

INVESTIGATING BIOMASS FAST PYROLYSIS AND CATALYTIC FAST PYROLYSIS:
MAPPING REACTION PATHWAYS AND EVALUATING CATALYSTS

By

Zhongyu Zhang

A DISSERTATION

Submitted to
Michigan State University
in partial fulfillment of the requirements
for the degree of

Biosystems Engineering – Doctor of Philosophy

2024

ABSTRACT

As the effects of global climate change become more apparent every year, renewable and environmental-friendly fuels are needed to replace fossil fuels. Biomass fast pyrolysis (BFP) produces a key intermediate, bio-oil, that can be upgraded to provide a needed alternative. BFP combined with catalysis, known as catalytic fast pyrolysis (CFP), is a method for green synthesis of valuable aromatic chemicals, such as benzene, toluene, ethylbenzene, and xylenes (BTEX), which are very important petrochemicals. BFP and CFP offer potential solutions to replace the current petroleum-based infrastructure and reduce the effects of climate change. However, the complex structure of biomass leads to multi-route reactions during pyrolysis that are not well defined. To better understand the reaction pathways, this study develops and deploys a methodology using isotopically labeled *Arabidopsis thaliana* cells as surrogate substrates. In this approach, plant cells are heterotrophically grown and preferentially labeled using ^{13}C -containing biosynthetic precursors (glucose for carbohydrate and phenylalanine for lignin). The harvested cells, containing different levels of ^{13}C -label, were subjected to pyroprobe-gas chromatography/mass spectrometry (py-GC/MS) to identify the products for both BFP and CFP. By tracking the ^{13}C from substrates to products, recognizing that either holocellulose or lignin are preferentially labeled in the plant cells, reaction pathways are revealed. Furthermore, HZSM-5 catalyst modified with several types of metals were tested during CFP for BTEX yield performance. Spent coffee was the selected feedstock as BTEX yields were highest amongst various biomass varieties. Chromium modified HZSM-5 exhibited the highest aromatic yields of the catalysts evaluated, with 1 wt.% Cr/HZSM-5 leading to the highest monoaromatic hydrocarbon yield.

Copyright by
ZHONGYU ZHANG
2024

Dedicated to my lovely family

ACKNOWLEDGEMENTS

As this long journey towards the destination, it is time to say thank you for all the support that I received during my doctoral degree. First and foremost, I would like to express my deepest appreciation and gratitude to my advisor, Dr. Christopher Saffron, for his immense contribution to my research. The knowledge and experience learnt from him has constantly benefited me throughout my graduate study at Michigan State University and will be for the rest of my life. I would like to extend my gratitude to Dr. James Jackson for his great advice on my work and all the discussions during the weekly meeting. I would also like to express my appreciation to my committee members, Dr. Wei Liao, Dr. Yair Shachar-Hill for their valuable guidance and feedback based on their exceptional expertise.

A sincere thank you to Dr. Steve Safferman for providing so much support and opportunities. His guidance on wastewater pretreatment broadened my scope and the understanding of my research.

I would also like to thank all past and present group members (Dr. Li Chai, Dr. Mahlet Garedew, Dr. Sabyasachi Das, Rachael Sak, and Meheryar Kasad) for all the help and support in my research. Thanks to my labmates (Dr. Ryan Stoklosa, Dr. Jacob Crowe, and Dr. Thanaphong Phongpreecha) for the happiness we shared in the lab. Thanks to the visiting scholars (Dr. Yi Yang, and Dr. Le Wu) for their friendships and collaborations. Thanks also to the staff at MSU (Dr. Peereboom, Cliff Foster, and Linda Danhof) for all the training and analysis they did for me.

Huge thanks to my friends (Pengchao, Zeyang, Chenchen, Peggy, Pei, Yuelin, Yang, Xing, Nusheng, and Xueliang) for all the fun we made together during my Ph.D. program. Finally, I would like to thank my parents for their support and encouragement from the beginning to the end. I owe them too much for this long-term absence. Lastly but not least, I want to thank my wife

Xinting for her love, support, and encouragement. This thesis would not have been possible without your help. Thank you!

TABLE OF CONTENTS

CHAPTER 1. INTRODUCTION	1
CHAPTER 2. LITERATURE REVIEW	5
CHAPTER 3. MAPPING REACTION PATHWAYS OF BIOMASS FAST PYROLYSIS USING ISOTOPICALLY LABELED PLANT CELL CULTURE	16
CHAPTER 4. MAPPING REACTION PATHWAYS OF CATALYTIC FAST PYROLYSIS USING ISOTOPICALLY LABELED PLANT CELL CULTURE	47
CHAPTER 5. MONOCYCLIC AROMATICS PRODUCTION BY CATALYTIC FAST PYROLYSIS OF BIOMASS WITH METAL MODIFIED HZSM-5.....	63
CHAPTER 6. CONCLUSIONS AND RECOMMENDATIONS	82
BIBLIOGRAPHY	85

CHAPTER 1. INTRODUCTION

More and more disasters caused by extreme weather, such storms, forest fires, floods, heat waves and cold waves, threaten human health in recent years.[1] Climate change is one of the greatest reasons leading to these phenomena.[2] Hansen et al. reported that the global surface temperature has been rising with a rate of 0.2 °C per decade starting from 1970s.[3] According to the Intergovernmental Panel on Climate Change (IPCC) synthesis report of 2023, global surface temperature was increased by 1.1°C in 2011-202 than 1950-1900.[4] The cumulative greenhouse gas emissions is a critical reaction caused the raised temperature.[5] IPCC indicated that 76% of global greenhouse gas emissions were carbon dioxide and 85% of these emissions were from petroleum and industrial activities.[6] A report from the International Energy Agency (IEA) said CO₂ emissions from energy consumption grew by 0.9% in 2022.[7] As the Paris Agreement hopes to keep the average temperature rise below 2 degrees Celsius, an effective way to cut down carbon footprint is to seek an environmentally friendly energy resource to reduce the reliance of petroleum-based fuels.

Biomass is the only sustainable source of organic carbon capable of replacing petroleum-based fuels and chemicals.[8] It is used to describe all organic materials including crops, trees, algae, land- or water-based plants and other organic waste. What has made biomass a unique source of energy is the stored chemical energy that is derived from the sun and stored in the bonds within the organic matter.[9] Moreover, plant-based biomass can have low sulfur and nitrogen contents, which can be advantageous when using many forms of heterogeneous catalysis to make clean energy products. These factors contribute to the growing interest in utilizing biomass as a clean and renewable energy resource.

Biomass is the largest single source of renewable energy consumption, accounting for 3.9 quadrillion of the 9.6 quadrillion renewable BTUs in 2015.[10] Various processes have been and are being researched to convert biomass into biofuels economically. Three main processes for bioenergy production are mentioned by McKendry: thermochemical conversion, biochemical conversion and mechanical extraction with esterification.[11] Fermentation-based alcohol biofuels have been and are being extensively considered, but they suffer from high cost, limited scalability, and incompatibility with the existing hydrocarbon-based infrastructure. In addition, the carbon efficiency is low and about 1/3 of the carbon will be released as carbon dioxide in the traditional alcohol conversion for biomass, such as the cellulose fermentation to ethanol. Instead, biomass fast pyrolysis (BFP) thermochemically converts biomass into gaseous, liquid, and solid products by heating biomass in the absence of oxygen.[12] This process can be carbon negative, an operational mode characterized by net carbon sequestration, if the solid product “biochar” is land applied as a nutrient amendment.[13] The liquid product, “bio-oil,” can be upgraded and used as an alternative to fossil fuels.[14] However, the mixture has deleterious properties, such as high viscosity, high acidity, and thermal instability, which makes bio-oil incompatible with current infrastructure or engine fuel systems.[15-20] As one example of an upgrading process, catalytic fast pyrolysis (CFP), is a process that combines BFP with catalysis (typically with zeolites) in a single step, to improve fuel quality and make valuable aromatic products which are dominantly produced by petroleum industry.

To develop the performance of BFP and CFP, a better understanding of BFP and CFP reaction mechanisms is sorely needed to optimize bio-oil production, select the proper feedstocks, and design effective stabilization approaches. Prior studies have attempted to map the flux of reactants to products using single small-molecule isotope studies such as glucose, cellulose, and

hemicellulose in BFP and CFP.[21-25] But those reaction mechanisms may be varied as lignocellulosic biomass has such a complex structure which could cause side reactions. Using plant tissue culture as a surrogate could be a solution to investigate pyrolysis reaction pathways. Plant cell culture exists cell wall fractions compared to single molecular model, and it could be harvested in a shorter time rather than a real plant. In this study, plant cell culture integrated with ^{13}C isotopic labeling procedure has been proposed with an aim to specifically label the cell fraction by feeding different ^{13}C labeled biosynthetic precursors into the media. Then the reaction pathway of BFP and CFP could be gained by tracking the ^{13}C isotope after subjecting the labeled cells into a pyroprobe-gas chromatography/mass spectrometer (Py-GC/MS).

The project goal is to improve the performance of biomass fast pyrolysis and catalytic fast pyrolysis by mapping the reaction pathways of BFP and CFP and investigating more effective catalyst for CFP. The objectives of this research are as follows:

- Map the reaction pathways during the fast pyrolysis of labeled T87 cell.
- Map the reaction pathways during the catalytic pyrolysis of labeled T87 cell.
- Evaluate several types of metals modified zeolite catalyst based on monoaromatic hydrocarbon yield.

To this end, we first develop a labelling methodology to preferentially label *Arabidopsis thaliana* (T87) cell wall components (Chapter 3). The characterization of T87 cells was done to examine the existence of plant cell walls and measure the cell wall fractions. Then the absorption of phenylalanine was observed to investigate the blocking biosynthetic pathway from glucose to phenylalanine. Then, the pyrograms, known as GC/MS results achieved after subjecting the materials into the py-GC/MS systems, were analyzed to map the reaction pathways of BFP. In Chapter 4, the procedure was similar as reporting in Chapter 3, but

packing the cells with HZSM-5 catalyst with a ratio of 1:5 for running through py-GC/MS system. Chapter 5 expands the evaluation of catalyst used in CFP. We begin with the selection of optimum feedstocks and optimum silicon: alumina ratio of HZSM-5 catalyst. Then seven types of metals were loaded on HZSM-5 to improve the monoaromatic hydrocarbon yield. Once the metal with the best performance was selected, a detailed analysis was studied for different amounts of the loadings.

CHAPTER 2. LITERATURE REVIEW

2.1 Biomass Fast Pyrolysis

The primary components of plant-based biomass (lignocellulosic biomass) are cellulose (20-50 wt.%), hemicellulose (20-40 wt.%), and lignin (10-20 wt.%).[26] Cellulose is a linear homopolymers of glucose linked by β -1,4-glycosidic bonds. Hemicellulose is heterogeneous polysaccharide mainly composed of glucose, xylose, arabinose, mannose, and galactose. Lignin, a highly branched polymer, is formed by phenyl propane units of coumaryl, coniferyl and sinapyl alcohol. Once these polymers are heated up without oxygen. Thermal decomposition occurs and creates three generalized products: non-condensable gas, bio-oil, and biochar. This thermochemical process is known as pyrolysis.

Pyrolysis product yields are dependent on temperature, heating rate, residence time, and the class of feedstock. In view of the three major fiber fractions of plant biomass, each degrades to a different extent under different heating conditions during pyrolysis. For example, lignin decomposes over a wide temperature range while cellulose and hemicellulose degrade fast in a narrower temperature range.[12] Residence time is another essential factor for pyrolysis products. Long residence time causes secondary cracking of primary products, which reduces the yield and quality of bio-oil.[12] Figure 2.1 shows pyrolysis with moderate temperature, high heating rates, and short residence times can convert woody biomass to bio-oil at a yield up to 70% by weight. To maximize bio-oil yield, pyrolysis is typically conducted under conditions of moderate temperature ($\sim 500^{\circ}\text{C}$), rapid heating (10^3 - 10^5 $^{\circ}\text{C}/\text{s}$), and short residence time ($<2\text{s}$), followed by immediate quenching of pyrolysis vapor.[27] When pyrolysis is performed under such conditions, it is known as “fast pyrolysis”.

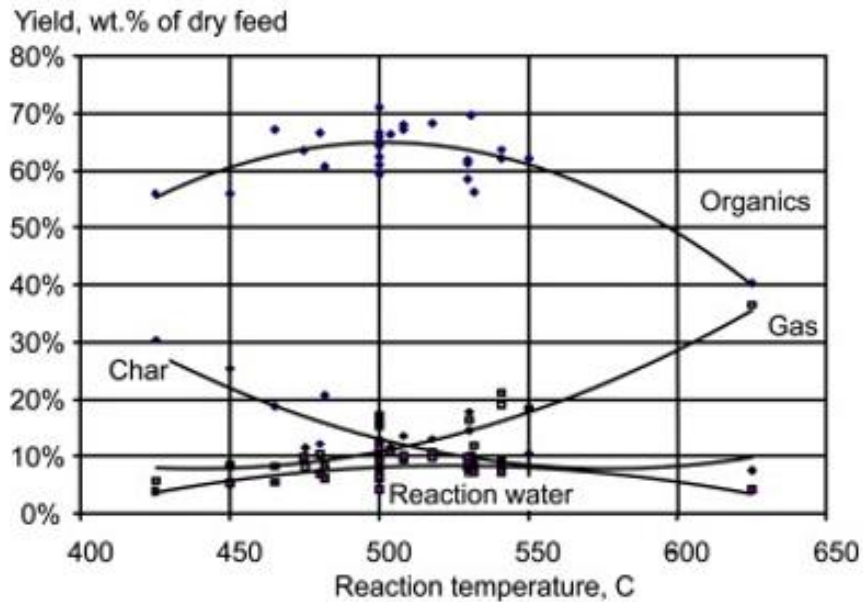


Figure 2.1 Variation of products from Aspen poplar with temperature.[28]

The quality of bio-oil, which affects its value and future utilization is also a function of pyrolysis temperature, heating rate, residence time and rapid quenching. Bio-oil is comprised of oxygenated organic compounds that are classified into aldehydes, alcohols, ketones, carbohydrates, aromatic hydrocarbons, and phenolics.[29] High oxygen content of bio-oil (35-40 wt.%) leads to a low energy density, where the heating value of bio-oil is 14-18MJ/Kg while that of engine oil is 42MJ/Kg.[30] Bio-oil is highly corrosive(pH 2-3) because it contains a large amount of organic acids (7-12 wt.%), especially acetic acid.[31] The poor thermal stability of bio-oil is due to its polymerization when heated over 80°C, in part because of condensation reactions between alcohols and aldehydes.[32]

Pyrolysis mechanisms of biomass are complicated because of the various composition of each biomass species and different reaction mechanism of each component at different conditions. Cellulose is primarily decomposed by cleaving β -1,4-glycosidic bonds in the temperature range of 315-400 °C.[33] Lin et al. proposed that cellulose firstly depolymerized to oligosaccharides and

then decomposed to anhydro-monosaccharides. The intermediate product, levoglucosan, can further produce to furan, ketones, and aldehydes.[23] The breakdown of hemicellulose occurs in a lower temperature range (200-350 °C) than cellulose. Xylan is typically considered as the model compound in the studies of hemicellulose pyrolysis due to the variance in polysaccharide constituents of hemicellulose. Because xylose cation cannot form any stable anhydride as glucose does, dianhydro-xylopyranose is formed from xylose by cleavage of glycosidic bond and dehydration reactions.[34] The final decomposition products of xylan are mainly acetic acid, furfural, hydroxy acetone, CO₂, CO, and H₂O. Compared to cellulose and hemicellulose, lignin has a much more complex mechanism during pyrolysis. The decomposition of lignin is classified into two stages by temperature because aromatic methoxy groups are stable at 200-400 °C and become highly reactive at 400-450 °C.[35, 36] As the pyrolysis temperature changes, the reaction mechanisms of each component of biomass are different and lead to a different fraction of products. Therefore, a study of reaction pathway is needed to improve the fuel quality and feedstock selection.

2.2 Catalytic Fast Pyrolysis

Bio-oil from biomass fast pyrolysis is not widely used as a liquid fuel because the process is not economically feasible compared with petroleum-based fuels. High oxygen and water content lower the values of pyrolysis products. Therefore, upgrading is a requisite step for the application of pyrolysis. Adding hydrogen at high pressure during pyrolysis (hydrotreating) is one way to reduce oxygenated molecules and increase the selectivity of hydrocarbons. This bio-oil hydrotreatment procedure typically includes two steps, 1) stabilization which transfers the carbonyl and carboxyl functional group into alcohols in the temperature range of 100-300 °C; 2) cracking and hydro-deoxygenation with metal catalyst, normally Ru, Ni or sulfided CoMo,

between 350-400 °C.[37] The pressure of hydrotreating process is between 50-200 bar.[38] Considering high pressure and the danger of hydrogen, catalytic fast pyrolysis (CFP), that combines pyrolysis and catalysis, may be a better solution to upgrade the bio-oil into desired products.

Catalytic fast pyrolysis likely occurs in two steps. The first step is thermal decomposition, the same as occurs during biomass fast pyrolysis.[39] Biomass is heated and converted into volatile organics, non-condensable gas, and solid coke. The volatile organics, mostly from the depolymerization of biomass, break up into water and dehydrated species in either the heterogenous catalyst or the homogeneous gas phase. The dehydrated species subsequently react in the catalyst or on the surface of the catalyst and then form the desired hydrocarbons based on the type of the catalyst selected (Figure 2.2).[40]

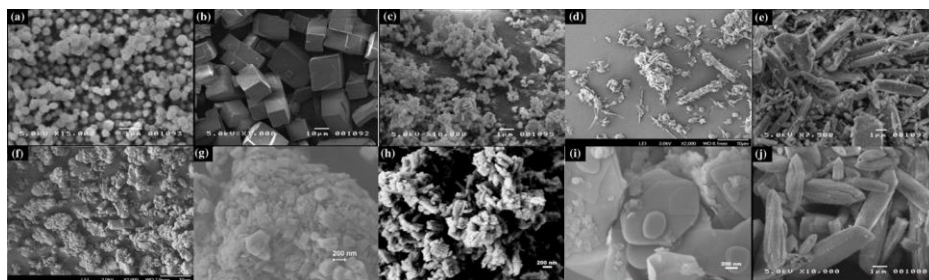


Figure 2.2 Scanning electron microscopy images of (a) ZK-5, (b) SAPO-34, (c) ZSM-23, (d) MCM-22, (e) SSZ-20, (f) ZSM-11, (g) ZSM-5, (h) IM-5, (i) TNU-9, and (j) SSZ-55.[41]

Several acid catalysts are used for catalytic fast pyrolysis, including sulfonated carbon, zeolites, heteropolyacids and metal oxides.[42] Of these, microporous acidic catalysts are widely known to crack the reactions that remove oxygen and catalyze the scission of carbon-carbon bonds of heavier oil fractions in oil refineries.[43] Highly acidic catalysts, like zeolites, are effective in selective of aromatic production during CFP.[44] Kelkar et al. found that HZSM-5 gave the highest aromatic conversion amongst ten different catalysts (five of them were HZSM-5 with different Si/Al ratio), while higher acidity HZSM-5 (lower Si/Al ratio) led to more monoaromatics and less

undesired coke production when using a pyrolyzer interfaced to a gas chromatography/mass spectrometer.[45] Aromatic compounds, especially monocyclic aromatics (benzene, toluene, ethylbenzene and xylenes, BTEX) are high value chemicals, that can be gasoline additives or precursors to terephthalic acid. Terephthalic acid that is used to produce polyethylene terephthalate is commonly synthesized by oxidation of *p*-xylene, where most of the *p*-xylene comes from catalytic re-forming of naphtha.[46, 47] Due to increasing demand, xylene isomers, along with other aromatics such as benzene and toluene, also produced from catalytic re-forming of naphtha are used to form *p*-xylene by reacting them over an acid zeolite catalyst.[48]

In this respect, catalytic pyrolysis with zeolite catalysts has been studied by many researchers.[39, 41, 45] Jae et al. investigated the conversion of glucose to aromatics in CFP was affected by zeolite pore size and shape selectivity. He concluded that the highest aromatic yields were obtained in the medium pore zeolites with a pore size range of 5.2-5.9 Å. Small pore zeolites do not produce aromatics from pyrolysis of glucose, while the large pore zeolites resulted in high coke yield, low aromatic yield and low oxygenate yields.[41] Wang et al. reported that cellulose (a glucose polymer) provided more aromatics than lignin, even lignin is derived from monomeric phenolics, in the catalytic pyrolysis of switchgrass.[39] On the other hand, metal modified catalysts have been studied by many researchers aiming to increase the acidity by ion exchange or incorporate into zeolite framework.[45, 49-57] The acid sites of ZSM-5 plays an critical role in deoxygenation and deactivating mechanisms in CFP as described by these research. According to Zheng's conclusion, all metal modified ZSM-5 (M-ZSM-5) yielded a higher yield of non-condensable gas, and the deoxygenation level of M-ZSM-5 catalysts followed the order: GaZSM-5 > Zn ZSM-5 > NiZSM-5 > CoZSM-5 > MgZSM-5 > CuZSM-5 > HZSM-5.[57] Veses et al. investigated that the incorporation of metals doped on ZSM-5 enhanced the deoxygenation mainly

through decarboxylation and/or decarbonylation reactions.[58] To promote the performance of CFP, a comprehensive study of its reaction pathways could support catalyst improvement, optimum product selectivity.

2.3 Prior Pyrolysis Mechanism Studies

Understanding the mechanisms and kinetics of pyrolysis has been a pursuit since the 1960s. Antal summarized the research output from the 1960s to early 1980s in two reviews that were published in “Advances in Solar Energy”. [59, 60] The reviews discussed the pyrolysis of cellulose, glucose, lignin, and whole biomass under low, moderate, and high temperature. All noncellulosic carbohydrates began rapidly decomposing to anhydrosugars, light volatile compounds, non-condensable gases (CO₂, CO) and char when pyrolysis temperatures were above 200°C. Cellulosic carbohydrates were found tolerant of a higher temperature (above 250°C) because of its crystalline structure.[61] Transglycosylation reactions were more effective than polymerization reaction at this temperature, resulting in the formation anhydrosugars composed primarily of levoglucosan.[62] The reaction pathways of cellulose were mapped by pyrolyzing ¹⁴C-labeled materials in thermal gravimetric analysis and differential thermal analysis (TGA/DTA).[63] The chemical mechanisms were projected to depend on using the isotopic materials labeled in different positions (C1, C2 or C6), including acid-catalyzed degradation pathway of carbohydrates, formation of the 3,6-anhydro rings under alkaline condition, fragmentation, dehydration and rehydration reactions.[63]

Molecular beam mass spectrometry (MBMS), a technique developed at the National Renewable Energy Laboratory (NREL), was applied to study pyrolysis mechanisms by Milne et al. in 1983.[64] This technique utilizes the molecular beam produced by hydrogen-oxygen combustion at high temperature (up to 900°C) to pass through a sample in a small orifice (~300

μm) and then the mixture is injected directly into a quadrupole mass spectrometer. The abrupt transition caused by high temperature steam quenches the chemical reaction, inhibits condensation, and also avoid contact with the instrument walls.[64] Evans et al. found higher than expected levels of levoglucosan when using the MBMS system compared to low-energy electron ionization using conventional sample volatilization (GC/MS). They also indicated that the levoglucosan formed in the conventional pyrolysis process was underestimated because of ionization fragmentation and thermal rearrangement.[65] Isolated lignins from different types of biomass were also subjected into MBMS by Evans et al.[66] The analysis of MBMS results showed that the first formed and predominant products were coniferyl and sinapyl alcohol where higher molecular weight oligomers, even dimers, were not confirmed.[66] They also found that product distribution varied with different lignin separation methods.[66] The same conclusion was drawn by Van der Hage et al. who examined the pyrolysis of steam-explosion lignin, Kraft lignin, bagasse lignin, wood-milled lignin and organosolv lignin.[67] On account of the severity of the isolation procedure, the alky-aryl linkages were altered to different degrees, leading to the diversity of pyrolysis products. Hence the reaction pathway of isolated lignin may not coincide with native lignin in natural biomass during pyrolysis.

To help gain a better understanding of pyrolysis chemistry, glucans that were labeled with ^{13}C at C1, C2 or C6 were applied to map the reaction pathways.[68] As reported by Ponder and Richard, glycolaldehyde was mainly derived from C1 and C2 labeled materials and about 50% of formic acid was enriched during pyrolyzing C1 labeled glucans. Acetol and acetic acid were mostly formed by three contiguous carbons that include a terminal carbon.[68] In latter research, Evans et al. grew *Acetobacter xylinum* cellulose on ^{13}C -labeled glucose medium for the study of pyrolysis chemistry.[21] They mentioned that glycolaldehyde was not enriched by using (1- ^{13}C)-

labeled cellulose even treating the sample with 0.1% aqueous KOH to increase the formation of glycolaldehyde. In contrast to pyrolysis of (2-¹³C)-labeled cellulose, a significant amount of labeled glycolaldehyde was detected by the mass spectrometer. The distinct conclusions reveal that the pyrolysis of cellulose differs from that of glucan.

More pyrolysis studies were extended by Paine et al. using ¹³C-labeled glycerin and glucose.[69-73] They discovered the cyclic Grob 1,3-diol fragmentation and the tandem alkaline pinacol rearrangement/retro-aldol fragmentation in pyrolysis of glycerin based on the position of labeled carbon and applied the mechanism to analyze breakage of the six-carbon chain of glucose.[70, 71] The unimolecular reaction mechanism was dominant in the formation of low molecular weight carbonyl compounds (C1:formaldehyde, formic acid, C2: acetaldehyde, acetic acid, glycolaldehyde,[70] C3: acetol, and C4: 2,3-butanedione[71]). Furan formation predominantly proceeds by a unimolecular reaction pathway, while some mechanisms showed that fructose was consistently involved during the co-pyrolysis of glucose and fructose.[72] In the formation of light alkane and alkenes (C2-C4), the least saturated compounds were first produced and then underwent hydrogenation induced by free radical chain reactions.[73]

A computational modeling method, density functional theory (DFT), was recently used to gain a more accurate simulation of the pyrolysis reactions. Broadbelt et al. reported the mechanistic models for pyrolysis of cellulose, glucose, and hemicellulose by DFT.[74-76] The activation energies of hundreds of reactions were calculated and compared with the experimental data from previous research. The reaction rate coefficients showed that the concerted mechanism was more favorable than either homolytic or heterolytic cleavage during cellulose pyrolysis.[76] The array of hemicellulose pyrolysis products were insignificantly affected by the degree of polymerization and the polydispersity index.[75] The computational results may predict the optimal conditions

for desired products and the modeling framework can be applied to study fast pyrolysis mechanisms for other polysaccharides and even whole biomass.

As most pyrolysis studies are focused on examining small-molecule compounds or single cell wall components, the pyrolysis mechanisms of whole biomass are barely investigated due to biomass 'complexity. Antal et al. supported the view biomass components interact during pyrolysis.[60] He noted that the pyrolytic behavior was not a linear superposition of each components. Therefore, further study of whole biomass pyrolysis is merited to better the understanding of biomass pyrolysis chemistry.

2.4 Labeling strategy

Mapping reaction pathways of biomass components to pyrolysis products should consider methodologies that aim to conserve the interactions that occur as cellulose, hemicellulose, and lignin are co-heated. ^{13}C -labelling offers one such route, provided that it is used to map cell wall components that are incorporated into the biomass fiber fractions. Emphasis on labelling individual fiber components provides a methodology for ascertaining the reactant source for label-containing products. Recognizing that sucrose, a photosynthetic sugar, is first converted into uridine diphosphate glucose (UDP-G), then to monosaccharides, and then into cellulose and hemicellulose polymers (Figure 2.3) is useful as ^{13}C labeled sucrose can serve as a carbon source for heterotrophically grown plant cells. Likewise, phenylalanine is a precursor to three monolignols—coniferyl, sinapyl, and *p*-coumaryl alcohol—that are incorporated into lignin through the phenylpropanoid pathway.[77, 78] Thus, ^{13}C labeled phenylalanine provides a tool for ascribing pyrolysis products to lignin.

The isotope effect on plant cell wall formation was considered for ^{13}C labeled cell culture studies. Schwender et al. described that labeling could be achieved by growing plant suspensions

in a ^{13}C -containing medium for several hours or growing excised plant components such as root tips in ^{13}C labeled glucose containing medium for 12-18 hours.[79] Sielbauer et al. examined that no significant difference in growth or isotope distribution when using universally labeled ^{13}C glucose or universally labeled ^{13}C sucrose as substrates.[80] Such results are important for ^{13}C -mapping experiments that depend upon known initial concentrations in cellulose, hemicellulose, and lignin fractions of plant cell walls.

Previous research has demonstrated that cell cultures from *Arabidopsis thaliana* (widely referred to as T87 cells) can be used as models to perform this labeling experiment. *Arabidopsis thaliana* is widely used in plant biology studies because it has a short generation period, small space requirements for growth and prolific productions. The other potential advantage is that the genomic sequence of *Arabidopsis* has been analyzed in 2000.[81] Even though mapping reaction pathways is not related to genomic works, but it may be beneficial from altering the composition of *Arabidopsis* plant via changing its genomes. Although *Arabidopsis* has an efficient and fast regeneration, sufficient time is needed to ensure that the labeled precursors reach a metabolic steady state, and the cells form secondary cell walls which have different composition than the primary cell wall.[82] To sum up, plant cell culture, such as T87 cells, could be a surrogate in pyrolysis reaction pathway study. If a methodology that can preferentially label plant cell wall fraction could be developed, pyrolysis reaction pathways from reactants to products would be easily investigated by tracking the labeled materials.

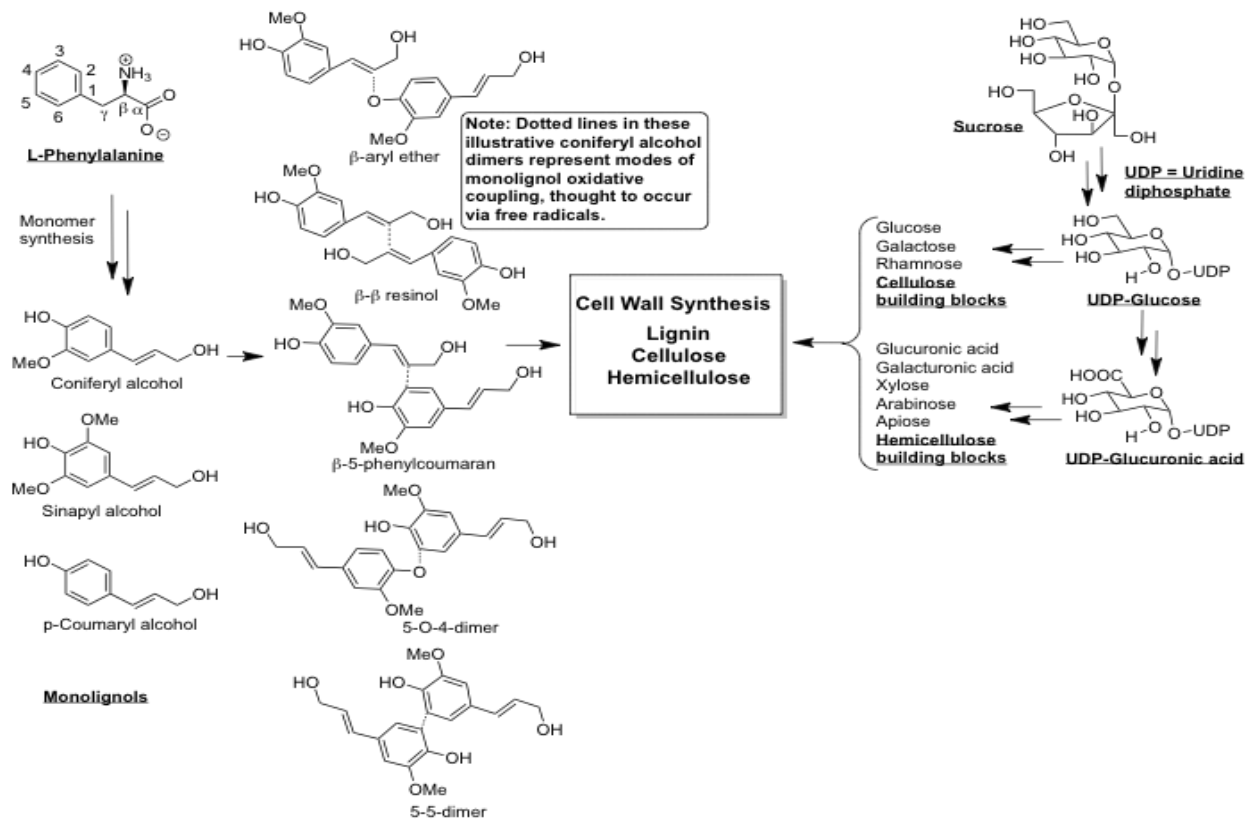


Figure 2.3 Cell wall synthesis scheme. Sucrose forms cellulose and hemicellulose through uridine diphosphate while phenylalanine is the biosynthetic precursor for lignin monomers.

CHAPTER 3. MAPPING REACTION PATHWAYS OF BIOMASS FAST PYROLYSIS USING ISOTOPICALLY LABELED PLANT CELL CULTURE

3.1 Abstract

Biomass fast pyrolysis has the potential to provide renewable fuels that can reduce greenhouse gas emissions. However, the pyrolysis reaction mechanism is not well established, especially for lignocellulose biomass with its complex structure. In this work, a methodology is developed that combines ^{13}C labeling and plant cell culture to simulate the biomass fast pyrolysis process and to map the reaction pathways by tracing isotopes. Plant cell wall components (carbohydrate and lignin) can be specifically labeled by feeding ^{13}C -labeled biosynthetic precursors (glucose and phenylalanine, respectively) into *Arabidopsis thaliana* “T87” cell cultures and growing the cell cultures heterotrophically. Excess phenylalanine is applied to the media to block the biological pathway from glucose to phenylalanine. In addition, T87 cells grown in media with high phenylalanine concentration (5 g/l) increases the lignin content 3.8-fold when compared to the cells cultivated without phenylalanine addition. Pyrograms for T87 cells with one of the two substrates labeled were used to map the reaction pathways. Based on the isotope distribution, light oxygenates, such as 3-methylbutanal, were derived from the carbohydrates, while the monoaromatic hydrocarbons were generated from lignin in pyrolysis of T87 cells. Interestingly, phenol was formed by both carbohydrates and lignin.

3.2 Introduction

Global climate change has already caused observable effects on the environment in recent years. With a high level of certainty, the Intergovernmental Panel on Climate Change (IPCC) and the U.S. Environmental Protection Agency have stated that humanity is responsible for the rapid

acceleration in climate change.[83, 84] Greenhouse gas emissions lead to a warmer climate that melts glaciers, shifts ocean currents, and thaws permafrost, which further exacerbates climate change. As reported by the International Energy Agency, global carbon dioxide emission from fuel combustion and industrial processes was over 36.8 gigatons in 2022. This number has increased by around 50% since 2000 and was raised by around 0.9% in 2022.[85] The Paris Agreement sets a long-term goal to limit average temperature rise to 2 degrees Celsius, compared to pre-industrial levels.[86] Reducing greenhouse gas emissions is the primary step to achieve this objective.

To replace fossil fuel and minimize the effect of climate change, a renewable and sustainable source of fuels is clearly needed, especially liquid fuels. Biomass is the largest single source of renewable energy consumption, accounting for 3.9 quadrillion of the 9.6 quadrillion renewable BTUs in 2015.[10] A thermochemical technology, fast pyrolysis, provides a possible solution to decrease fossil fuel-derived atmospheric carbon dioxide by utilizing abundant plant biomass resources. This process converts biomass into gaseous, liquid, and solid products by heating biomass in the absence of oxygen.[12] The liquid product, “bio-oil,” can be upgraded and used as an alternative to fossil fuels.[14] “Biochar,” the solid product, can be land applied as a nutrient amendment, while also sequestering carbon and promoting regenerative agriculture.[13]

Despite the growing interest in biomass fast pyrolysis, there is no consensus about its reaction mechanisms. A better understanding of reaction mechanisms is needed to optimize bio-oil production and design effective stabilization approaches. Due to the complex structure of lignocellulosic biomass, many studies have attempted to map the flux of reactants to products using single small-molecules such as glucose, cellulose, and hemicellulose.[23-25] Though such investigations can be informative, the complexity of lignocellulosic biomass will invariably trigger side reactions that result in difficult-to-explain product slates. Therefore, it is important to map the

reaction pathways of biomass fast pyrolysis from reactants to products. Isotope analysis can provide a clear material flow in the uncertain pyrolysis reaction mechanism studies. For example, Ponder and Richards found that about 50% of formic acid was isotopically enriched when pyrolyzing isotope-labeled glucans.[68] In another isotope study, Evans et al. grew *Acetobacter xylinum* cellulose on ^{13}C -labeled glucose medium for examining pyrolysis chemistry.[21] However, these isotope studies used single molecules and did not consider molecular interactions that occur as cellulose, hemicellulose, and lignin are co-heated in biomass fast pyrolysis.

This work aims to probe the reaction pathways in pyrolyzing biomass' cell wall components. ^{13}C -labeling is used to map reaction pathways, assuming no isotope effect leading to unwanted changes in cell wall composition. Supporting this assumption, Schwender et al. described that labeling could be achieved by growing plant suspensions in a ^{13}C -containing medium for several hours or growing excised plant components such as root tips in ^{13}C labeled glucose containing medium for 12-18 hours.[79] Sielbauer et al. found no significant difference in growth or isotope distribution when using universally labeled ^{13}C glucose or universally labeled ^{13}C sucrose as substrates.[80] Compared to labeling real plant biomass in a ^{13}C - CO_2 environment, isotope labeled cell culture could be harvested every one or two weeks, resulting in a much faster and less expensive labeling process. On the other hand, labeling biomass by using ^{13}C - CO_2 will label the entire cell wall, making it difficult to trace pyrolysis product origin to cell wall components.

Herein, we explore a labeling strategy that specifically labels *Arabidopsis thaliana* "T87" cell cultures in carbohydrate or lignin fractions by feeding ^{13}C -containing biosynthetic precursors (sucrose or glucose for carbohydrates, phenylalanine for lignin). Sucrose, a photosynthetic disaccharide made of glucose and fructose, is first converted into uridine diphosphate glucose

(UDP-G), then to monosaccharides, and then into cellulose and hemicellulose polymers. The phenylpropanoid pathway (Figure 3.1) provides the formation of three hydroxycinnamic acids from phenylalanine, where their alcohol derivatives—coniferyl, sinapyl, and *p*-coumaryl alcohol—are known as three basic building blocks of lignin. Due to a higher cost of ¹³C labeled sucrose, glucose is substituted for sucrose as the source of carbon and energy in liquid medium.

However, glucose is not only a precursor to cellulose and hemicellulose, as it is also converted to lignin. Following the glycolysis metabolism pathway (Figure 3.2), glucose is converted into phosphoenolpyruvate (PEP) before forming pyruvate. As a key metabolite, PEP can react with erythrose-4-phosphate and form phenylalanine through the shikimate pathway (Figure 3.3). A reaction route to lignin starting from glucose is shown by combining these three metabolic pathways (Figure 3.1-3.3) that occur in plants. Hypothetically, the pathway from glucose to phenylalanine could be blocked if excess phenylalanine was provided in liquid medium. This excess phenylalanine then serves as the sole precursor to lignin.

After cultivation of labelled plant cells, they are harvested and injected into a micropyrolyzer-gas chromatography/mass spectrometry (py-GC/MS) system. The results of this analysis are used to map the reaction pathways of pyrolysis for several reactants into products. An improved understanding of how biomass is transformed into energy products is gained and will contribute to developing biomass fast pyrolysis techniques and optimizing feedstock for desired products.

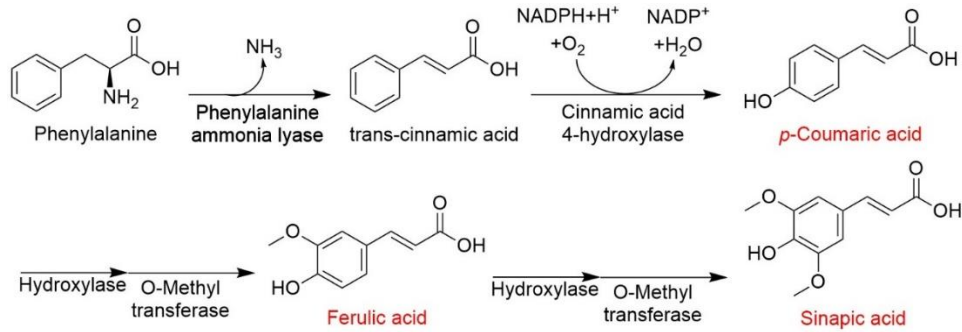


Figure 3.1 Synthesis of three hydroxycinnamic acids from phenylalanine.

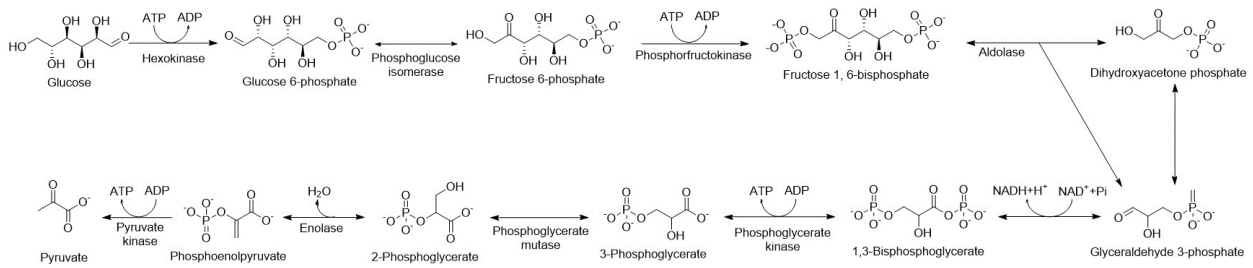


Figure 3.2 Glycolysis metabolism from glucose to pyruvate in plant biomass.

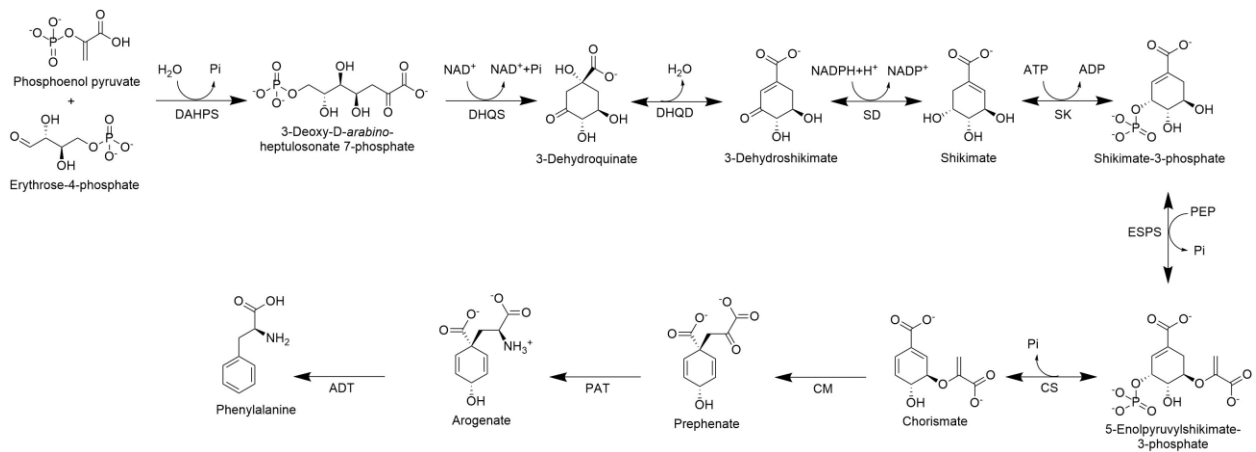


Figure 3.3 Shikimate pathway from phosphoenolpyruvate to phenylalanine in plants.

3.3 Methods and Materials

3.3.1 *Arabidopsis thaliana* liquid cell culture (T87 cells)

T87 cells from *A. thaliana* Columbia plants, were routinely grown in liquid media with glucose (30 g/l), and phenylalanine (5 g/l). The liquid medium consisted of the Murashige and Skoog basal salt mixture (4.3 g/l) supplemented with 2,4-dichlorophenoxyacetic acid (0.2 mg/l), thiamine (1 mg/l), myo-inositol (0.1 g/l), ethylenediaminetetraacetic acid (2.9 µg/l), and potassium dihydrogen phosphate (0.18 g/l) in a pH value of 5.7. Briefly, each flask was filled with 10 ml of liquid culture from a previous trial and 40 ml of fresh liquid media. The cells were incubated in 250 ml baffled culture flasks in an incubator at 21 °C with a speed of 140 rpm in darkness. After seven days, the cells were filtered and rinsed three times in RO water and then dried at 60 °C overnight prior to pyrolysis. ¹³C labeled glucose and ¹³C labeled phenylalanine were purchased from Cambridge Isotopes and used without further treatment. All six carbons in glucose were labeled and nine carbons and nitrogen in phenylalanine were labeled.

3.3.2 Labeling strategies for T87 cells

To preferentially label the cell wall fraction, T87 cells were grown heterotrophically to avoid photosynthesis; the only carbon source was the sugar provided in the liquid medium. Using this approach, each cell wall fraction, i.e., carbohydrate and lignin, will be labeled as its biosynthetic precursor is labeled. T87 cells grown with labeled glucose and unlabeled phenylalanine predominantly forms labeled carbohydrates (cellulose and hemicellulose) and unlabeled lignin. Likewise, labeled phenylalanine mostly forms lignin when unlabeled glucose is present. Three different feeding rates (20, 50, and 100 wt.%) of labeled materials were applied in the labeling process to better trace the isotopes and find the relationship from the reactants to products during pyrolysis. ¹³C labeled glucose and phenylalanine (Cambridge Isotopes) were used

without any purification. All six carbons in glucose were labeled, while all the carbons and nitrogen in phenylalanine were labeled.

3.3.3 Proximate analysis of T87 cells

Harvested T87 cells were subjected to proximate analysis using a thermogravimetric analyzer (TGA, Model TGA/DSC 1, Mettler-Toledo, OH). Three samples harvested from different batches were run on the TGA. The temperature program was first heated to 105 °C for removing moisture, and then to 925 °C for driving off the volatile matter. Moisture and volatiles were removed by nitrogen carrier gas. The residue was reheated to 800 °C in the presence of air to determine ash content at a heating rate of 10 °C/s.

3.3.4 Cell wall compositional analysis

Cell wall polymer composition was determined with an NREL method[87] that uses a two-step sulfuric acid hydrolysis to fractionate the biomass. Polymeric carbohydrates are hydrolyzed into the monomeric forms, which are measured by HPLC. The insoluble lignin and ash are filtered, dried, and weighed.

3.3.5 Lignin staining

The presence of lignin was confirmed using the phloroglucinol-hydrochloric acid staining method developed by Herr.[88] Phloroglucinol-hydrochloric acid solution was made of 1% phloroglucinol in 20% calcium chloride solution and concentrated hydrochloric acid with a volume ratio of 25:4. One drop of this solution was mixed with a small amount of liquid-cultured T87 cells and placed on a glass microscope slide for observation by light microscopy.

3.3.6 Pyrolysis-GC/MS

Samples were heated using a microscale pyrolyzer (Proprobe 5250, CDS Analytical Inc, PA) interfaced with gas chromatography/mass spectrometry (QP-5050A, Shimadzu Corp, MD) to

simulate biomass fast pyrolysis. The input was dried at 60 °C and ground to a particle size of less than 0.5 mm (35 mesh). Approximately 3 mg of sample was packed between quartz wool in a quartz tube that is dropped into a pyroprobe chamber at 650 °C for 20 seconds with a heating rate of 999 °C/s. The pyrolysis vapor was entrained in a helium stream and sent to a GC/MS through a heated transfer line at 300 °C. A Restek rtx-1701 column (60m × 0.25mm × 0.25µm) was heated in a GC oven to perform the chromatographic separation using a column gas flow rate of 1 cm³/s with an inlet split ratio of 1:100. The GC oven temperature program began at 40 °C with a one-minute hold and then ramped to 270 °C at an 8 °C/min heating rate. Each peak's mass spectrum was compared with standard spectra in the 2005 NIST library for compound identification.

3.4 Results and Discussion

3.4.1 Characterization of T87 cells

Confirmation that T87 cells are forming cell walls is needed to support reaction mapping studies. As the purpose of this study is mapping the reaction pathway using liquid cell culture, confirmation of cell wall existence in T87 cells was necessary prior to pyrolysis. Analysis of TGA results in Figure 3.4 revealed that oven dried T87 cells were mostly comprised of volatile matter (Table 3.1) that was liberated from 200 to 500°C (Figure 3.4), a result consistent with cell wall deconstruction by pyrolysis. The high ash content in Table 3.1 is likely due to intracellular mineral salts that failed to wash away prior to TGA.

Table 3.1 Proximate analysis of T87 cells in triplicates (wt.%).

	Average	Standard Deviation
Moisture	5.81%	0.32%
Volatile matter	83.62%	1.27%
Ash	7.58%	0.81%
Total	97.01%	

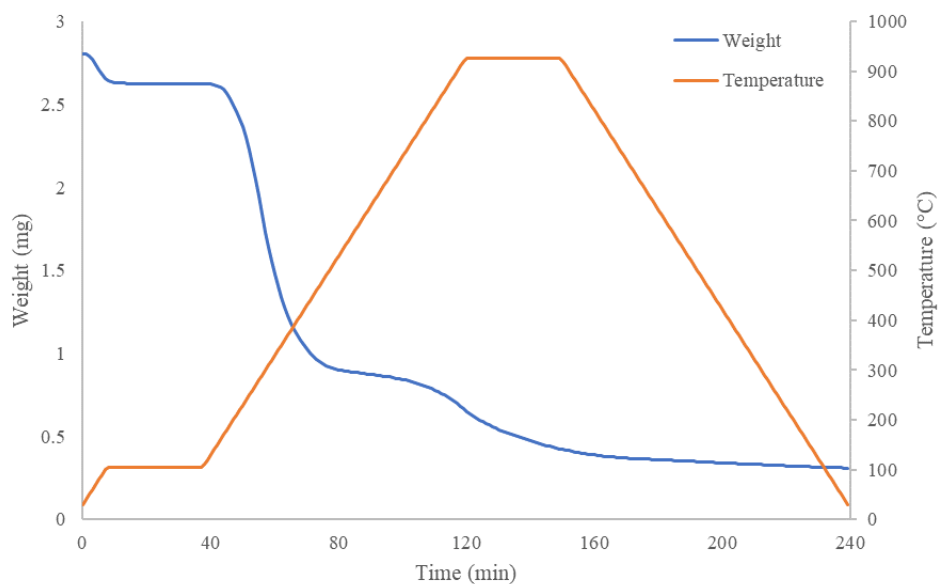


Figure 3.4 Thermal gravimetric analysis (TGA) of T87 cells in the presence of nitrogen.

The structural carbohydrate and lignin contents of three different feedstocks (raw *A. thaliana* stem cuttings, and T87 cells, with and without feeding PHE) were examined by NREL compositional analysis. *A. thaliana* has a lower cell wall mass total than woody plants, like poplar, which can exceed 80 wt.%. As seen in Table 3.2, the amounts of cellulose, hemicellulose, and lignin in T87 cells, without adding phenylalanine in the growth medium, were much lower than *A. thaliana* stem cuttings. However, the lignin content of T87 cells was significantly increased when adding phenylalanine into the medium.

Table 3.2 NREL compositional analysis of feedstocks in triplicates (wt.%).

	Glucan	Xylan	Lignin	Total
Raw <i>A.thaliana</i>	22.79% ± 0.02%	11.65% ± 0.08%	16.39% ± 0.03%	50.83%
T87 cells without PHE	8.83% ± 0.10%	4.86% ± 0.06%	1.39% ± 0.38%	15.08%
T87 cells with PHE	11.12% ± 0.12%	5.62% ± 0.03%	5.30% ± 1.83%	22.03%

Elemental analysis was applied to quantify the composition of carbon, hydrogen, and nitrogen, while oxygen content was calculated by difference. The replicated results reported that T87 cells contained 7.19 wt.% nitrogen, much greater than 1.83 wt.% observed in raw *Arabidopsis* biomass. The high nitrogen content indicated a high amount of protein in T87 cells, that reduced the cell wall fraction of total cell weight. Also, raw *Arabidopsis* biomass has a higher nitrogen content than a typical lignocellulosic biomass, such as poplar (0.15 ±0.02 wt.%) or switchgrass (0.42 ±0.04 wt. %). As nitrogenous substances are indispensable for cell culture, this problem may not be resolved. Moreover, high nitrogen content was observed because excess phenylalanine was added to block the synthesis of phenylalanine from glucose.

Noting the low observed lignin levels, several methods were used to confirm the existence of lignin in T87 cells. The phloroglucinol-hydrochloric acid staining method is an obvious way to show the existence of lignin. Confirming the presence of lignin, cinnamaldehyde end groups of lignin reacted with phloroglucinol in the acidic environment, resulting in a red color (Figure 3.5).[89]

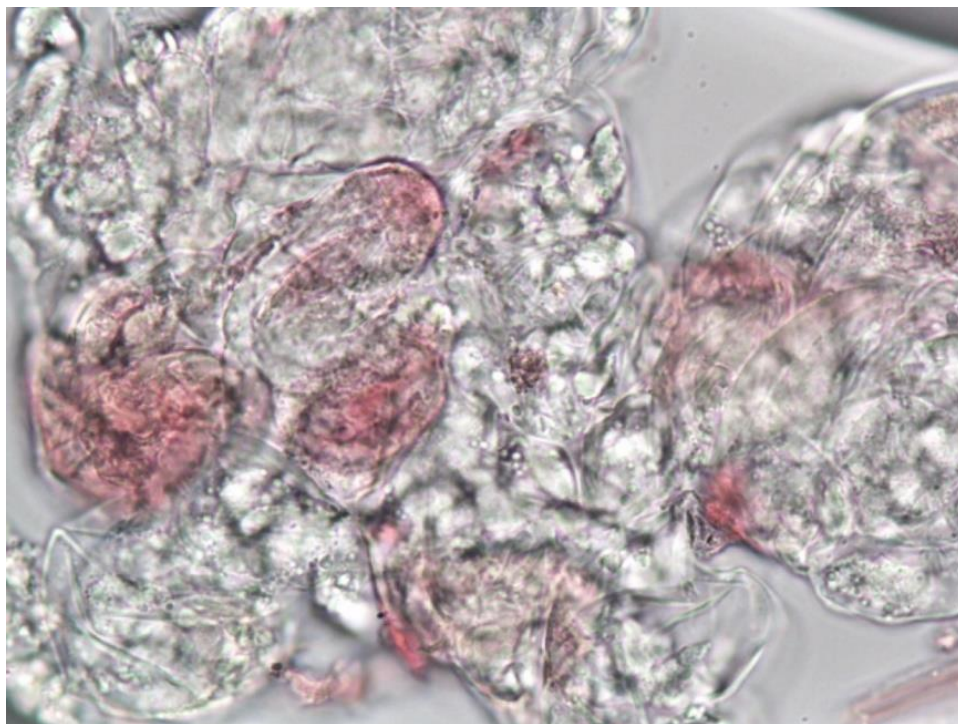


Figure 3.5 Phloroglucinol-hydrochloric acid staining of T87 cells observed by light microscopy with a 40X objective lens.

Thioacidolysis was also applied to dried T87 cells to obtain the composition of thioethylated lignin monomers through the cleavage of β -O-4 ether linkage. Small amounts of guaiacyl and hydroxyphenyl (376 and 197 $\mu\text{g/g}$) lignin were detected, while no syringyl lignin was released from the T87 cells. Zhao et al. indicated that syringyl lignin was not produced in angiosperms generally.[90] T87 cells also did not make syringyl lignin as *A. thaliana* is an angiosperm. Even though the lignin monomer content was lower than that of lignocellulosic biomass, such as poplar, similar results were reported by other researchers who analyzed *A. thaliana* cell culture. As examples of prior work, Derikvand et al. found the amounts of ferulic acid and *p*-coumaric acid produced were 27 and 32 $\mu\text{g/g}$ for *A. thaliana* inflorescence stems,[91] while only 31.5 $\mu\text{g/g}$ of ferulic acid and 2.7 $\mu\text{g/g}$ of *p*-coumaric acid were found in T87 cells by Yamamura et al.[92]

3.4.2 Phenylalanine absorption

To avoid photosynthesis, T87 cells were grown heterotrophically in liquid culture with a carbon source in the liquid medium. Hypothetically, T87 cell wall components can be preferentially labeled by feeding ^{13}C -labeled biosynthetic precursors. Specifically, ^{13}C -labeled glucose only labels the carbohydrate polymers if excess phenylalanine is present to block the pathway from glucose to phenylalanine, while ^{13}C -labeled phenylalanine forms lignin.

Method efficacy depends, in part, on T87 cells absorbing phenylalanine from culture media. To demonstrate uptake, 5 g/l of phenylalanine was initially added into regular trials containing T87 cells. One ml of cell suspension was sampled daily beginning from the date that T87 cells were originally transferred from tissue culture. These samples were filtered through a 0.22-micron syringe filter to remove cells. The phenylalanine concentration in the filtrate was estimated by high performance liquid chromatograph (HPLC) with a C18 column followed by a diode array detector (HPLC-DAD) set at 260 nm. As shown in Figure 3.6, the phenylalanine concentration reduced 1 g/l after seven days, indicating that about 50 milligrams of phenylalanine were absorbed. Error bars show the variability of plant cell culture performance between replicates. Large error bars were due to the variability of plant tissue performance from different weeks.

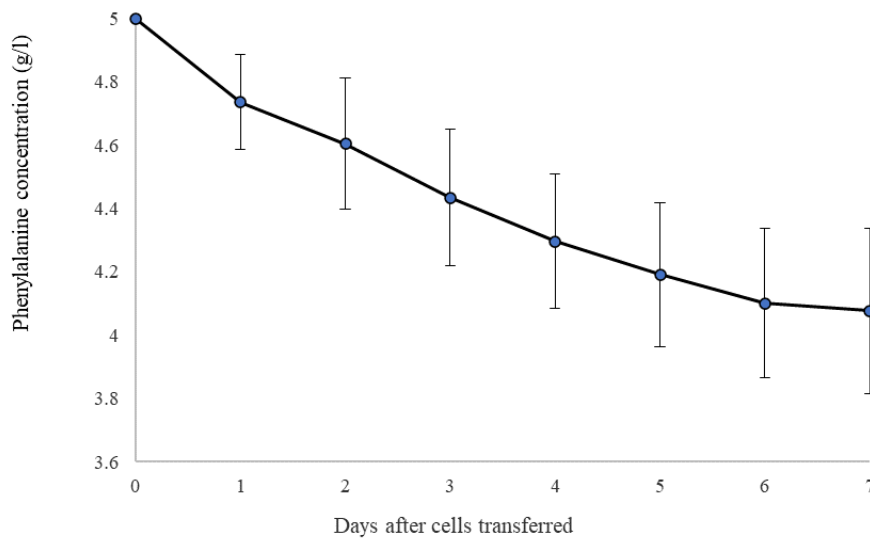


Figure 3.6 Phenylalanine absorption of T87 cells days after the cells were transferred.

To block phenylalanine synthesis from glucose, an excess of unlabeled phenylalanine was added to block this undesired pathway (Figure 3.2-3.3). As Figure 3.7 demonstrated, about 10% more glucose was consumed after 7 days for T87 cells when phenylalanine concentration was reduced from 5 g/l to 1 g/l, indicating that glucose metabolism to phenylalanine could be blocked by adding excess phenylalanine. More phenylalanine may also result in greater lignin content in T87 cells, as lignin content rose four times when phenylalanine (5 g/l) was added into the liquid medium when compared to T87 cells grown without adding phenylalanine (Table 3.2). Likewise, phenylalanine consumption was measured under different amounts of glucose added in the media (Figure 3.8). More glucose in the media lowers phenylalanine absorption by liquid cell culture, a result confirming that glucose and phenylalanine are interconverted.

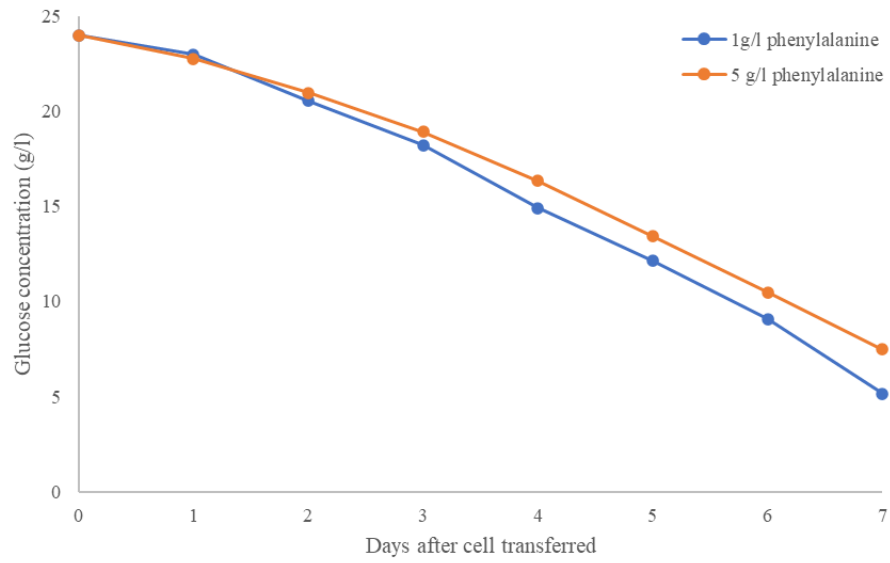


Figure 3.7 Glucose consumption under differing phenylalanine concentrations. Each point is the average of two replicates.

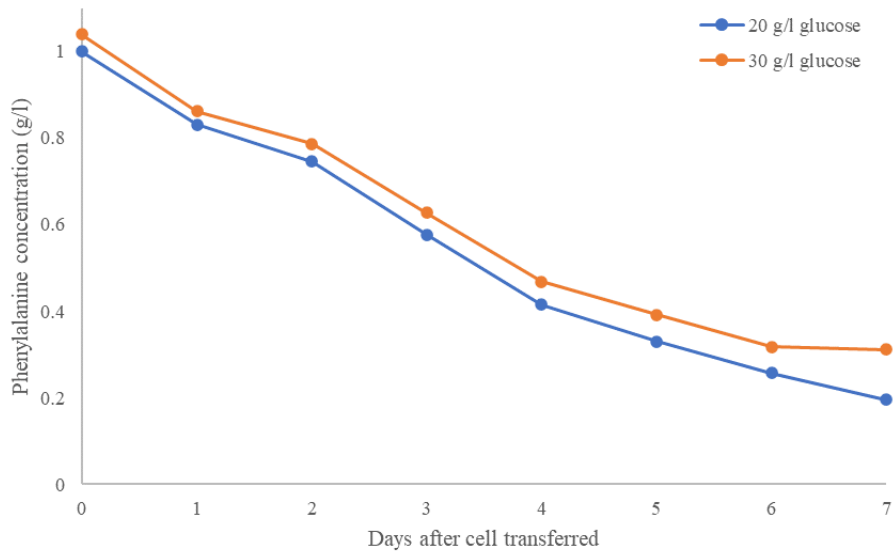


Figure 3.8 Phenylalanine consumption under differing glucose concentrations. Each point is the average of two replicates.

3.4.3 Pyrolysis-GC/MS results comparison

To examine whether T87 cells are better surrogates than other materials, a series of T87 pyrograms were compared to those of *A. thaliana* stem cuttings in Figure 3.9. The major pyrolysis product of *A. thaliana* stem cuttings is toluene with a retention time of 8.05 minutes, which was notably different than other lignocellulosic biomass types (poplar, switchgrass, or corn stover). Two other aromatic hydrocarbons products, ethylbenzene, and styrene were also produced in relative abundance in its pyrograms. Such aromatic hydrocarbons are normally generated in catalytic fast pyrolysis, not directly by BFP. T87 cell pyrograms are consistent with *A. thaliana* stem cuttings, in that the dominant products are toluene, ethylbenzene, and styrene. Unlike stem cuttings, the abundance of ethylbenzene and styrene was much higher in T87 cell pyrograms because excess phenylalanine in the media pyrolyzes to form ethylbenzene and styrene.

The pyrograms of Avicel® (cellulose) and post corn stover fermentation lignin were also compared to the pyrolysis of *A. thaliana* stem cuttings. Anhydrosugars, especially levoglucosan, were produced by pyrolyzing cellulose, while the levoglucosan peak, at a retention time of 26.30 minutes, was barely noticeable in both pyrograms of *A. thaliana* stem cuttings and T87 cells. Corn stover lignin after fermentation and filtration formed phenolic compounds after pyrolysis, such as guaiacol. However, guaiacol was rarely found in *A. thaliana* stem cuttings and T87 cell pyrolysis products. Among the pyrograms listed in Figure 3.9, T87 cell pyrograms were more similar to *A. thaliana* stem cuttings. Such similarity suggests that plant cell liquid culture can be used as a surrogate for whole plant tissue to conduct ^{13}C labeling studies.

Figure 3.9 reveals that the T87 cell pyrolysis results in aromatic hydrocarbons, some of which may be directly made from pyrolyzing excess phenylalanine. As the T87 cells were rinsed during harvesting, the residual phenylalanine mainly existed in the T87 cell cytosol as opposed to

the cell wall surface. To remove cytosolic phenylalanine, harvested T87 cells were ground by a mortar and pestle and rinsed again to remove the possible remaining phenylalanine. Approximately, 39.4 wt.% of cell mass was lost after drying the double rinsed T87 cells. Figure 3.10 represents the pyrograms of *A. thaliana* stem cuttings, T87 cells, and double-rinsed T87 cells. After rinsing away the soluble cytosol components, the aromatic hydrocarbon (toluene, ethylbenzene, and styrene) production from double rinsed T87 cells was significantly decreased versus the harvested T87 cells that were only rinsed once with no grinding to expose cytosolic compounds. Double rinsing T87 cells increased the similarity of *A. thaliana* stem cutting pyrograms and T87 cells. Therefore, double-rinsed T87 cells were used as the probe material for experiments. Figure 3.11 shows the double rinsed T87 cells pyrogram with ten important compound peaks. Peak identification is provided in Table 3.3 with retention time and the similarity value provided by the NIST library. Pyrolysis products of double rinsed T87 cells contained more heterocyclic amines, likely due to the high nitrogen composition as described previously. Small molecule products were mostly aldehydes, such as 2-methylpropanal, 3-methylbutanal and 2-methylbutanal. Phenol and methyl phenol were found in the pyrogram, while other phenolic compounds, like guaiacol, were not produced. Compared to single-rinsed T87 cells, levoglucosan is a main product after pyrolysis of double rinsed T87 cells. This implies that interactions may occur between soluble cytosol materials and cellulose that prevented the cellulose dehydration to form levoglucosan. Those important compounds, such as 3-methylbutanal, toluene, and phenol, were further analyzed based on mass spectra results under ^{13}C labeling studies to understand the reaction route in the pyrolysis of T87 cells.

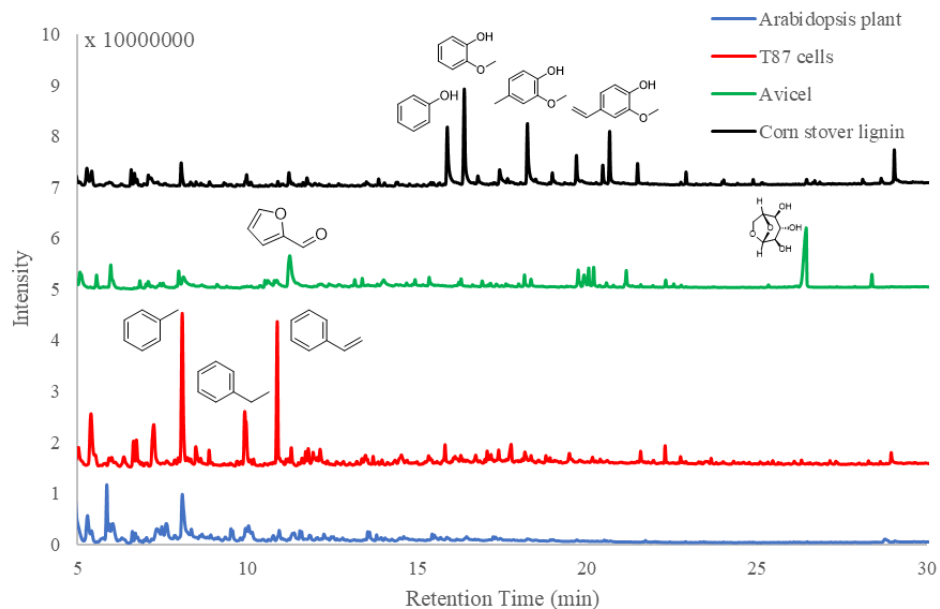


Figure 3.9 Pyrogram comparison between *A. thaliana* stem cuttings, T87 cells, Avicel® (cellulose), and lignin after fermentation of corn stover.

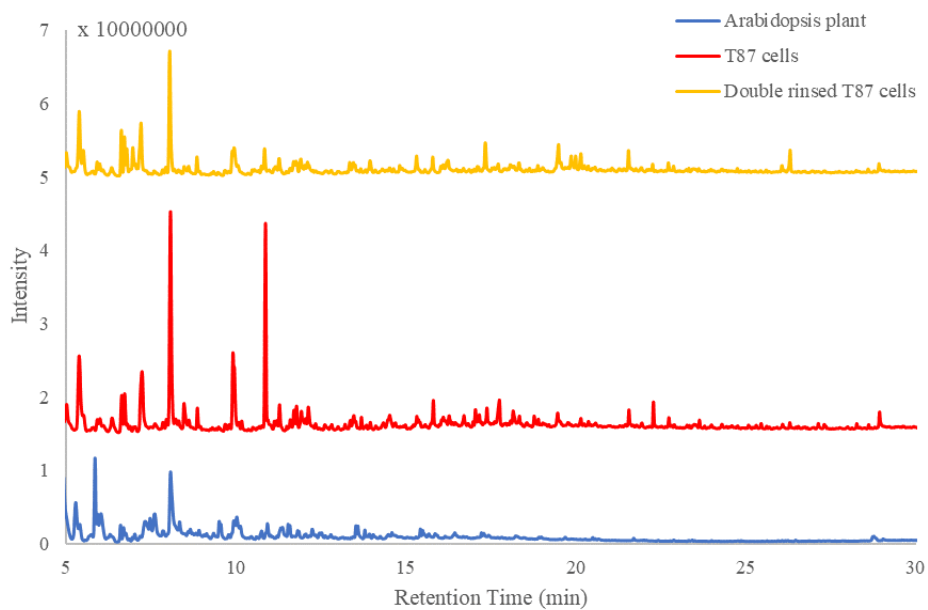


Figure 3.10 Pyrogram comparison between *A. thaliana* stem cuttings, T87 cells, and double rinsed T87 cells.

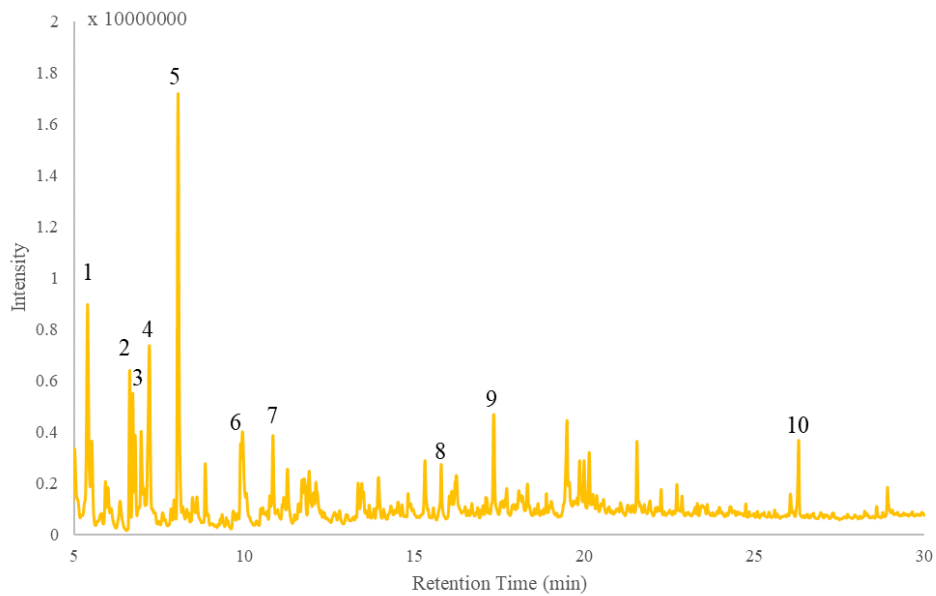


Figure 3.11 Double rinsed T87 cell pyrograms with important compounds identified by NIST library. 1: 2-Methylpropanal, 2: 3-Methylbutanal, 3:2-Methylbutanal, 4: Acetic acid, 5: Toluene, 6: Ethylbenzene, 7: Styrene, 8: Phenol, 9: 4-Methylphenol, 10: Levoglucosan.

Table 3.3 Double-rinsed T87 cell pyrolysis products identified using the NIST library.

No.	Retention time (min)	Compound	Similarity
1	5.01	Acetone	95
2	5.39	Propanal, 2-methyl-	89
3	5.51	Furan, 2-methyl-	94
4	5.92	2,3-Butanedione	93
5	5.95	2-Butanone	97
6	6.63	Butanal, 3-methyl-	95
7	6.72	Butanal, 2-methyl-	92
8	6.79	Furan, 2,5-dimethyl-	94
9	6.97	3-Buten-2-one, 3-methyl-	96
10	7.21	Acetic acid	97
11	8.05	Toluene	97
12	8.47	Pyridine	95
13	8.85	Butanenitrile, 3-methyl-	95
14	9.89	Ethylbenzene	91
15	9.95	Pyrrole	92
16	10.84	Styrene	97
17	11.11	Furfural	96
18	11.27	Pentanenitrile, 4-methyl-	90
19	11.70	1H-Pyrrole, 3-methyl-	92
20	11.76	L-Phenylalaninol	74
21	11.91	2-Pyrrolidinone, 1-methyl-	73
22	12.11	2-Propanone, 1-(acetyloxy)-	94
23	13.35	Cyclopentanone, 2-methyl-	82
24	13.46	Hexanal	79
25	13.95	Butane, 1-propoxy-	78
26	15.31	1,2-Cyclopentanedione, 3-methyl-	92
27	15.79	Phenol	97
28	16.24	2,5-Dimethyl-4-hydroxy-3(2H)-furanone	86
29	17.34	Phenol, 4-methyl-	96
30	19.49	3-Pyridinol	92
31	19.86	3,4-Anhydro-d-galactosan	76
32	19.99	2,3-Anhydro-d-mannosan	87
33	20.14	1,4:3,6-Dianhydro-.alpha.-d-glucopyranose	89
34	21.55	Indole	94
35	26.30	Levogluconan	95

3.4.4 Biomass fast pyrolysis using labeled T87 cells

Two methodologies were used to enrich T87 cells with isotopes: 1) T87 cells with labeled glucose and unlabeled phenylalanine to label cell wall carbohydrates, and 2) T87 cells with unlabeled glucose and labeled phenylalanine to label cell wall lignin. Experiments used substrates

that contained a labeled substrate fraction at three different levels: 20 wt.%, 50 wt.% and 100 wt.% of the entire substrate. Note, these fractions refer to the mass percentage of fully ^{13}C labeled substrate used in the experiments. The other steps of the two methodologies are identical. If one compound is partially or entirely labeled, the other is always unlabeled, i.e., if glucose is labeled, PHE is always unlabeled and vice versa. As shown in Figure 3.12, the pyrograms for the three different labeling levels were identical, showing no isotope effect in the GC results. As expected, the MS results in Figures 3.13-3.15 do vary depending on the type of labeled substrate and the labeled substrate level used in the medium.

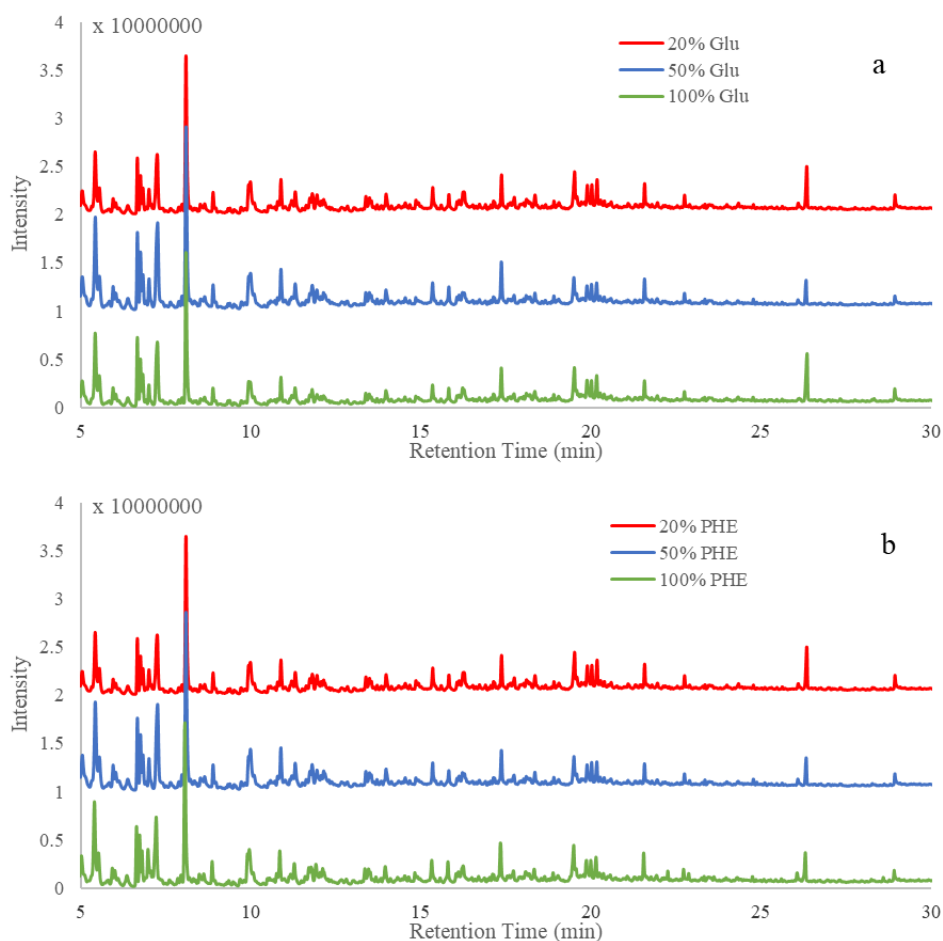


Figure 3.12 Results of T87 cell pyrolysis. (a) pyrogram of T87 cells with different glucose labeling fractions and unlabeled phenylalanine, (b) pyrogram of T87 cells with different phenylalanine labeling fractions and unlabeled glucose (all T87 cells were double rinsed).

3.4.5 Mass spectra of T87 cells

Mass spectra results were used to measure isotopic enrichment in the major products that were listed in Figure 3.11. T87 cells with labeled glucose showed isotopic enrichment (example in Figure 3.13b) in 3-methylbutanal, 2-methylbutanal, and negligible isotopes (example in Figure 3.14b) in toluene, ethylbenzene, styrene, and partial isotopes in phenol (example in Figure 3.15b). When phenylalanine was labeled, pyrograms show isotopic enrichment of toluene, ethylbenzene, and styrene (example in Figure 3.14c). Phenol produced from T87 with labeled phenylalanine was also partially labeled in Figure 3.15c.

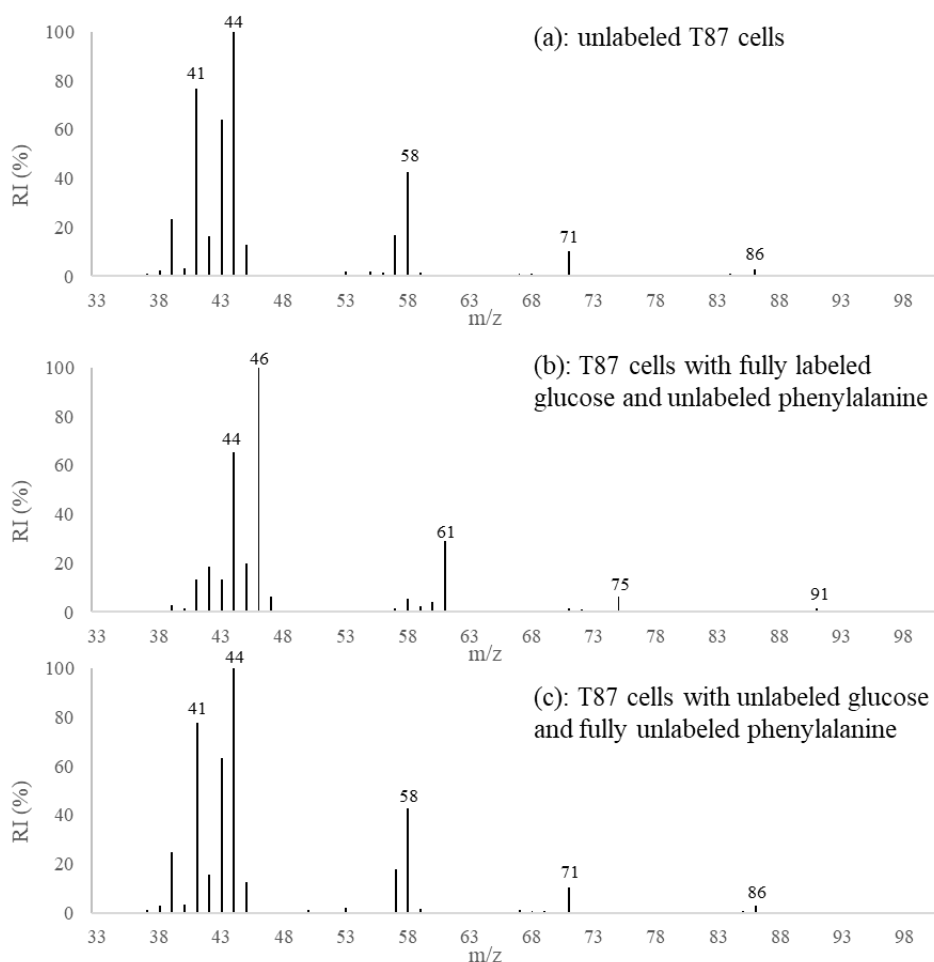


Figure 3.13 Mass spectra results of 3-methylbutanal: (a) unlabeled T87 cells, (b) T87 cells with fully labeled glucose and unlabeled phenylalanine, (c) T87 cells with unlabeled glucose and fully unlabeled phenylalanine. RI: relative intensity; m/z: mass to charge ratio.

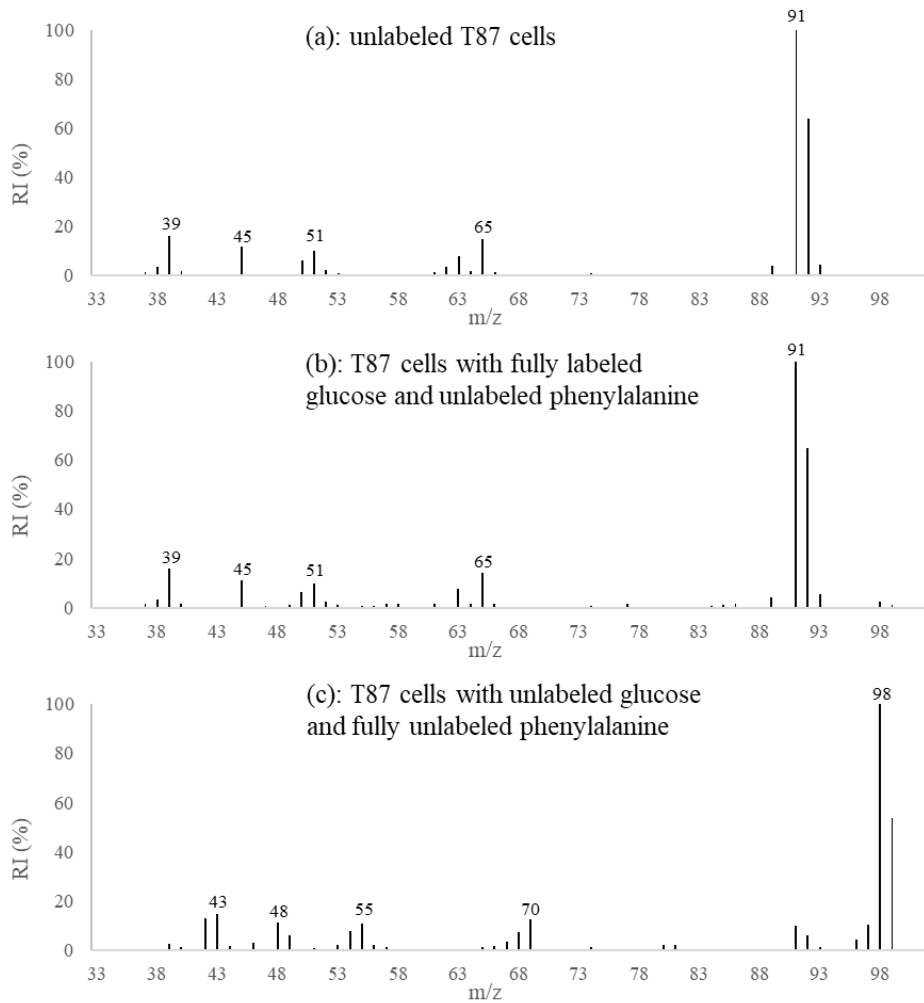


Figure 3.14 Mass spectra results of toluene: (a) unlabeled T87 cells, (b) T87 cells with fully labeled glucose and unlabeled phenylalanine, (c) T87 cells with unlabeled glucose and fully unlabeled phenylalanine. RI: relative intensity; m/z: mass to charge ratio.

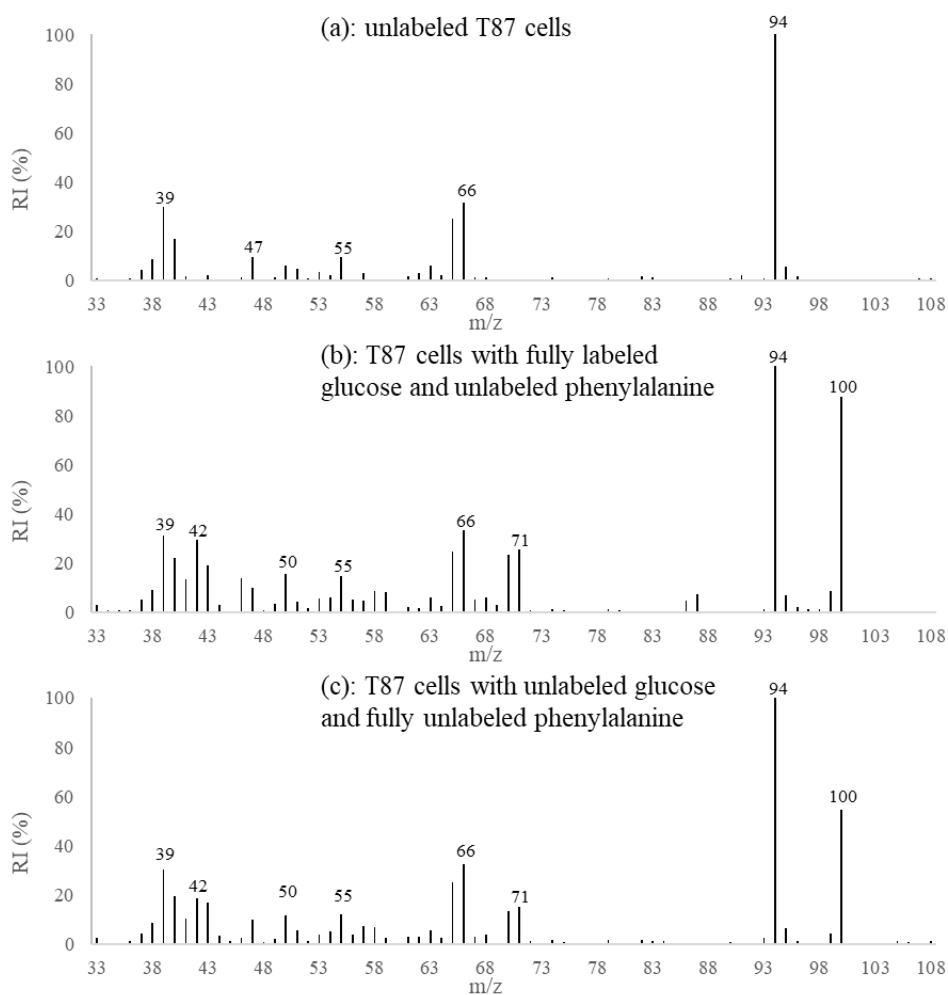


Figure 3.15 Mass spectra results of phenol: (a) unlabeled T87 cells, (b) T87 cells with fully labeled glucose and unlabeled phenylalanine, (c) T87 cells with unlabeled glucose and fully labeled phenylalanine. RI: relative intensity; m/z: mass to charge ratio.

3.4.6 ^{13}C distribution and possible pathways to the products during fast pyrolysis of T87 cells

Based on Figure 3.11 and the previous mass spectra results (Figure 3.13-3.15), the main products of biomass fast pyrolysis can be divided into three classes: 1) isotopic enrichment only observed with labeled glucose, 2) isotopic enrichment only observed with labeled phenylalanine, 3) isotopic enrichment found with either labeled glucose or labeled phenylalanine. After pyrolyzing different fractions of labeled material, the isotopic ratio of labeled carbon was calculated according to the mass spectra results.

Figure 3.16 represents the isotopic distribution of 3-methylbutanal formed by pyrolysis of unlabeled T87 cells and T87 cells with different labeling levels. Unlabeled T87 cells with a $6.12 \pm 0.86\%$ of M+1 isotopologue (Figure 3.16) results because the natural abundance of ^{13}C is about 1.11 wt.% and 3-methylbutanal has five carbons that leads to its M+1 isotope level of 5.55%. From comparison to its natural abundance, 3-methylbutanal was only sparingly made from labeled phenylalanine. Contrastingly, 88.81% of 3-methylbutanal was fully labeled when all glucose in the media was labeled. In addition, about 9% of 3-methylbutanal was unlabeled because the T87 cell culture was started using 10 ml of liquid culture from a previous trial that was unlabeled. This starter culture was mixed with 40 ml of new medium containing fully labeled glucose. When the glucose labelling level increased, the 3-methylbutanal labelling level also increased. Interestingly, all five isotopes of 3-methylbutanal were nearly equally distributed when feeding the T87 cells 50% labeled glucose. This implies that 3-methylbutanal is not directly formed through glucose decomposition. Instead, glucose is first decomposed, or catabolized, to light molecules, which are then recombined to form 3-methylbutanal. Therefore, the proposed reaction routes were presented in Figure 3.17 proposes a reaction route where leucine, formed from pyruvate that was derived from glucose,[93] serves as an intermediate to 3-methylbutanal. In Figure 3.17A, deamination converts the amino group to a methyl radical, which then reacts to form 3-methylbutanal.[94] A second proposed pathway (Figure 3.17B) is the Strecker degradation that occurs between a dicarbonyl group and an amino acid to form flavor-active aldehydes.[95] In the Strecker degradation, leucine reacts with a sugar that is subsequently decarboxylated and then deaminated to generate 3-methylbutanal.[96] Carbon flow through these proposed pathways can explain the isotope distribution observed by the T87 cell labeling studies, though further interrogation of these reaction is warranted. The same trend in isotope distribution was observed in other light

to the isotopic ratio of 3-methylbutanal, the result was not evenly distributed for the isotopologues. Most of the isotopologues were M+6 and M+7, indicating that the aromatic ring was not opened by pyrolysis. The sum of M+6 and M+7 composition was over 80% when fully labeled phenylalanine was added into the media. As stated previously, 20 vol% of the liquid media was from the previous trial, which contained only unlabeled carbon, resulting in an unlabeled toluene level of 13% when pyrolyzing T87 cells with fully labeled phenylalanine. Only about 2% of fully labeled toluene was found in the pyrogram of T87 cells grown with 100% labeled glucose. This indicates that the biosynthetic pathway from glucose to phenylalanine was not entirely blocked. Proposed reaction pathways from lignin to toluene or ethylbenzene are illustrated in Figure 3.19, which starts with a lignin dimer containing a β -aryl ether linkage to serve as a lignin model. If the R group on C_α is a hydroxy group in Pathway (A), oxidation of C_α -OH to ketone is the first step. Wang et al. investigated that the C_α - C_β bond in β -O-4 ketone was weaker than in β -O-4 alcohol.[97-100] C_α - C_β cleavage followed by C-O cleavage resulted in the formation of benzoic acid, which was then reduced to benzyl alcohol. Toluene can be generated by further reduction. Pathway (B) shows a typical C_β -O cleavage as studied by many researchers.[101-104] Both Huang and Shen calculated the bond dissociation energies of possible pyrolysis paths of the β -O-4 lignin dimer model and concluded that the bond dissociation energy of C_β -O was the lowest. When the R group on C_α is hydroxyl, the model compound can decompose into two radicals. The radical containing the phenylpropane unit of the dimer is converted to 1-phenylpropane-1,3-diol by receiving a proton and removing the side chains through demethoxylation. 1-Phenylpropane-1,3-diol then undergoes dehydration, rearrangement, and decarbonylation to form ethylbenzene. The other aromatic hydrocarbon products in BFP pyrograms follow a similar trend in isotope distribution, illustrating that ethylbenzene and styrene are lignin derived.

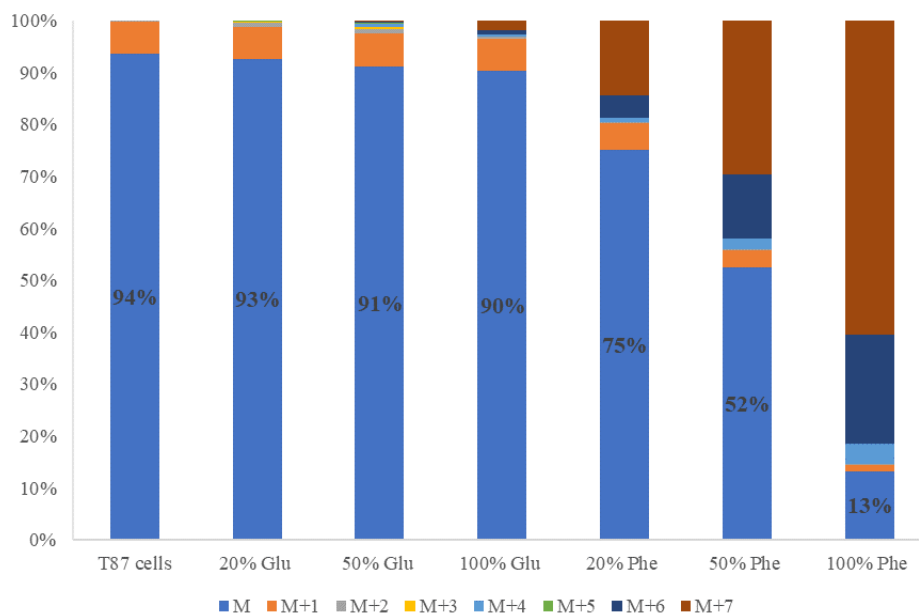


Figure 3.18 ^{13}C distribution of toluene in T87 cells with different labeling strategies after BFP indicating that toluene is lignin derived.

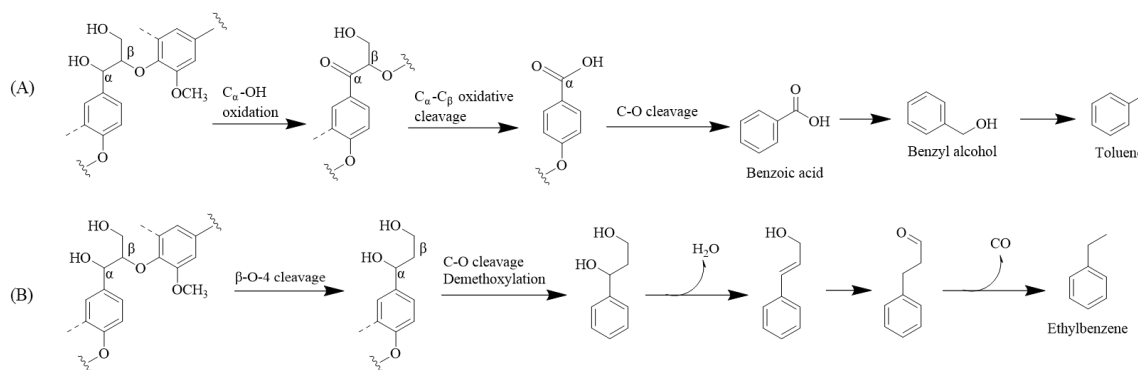


Figure 3.19 Proposed reaction pathway from β -aryl ether linkage to toluene. (A) C_α oxidation followed by C-C oxidative cleavage to form toluene. (B) $\text{C}_\beta\text{-O}$ cleavage to form toluene if R group on C_α is -OH.

As presented in Figure 3.20, phenol appears to be made by either labeled substrate, although by different routes. From the isotope distribution trends, the phenol from labeled phenylalanine formed by bond scissions and not ring opening, while phenol from glucose formed after glucose decomposition into small hydrocarbon fragments. The abundance of M+6 phenol by

T87 cells when feeding fully either labeled glucose and phenylalanine was 51% and 27%, respectively. As levoglucosan, furfural, 2-methyl-cyclopentanone, and methylphenol were observed in the pyrogram, a possible reaction route including these molecules is proposed for cellulose to phenol in Figure 3.21. Zhang et al. proposed a similar reaction route and indicated that 2-methyl-2-cyclopentene-1-one, was the most important intermediate during the phenol formation,[105] though the pyrolysis reactions from Zhang's article were catalyzed by phosphoric acid-activated carbon. Although this work does not include catalytic fast pyrolysis, MS salts contain metals such as K, Ca, Mg and Fe^{2+} , that when absorbed by T87 cells can catalyze reactions.

According to Figure 3.20, phenol can also be formed from lignin. Possible reaction pathways were proposed in Figure 3.22. Pathway (A) shows the $\text{C}_\beta\text{-O}$ cleavage reaction mentioned previously. As S-type lignin monomer was not detected in thioacidolysis of T87 cells, a guaiacol-like molecule is first converted when the radical absorbs a proton, after which phenol is then formed by a demethoxylation reaction. Pathway (B), introduced by Yan et al., generates phenol by directly deconstructing the aryl C-C bond and $\text{C}_\beta\text{-O}$ bond. Aryl C-C bond breakage was catalyzed by a zeolite via dihydroxylation, γ -methyl shift, and C-C β scission under mild conditions. In this reaction sequence, $\text{C}_{\text{sp}2}\text{-C}_{\text{sp}3}$ cleavage occurs above 400 °C, a possibility noting that the pyrolysis temperature in this work is about 550 °C, so Pathway (B) is a possible reaction route to form phenol from lignin.

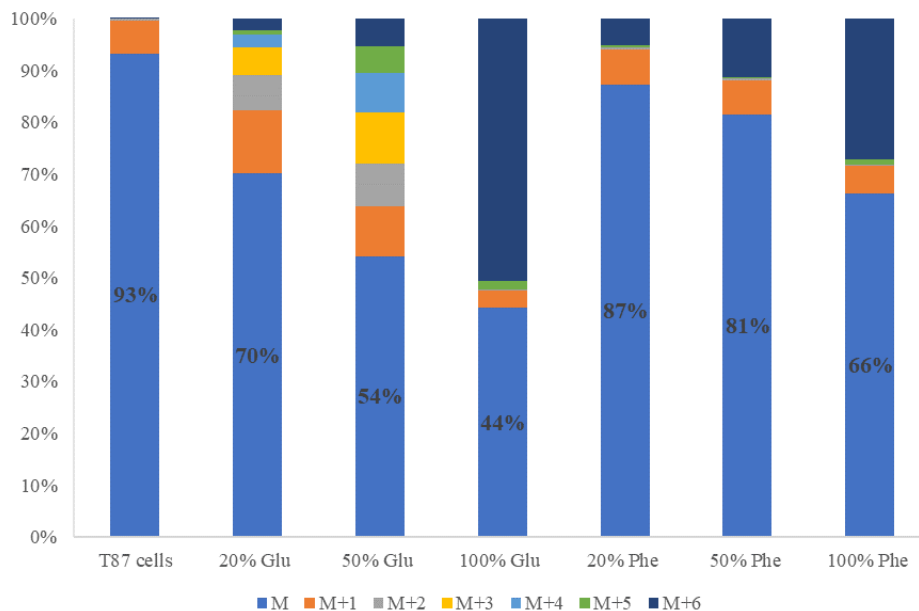


Figure 3.20 ^{13}C distribution of phenol in different T87 cells with different labeling strategies after BFP indicated that phenol was produced by both carbohydrates and lignin.

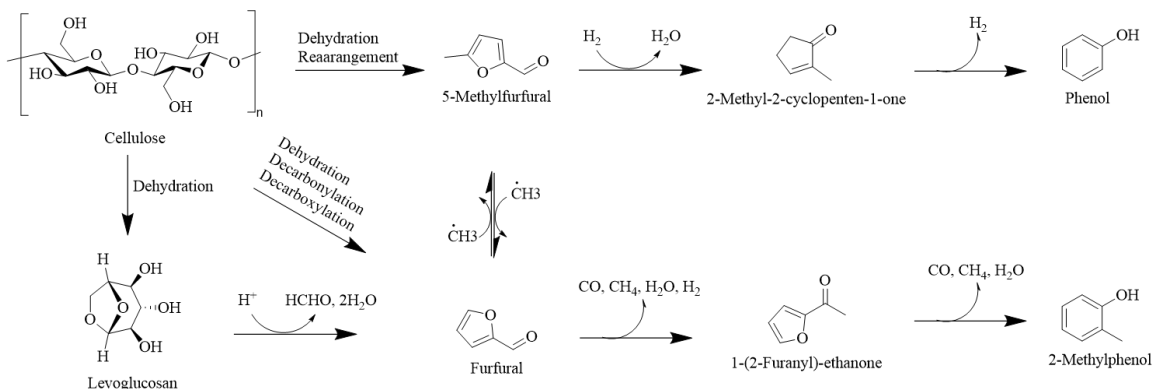


Figure 3.21 Proposed reaction pathway from cellulose to phenol.

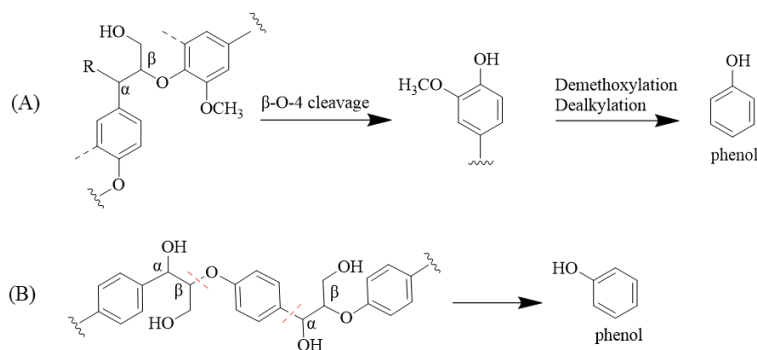


Figure 3.22 Proposed reaction pathway from β -aryl ether linkage to phenol. (A) C_{β} -O cleavage followed by demethoxylation and dealkylation to remove the side chains. (B) Direct bond scission of a C-C bond and a C_{β} -O bond to form phenol.[106]

3.5 Conclusion

Methodologies were developed to preferentially label *A. thaliana* cell culture by feeding ^{13}C -containing biosynthetic precursors (glucose for carbohydrate and phenylalanine for lignin). NREL compositional analysis confirms that cell wall mass content increases when T87 cells are grown on the liquid media with added phenylalanine. Adding phenylalanine promotes cell wall formation, especially the lignin fraction, which was observed through phloroglucinol-hydrochloric acid staining. Thioacidolysis of the dried T87 cells detects 376 $\mu\text{g/g}$ of guaiacyl lignin and 197 $\mu\text{g/g}$ of hydroxyphenyl lignin. A second rinsing procedure was necessary to remove the residual cytosolic phenylalanine to improve the use of labelled T87 cells and cell wall models. Reaction mapping studies, performed on plant cell cultures with preferential fiber labeling, can reduce the cost and time needed to investigate heat catalyzed transformations. Upon analyzing partially labeled materials with varying label levels, most aldehydes are derived from holocellulose while the monoaromatic hydrocarbons generally form from lignin after BFP. Interestingly, phenol was produced by both holocellulose and lignin, not lignin alone. Increasing reaction yields from holocellulose and lignin might establish a viable pathway to phenol, which is a valuable

commodity chemical. This labeling methodology, using plant cell culture, can ultimately be used to improve feedstock selection for conversion strategies like BFP.

CHAPTER 4. MAPPING REACTION PATHWAYS OF CATALYTIC FAST PYROLYSIS USING ISOTOPICALLY LABELED PLANT CELL CULTURE

4.1 Abstract

Prior research (Chapter 3) developed a methodology to investigate biomass fast pyrolysis reaction pathways using ^{13}C labeled T87 cells. In the present chapter, this methodology was applied to study the reaction pathways of catalytic fast pyrolysis. HZSM-5 with a silicon-to-alumina ratio of 23:1 was selected to catalyze pyrolysis at 650 °C. A catalyst-to-biomass ratio of 5:1 was used during catalytic pyrolysis. Pyrolysis was performed in a pyroprobe, sending the vapor products to a GC/MS for analysis. ^{13}C distribution results confirm that the reaction pathway from carbohydrate to BTEX began with decomposition reactions to form a “hydrocarbon pool” and then produce BTEX. Contrastingly, the reaction pathway from lignin to BTEX was more likely by side-chain cleavage. Carbohydrates form all BTEX products, while lignin primarily leads to benzene while making almost no xylene.

4.2 Introduction

As global warming rates accelerate, the demand for sustainable energy resources increases. Photosynthetic biomass, a well-known renewable source, is broadly appealing for green energy production due to wide availability and low price.[107] Various applications to convert biomass into energy have been investigated through either thermochemical or biochemical processes.[108] Biomass fast pyrolysis (BFP) is one promising technique that makes “bio-oil” as a main product by heating the biomass without oxygen.[28] Bio-oil is a complex mixture including hundreds of organic compounds, such as alcohols, ketones, aldehydes, and phenols.[109] However, these compounds are undesirable because of high oxygen content, high water content, low energy

content, and high acidity.[110] Thus, catalytic upgrading is necessary prior to bio-oil's application as an energy intermediary.

Catalytic fast pyrolysis (CFP) integrates fast pyrolysis and catalysis to obtain valuable chemicals either *in situ* or *ex situ* formats. Wang et al. concluded that *ex situ* CFP makes more olefins and less aromatic hydrocarbons than *in situ* CFP.[111] Zeolites, especially ZSM5, are commonly used by CFP to make aromatic hydrocarbon because of ideal pore structure and acidity.[112, 113] Kelkar et al. compared the CFP performance of HZSM-5 with different silicon-to-alumina ratios (SAR) and concluded that low SAR resulted in strong acidity that leads to lighter monoaromatic hydrocarbons.[45]

The main components in lignocellulosic biomass, cellulose, hemicellulose, and lignin, are initially depolymerized and decomposed during catalytic pyrolysis. Next, the volatile products are deoxygenated to form hydrocarbons.[114] Both cellulose and hemicellulose are polysaccharides accounting 30-55 wt.% and 25-30 wt.% of dry biomass, respectively.[115] Compared to cellulose, consisting of a linear chain of glucose, hemicellulose is a branched amorphous polymer composed of various C5 and C6 sugars. Lignin, constituting 25-30 wt.% of biomass, is a much different polymer that is highly branched and derived from three monolignols (coumaryl, coniferyl and sinapyl alcohol).[116] Many researchers have investigated catalytic pyrolysis of individual biomass components with ZSM-5 catalyst.[39, 117, 118] Srinivasan et al. observed that the aromatic yield from CFP of cellulose was about 17 wt.% at 600°C (carbon yield).[117] Wang et al. reported that the carbon yields of aromatics from cellulose, hemicellulose and lignin CFP were 28.8%, 19.4%, and 7.4% at 600°C, respectively.[39] They also observed no significant interaction among the three cell wall components when pyrolyzing switchgrass. Meanwhile, Mullen et al. found an equal conversion of cellulose and lignin to aromatic hydrocarbons during CFP.[118] These three studies

used HZSM-5 catalyst via a micro-pyrolyzer-GC/MS system for experiments. In addition, some researchers presented that there existed interaction when pyrolyzing the mixture.[119, 120] Wu et al. indicated that the formation of levoglucosan was inhibited due to the interactions between cellulose and lignin.[119] Liu et al. concluded that the interactions among biomass components were significant. Lignin decreased the production of 2-furaldehyde and C=O containing compounds, while hemicellulose decreased the yield of levoglucosan, and enhanced the formation of hydroxyacetaldehyde.[120] The different behavior reveals a lack of knowledge to catalytic pyrolysis mechanisms.

The goal of this study is to map the reaction pathways of catalytic fast pyrolysis for a better understanding of how the cell wall components react during CFP. Our prior research developed a methodology using ^{13}C labeled *Arabidopsis* cell (T87 cell) culture as a surrogate for investigating BFP reaction pathways, while this work uses CFP. As with the BFP study, different T87 cells with preferentially labeled fractions (carbohydrate or lignin) were used in this investigation. T87 cells grown with labeled substrates preferentially labeled holocellulose or lignin cell wall components, allowing for the interaction affects during CFP to be observed. Monoaromatic hydrocarbons, such as benzene, toluene, ethylbenzene, and xylenes (BTEX), were mainly analyzed as they are important industrial chemicals that can be used as gasoline additives, solvents, and in leather industry.

4.3 Methods and Materials

4.3.1 ^{13}C labeled T87 cells

The methodology to preferentially label cell wall fraction of T87 cells was introduced in Chapter 3. The same procedure was applied to this study. Briefly, T87 cells from *A. thaliana* Columbia plants, were routinely grown in liquid media with glucose (30 g/l), and phenylalanine

(5 g/l). Ten milliliters of liquid culture from a previous trial were transferred into 40 ml of fresh media. The cells were incubated at 21 °C with a speed of 140 rpm in darkness for a week. The cells were then harvested by filtration and dried at 60 °C overnight. By comparing the pyrograms for T87 cells and *Arabidopsis* plant, it was assumed that residual phenylalanine in the T87 cell cytosol was the precursor to toluene, ethylbenzene, and styrene. To remove this phenylalanine, harvested cells were ground and double-rinsed again to obtain a higher similarity of pyrolysis performance to whole *Arabidopsis* plants. Double rinsed T87 cells were then filtered and dried prior to the experiments.

4.3.2 Sample preparation and py-GC/MS settings

Commercial NH_4^+ ZSM-5 catalyst with SAR 23 were brought from Zeolyst Co. (Conshohocken, PA). Original ZSM-5 is in ammonium cation form and needs to be calcined at 550 °C for 4 hours to convert it into HZSM-5. The prepared zeolite catalyst was well mixed with each type T87 cells (T87 cells, T87 cells feeding with 20, 50 and 100 wt.% ^{13}C labeled glucose, and T87 cells feeding with 20, 50 and 100 wt.% ^{13}C labeled phenylalanine) with a ratio of 5:1. Approximately, 3 mg of mixed samples (~0.5 mg of cells and ~2.5 mg of catalyst) was covered by quart wool and filled into a quartz tube with a filler rod. Then, the packed sample was injected into the py-GC/MS (Proprobe 5250, CDS Analytical Inc, PA, QP-5050A, Shimadzu Corp, MD) for further analysis. Three replicates of each sample were tested. Py-GC/MS settings were the same as described in Chapter 3. Briefly, the pyroprobe holds the sample for 20 seconds in the chamber at 650 °C and the heating rate is 999 °C/s. The vapors produced in the pyroprobe was blew into GC/MS by a helium stream through a transfer line at 300 °C. A Restek rtx-1701 column (60m \times 0.25mm \times 0.25 μm) was applied for the separation. The column gas flow rate was 1 cm^3/s with a split ratio of 100, The GC oven was initially at 40 °C and was heated with a heating rate of 8 °C/min

after the first minute. Once the oven temperature reached 270 °C, the temperature was kept for 10 more minutes. The products were identified by the 2005 NIST library.

4.4 Results and Discussion

4.4.1 Pyrolysis-GC/MS results and a comparison between BFP with CFP of T87 cells

Unlabeled T87 cells were pyrolyzed with and without HZSM-5 to compare biomass fast pyrolysis to catalytic fast pyrolysis (Figure 4.1). The products during BFP of T87 cells were dominantly light oxygenated molecules, toluene, and levoglucosan, while aromatic hydrocarbons were the main products during CFP. The compounds observed by T87 cell CFP are listed in Table 4.1 as identified by the 2005 NIST library. The retention times for the three xylene isomers were verified by injecting pure standards in GC/MS. The largest peak, at a retention time of 10.1 minutes, was a mixture of *p*-xylene and *m*-xylene owing to similar boiling points. Because of high instrument responses and interest in them as valuable products, monoaromatic hydrocarbons were analyzed to probe their reaction pathways.

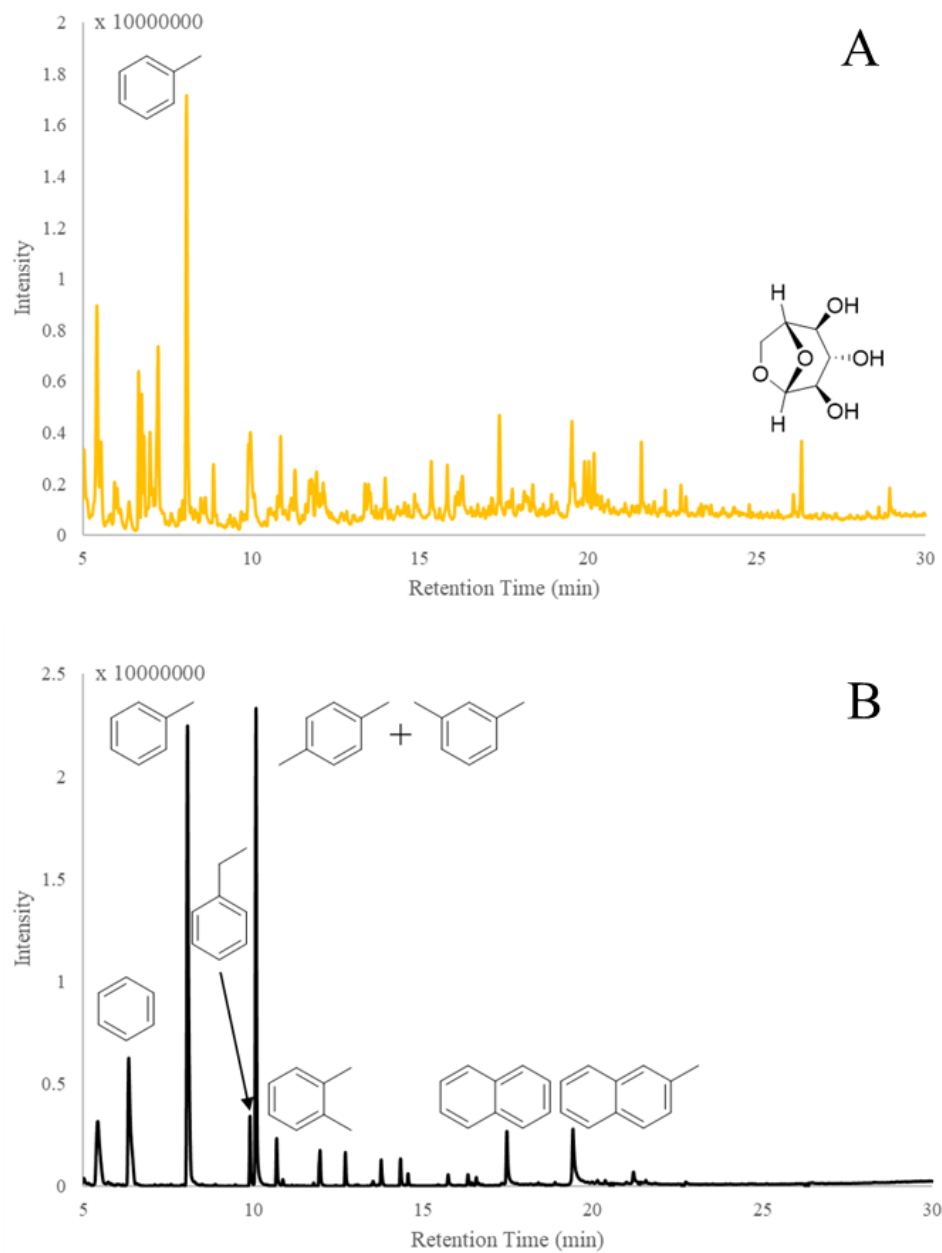


Figure 4.1 Pyrogram comparison of T87 cell with no catalyst (A) and HZSM-5 (B).

Table 4.1 Catalytic pyrolysis products from double rinsed T87 cells pyrogram identified by NIST library.

No.	Retention time (min)	CompoundName	Similarity
1	5.43	Acetonitrile	98
2	6.34	Benzene	98
3	8.07	Toluene	97
4	9.91	Ethylbenzene	98
5	10.08	p-Xylene/m-Xylene	98
6	10.69	o-Xylene	97
7	11.97	Benzene, 1-ethyl-2-methyl-	97
8	12.71	Benzene, 1,2,3-trimethyl-	97
9	13.77	Indane	96
10	14.34	Indene	97
11	14.56	1H-Indene, 2,3-dihydro-2-methyl	93
12	15.74	1H-Indene, 2,3-dihydro-5-methyl-	88
13	16.32	1H-Indene, 1-methyl-	95
14	17.47	Naphthalene	99
15	19.41	Naphthalene, 2-methyl-	93

4.4.2 Mass spectra of T87 cells

Three levels of labeled substrates (20 wt%, 50 wt.%, and 100 wt.%) were used to label T87 cells. A total of seven types of T87 cells were applied to this study: unlabeled T87 cells and labeled T87 cells containing 20% Glu, 50% Glu, 100% Glu, 20% Phe, 50% Phe, and 100% Phe. “T87 cells” in the figures refer to unlabeled T87 cell, while “20% Glu” contains T87 cells grown in a media with 20 wt.% labeled glucose and unlabeled phenylalanine.

Mass spectra results were initially compared for three types of T87 cells (unlabeled, with fully labeled glucose and unlabeled phenylalanine, and with unlabeled glucose and fully labeled phenylalanine). Examples of mass spectra for benzene, toluene, and m- and p-xylene are presented in Figures 4.2-4.4, each showing the results for unlabeled, 100% Glu-labeled, and 100% Phe-labeled experiments. T87 cells with fully labeled glucose and unlabeled phenylalanine (100%-Glu T87 cells) displayed a ^{13}C enrichment in all three products (Figure 4.2b, 4.3b, and 4.4b). The isotope enrichment in 100%-Glu T87 cells follows the order: benzene < toluene < the mixture of

p-xylene and *m*-xylene (Figure 4.2, 4.3, 4.4b). However, T87 cells with unlabeled glucose and fully labeled phenylalanine (100%-Phe T87 cells) show a reversed order compared to 100%-Glu T87 cells, with almost no labeled xylene mixture observed in 100%-Glu T87 cells. Even in mass spectra of benzene, 100%-Glu T87 cells have much less ^{13}C labeled product than 100%-Glu T87 cells. The other two important peaks (ethylbenzene and *o*-xylene) were not listed, but the same trend was found as in toluene and the xylene mixture, respectively.

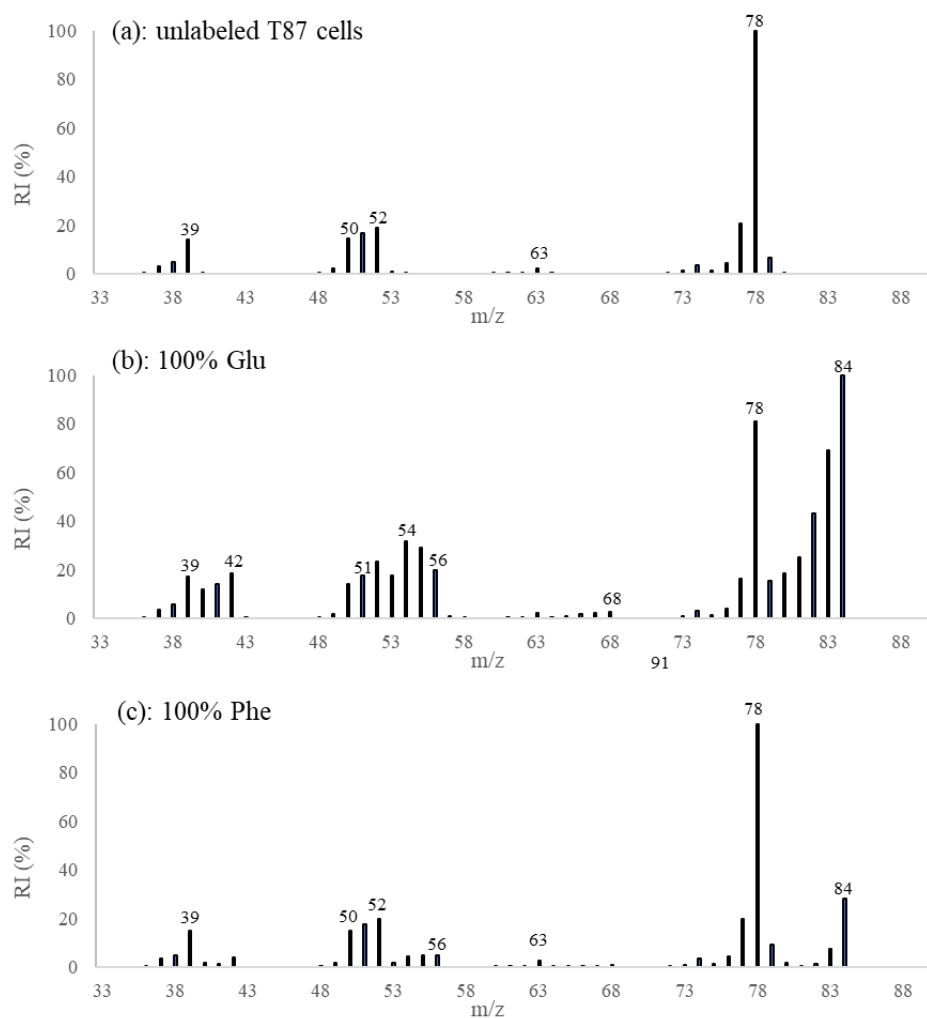


Figure 4.2 Mass spectra results of benzene during CFP: (a) unlabeled T87 cells, (b) T87 cells with fully labeled glucose and unlabeled phenylalanine, (c) T87 cells with unlabeled glucose and fully labeled phenylalanine. RI: relative intensity; m/z: mass to charge ratio.

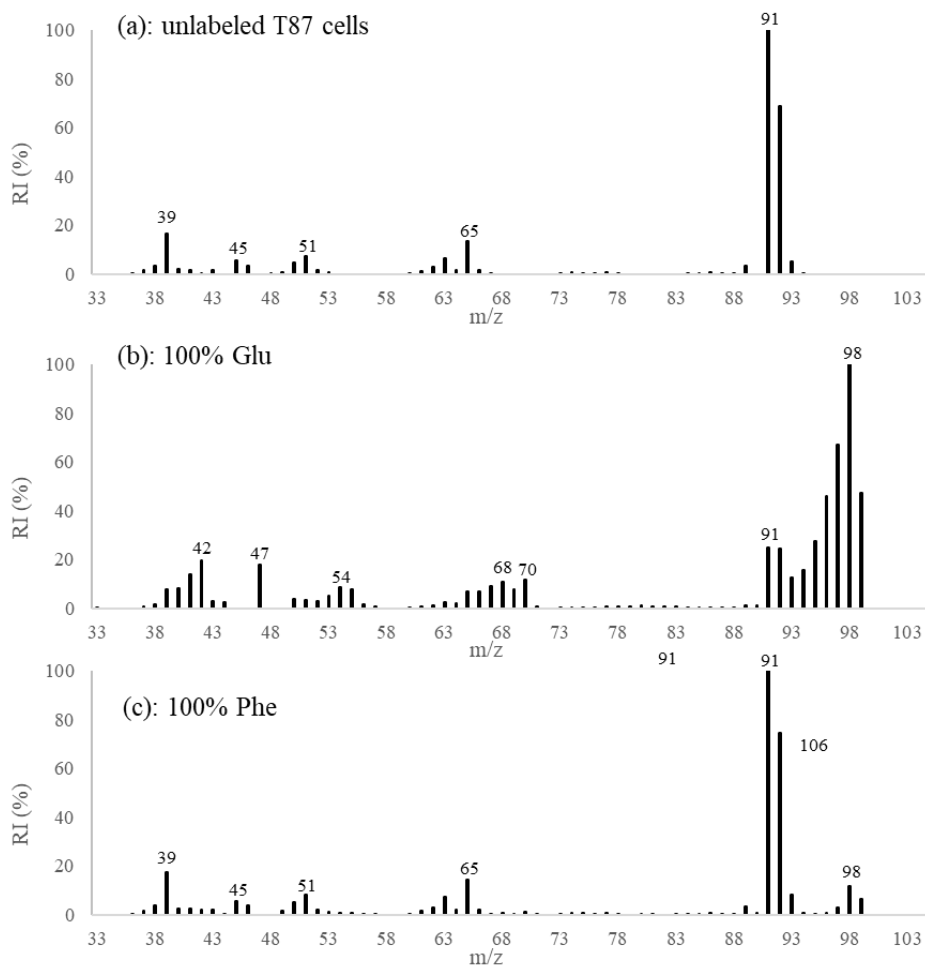


Figure 4.3 Mass spectra results of toluene during CFP: (a) unlabeled T87 cells, (b) T87 cells with fully labeled glucose and unlabeled phenylalanine, (c) T87 cells with unlabeled glucose and fully labeled phenylalanine. RI: relative intensity; m/z: mass to charge ratio.

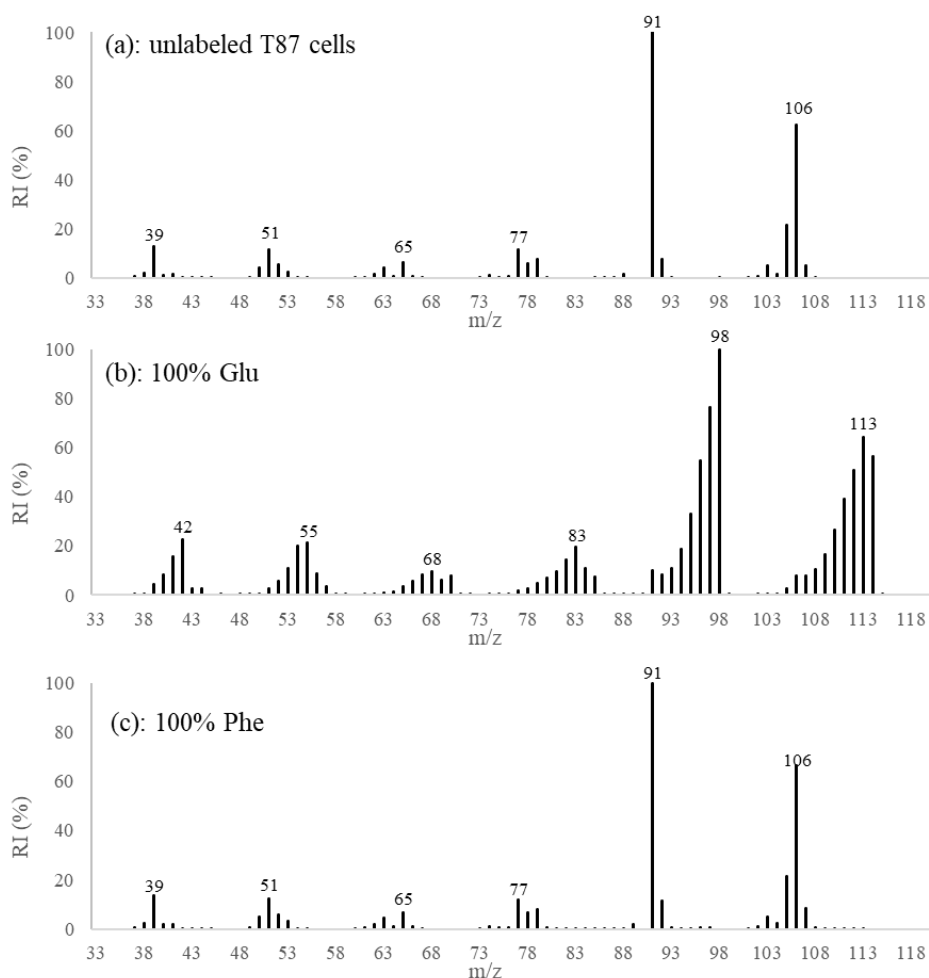


Figure 4.4 Mass spectra results of the mixture of *p*-xylene and *m*-xylene during CFP: (a) unlabeled T87 cells, (b) T87 cells with fully labeled glucose and unlabeled phenylalanine, (c) T87 cells with unlabeled glucose and fully labeled phenylalanine. RI: relative intensity; m/z: mass to charge ratio.

4.4.3 ^{13}C distribution and possible pathways to the products during fast pyrolysis of T87 cells

The ^{13}C distribution analysis of mass spectra results is shown in Figures 4.5-4.7. As seen in the ^{13}C distribution for benzene, only 20% M+6 benzene was produced when pyrolyzing T87 cells by feeding with fully labeled phenylalanine, while 26% of the total benzene was unlabeled during CFP of T87 cells grown with fully labeled glucose. The difference in these values results from routine cultivation that starts with a seed stock of unlabeled T87 cells that is transferred into the media containing labeled feedstocks. The first column in Figure 4.5, for unlabeled T87 cells,

shows that 6% of the benzene contains an M+1 label, which is caused by 1.11 wt.% of ^{13}C natural abundance.

Regarding aromatic compounds, the amount of labeled benzene increased significantly when the amount of labeled phenylalanine was increased in the media. Even when only 20% labeled phenylalanine was added into the media, the M+6 isotopologue remained the most abundant isomer for labeled benzene while the other isotopologues were barely observed. This trend is also found in the ^{13}C distribution of toluene, ethylbenzene, and xylenes as seen in Figures 4.6-4.8. The dominance of the M+6 or higher isotopologue reveals that the aromatic ring of phenylalanine was not broken as lignin was formed and then subsequently converted to benzene. The reaction pathways from lignin to monoaromatics first proceeds by side chain removal. As in previous work, aromatic product selectivity is a function of the internal pore size of ZSM-5 catalysts. Jae et al. reported that ZSM-5's internal pore diameter was 6.36 Å.[41] Choudhary et al. found that the kinetic molecular sizes of benzene, toluene, ethylbenzene, *p*-xylene, *o*-xylene and *m*-xylene at 308 K were 5.9 Å, 6.1 Å, 6.7 Å, 6.7 Å, 7.1 and 7.4 Å, respectively.[121] Though the pore size is slightly smaller compared to the aromatics' molecular sizes, molecules can still enter pores owing to ZSM-5's pore size variability. Even so, larger BTEX molecular size likely leads to transport limitations through the catalyst, a view consistent with the observed ^{13}C distribution of benzene, toluene, and ethylbenzene, which are likely formed from small molecules derived from carbohydrate pyrolysis.

The amount of highly labeled BTEX grew with the rising amount of labeled glucose to a greater degree than with labeled phenylalanine. However, a significant amount of smaller isotopologues (M+1, M+2, and M+3) were generated versus using labeled phenylalanine. This indicates that the reaction pathways from carbohydrate to BTEX is an aromatic ring formation

process by light olefin molecules, which is consistent with the formation of a “hydrocarbon pool” made by decomposition, decarbonylation, and decarboxylation of cellulose, hemicellulose, and lignin.[111, 118, 122] Interaction between carbohydrates and lignin likely occurs in this hydrocarbon pool, as evidenced by ^{12}C in BTEX when pyrolyzing T87 cells with fully labeled glucose, which may be explained by alkyl group excision from lignin. Finally, a proposed reaction pathway during CFP was demonstrated in Figure 4.10.

By considering the mass fraction of cell wall components (Table 3.2) and the distribution of BTEX production of T87 cells during catalytic pyrolysis (Figure 4.5-4.8), aromatic production per mass could be calculated using Equation 1 and 2:

$$\text{BTEX production from carbohydrates} = \frac{\sum_{i=1}^a (M + i) * \frac{i}{a} - M * 1.11\%}{(\text{Glucan} + \text{Xylan})\text{wt.}\%} \quad (1)$$

$$\text{BTEX production from phenylalanine} = \frac{\sum_{i=6}^a M + i}{\text{Lignin wt.}\%} \quad (2)$$

where, i represents the number of labeled carbons, a is the total carbons in the molecule, and $M+i$ is the relative fraction of the isotopmer $M+i$. As the possible proposed reaction pathways described above, BTEX production from carbohydrates is computed by adding up the labeled carbon from each isopomer. BTEX production from phenylalanine only counts the $M+6$ or higher isotopmers as the aromatic ring does not break. The overall information is summarized in Table 4.2. As the molecular size of BTEX increases, the production from lignin decreases due to the difficulties absorbing into the pores of catalyst.

Table 4.2 BTEX production from carbohydrates and phenylalanine per mass compared to their kinetic molecular sizes.

Compound	Kinetic molecular size (Å)	Relative production from carbohydrates	Relative Production from phenylalanine
Benzene	5.9	1	1.09
Toluene	6.1	1	0.51
Ethylbenzene	6.7	1	0.38
<i>p</i> -Xylene	6.7	1	0.04
<i>m</i> -Xylene	7.1	1	0.04
<i>o</i> -Xylene	7.4	1	0.05

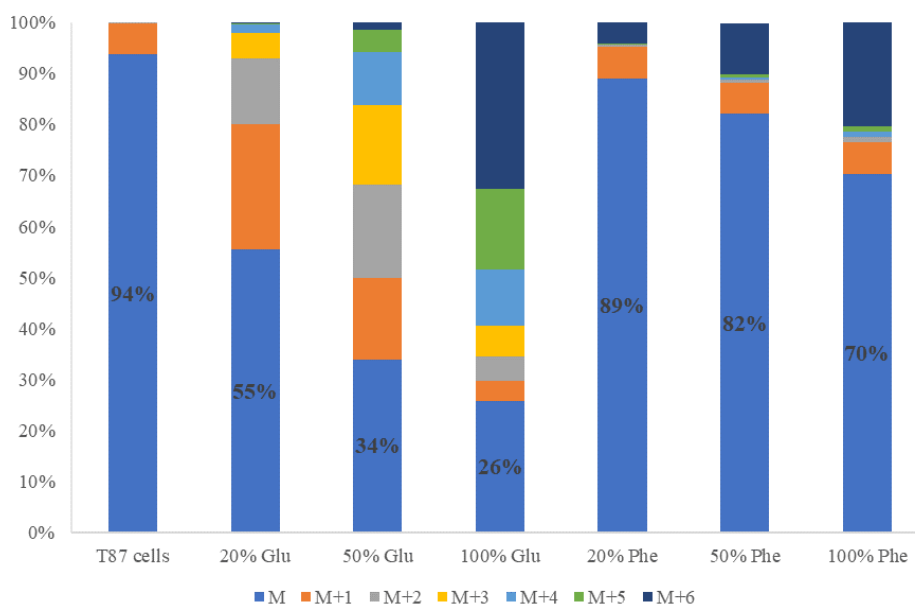


Figure 4.5 ¹³C distribution of benzene in T87 cells with different labeling strategies after CFP indicating that more benzene is derived from carbohydrate than from lignin.

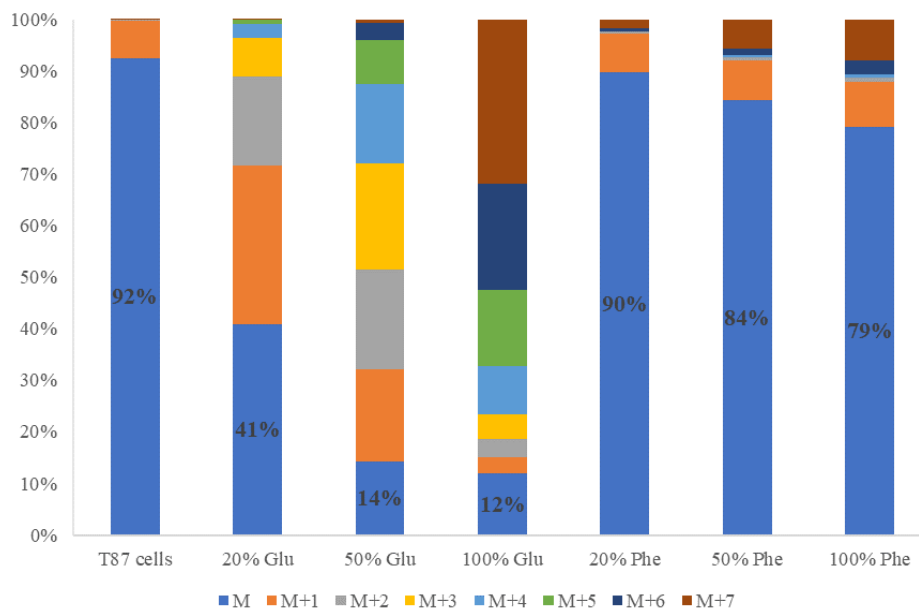


Figure 4.6 ^{13}C distribution of toluene in T87 cells with different labeling strategies after CFP indicating that only a few toluene is derived from lignin and the rest is formed by carbohydrate.

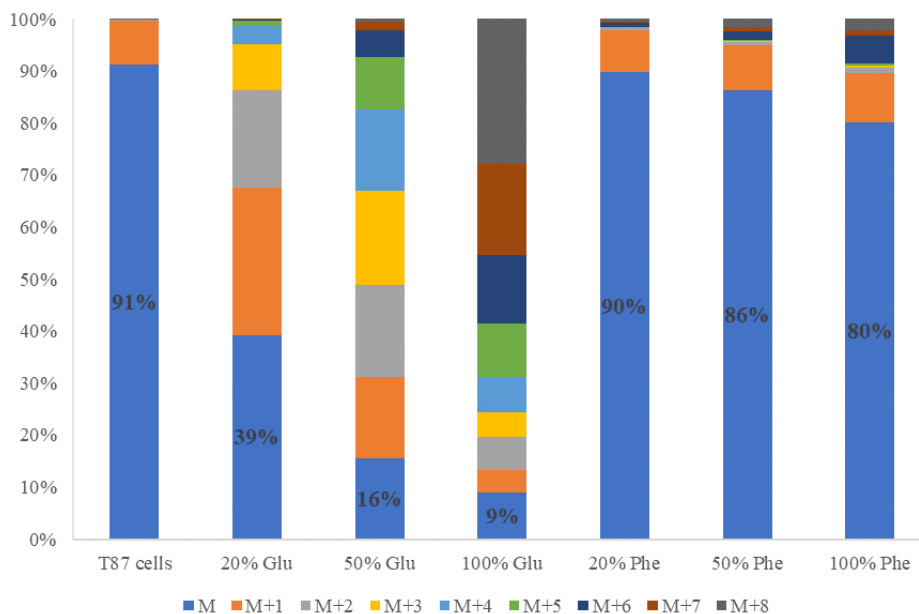


Figure 4.7 ^{13}C distribution of ethylbenzene in T87 cells with different labeling strategies after CFP indicating that small amount of ethylbenzene is derived from lignin and the rest is formed by carbohydrate.

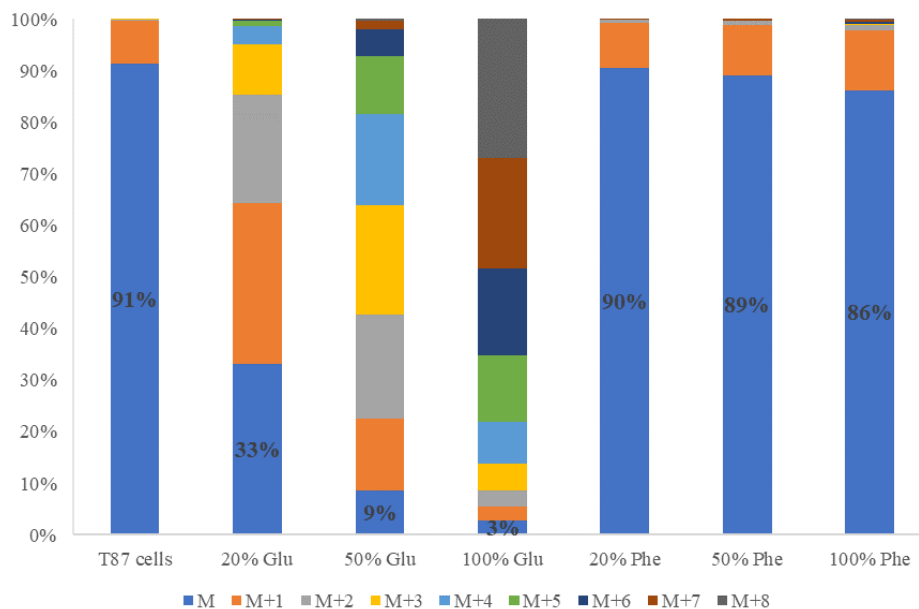


Figure 4.8 ^{13}C distribution of the mixture *p*-xylene and *m*-xylene of in T87 cells with different labeling strategies after CFP indicating that *p*-xylene and *m*-xylene are derived from carbohydrate.

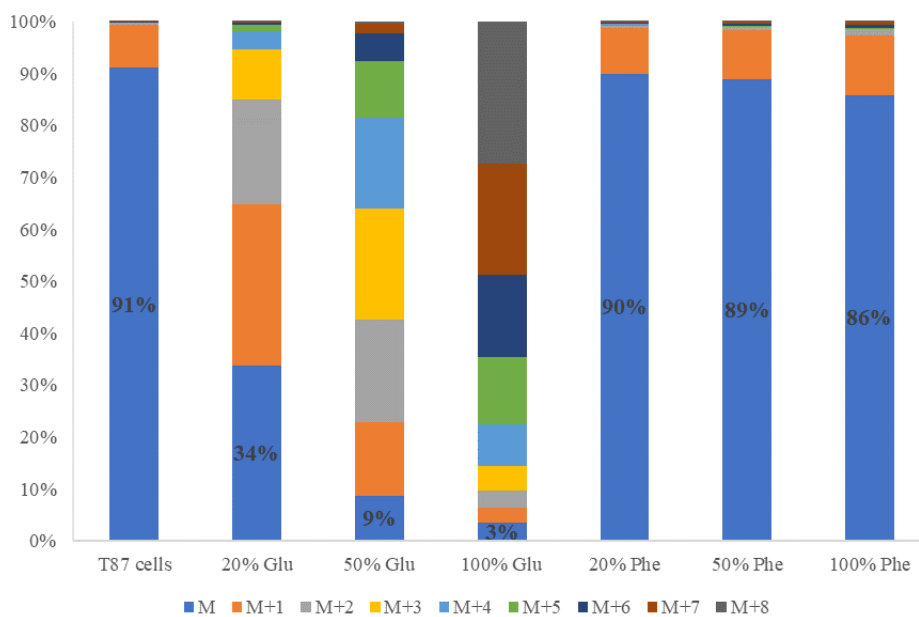


Figure 4.9 ^{13}C distribution of *o*-xylene of in T87 cells with different labeling strategies after CFP indicating that *o*-xylene are derived from carbohydrate.

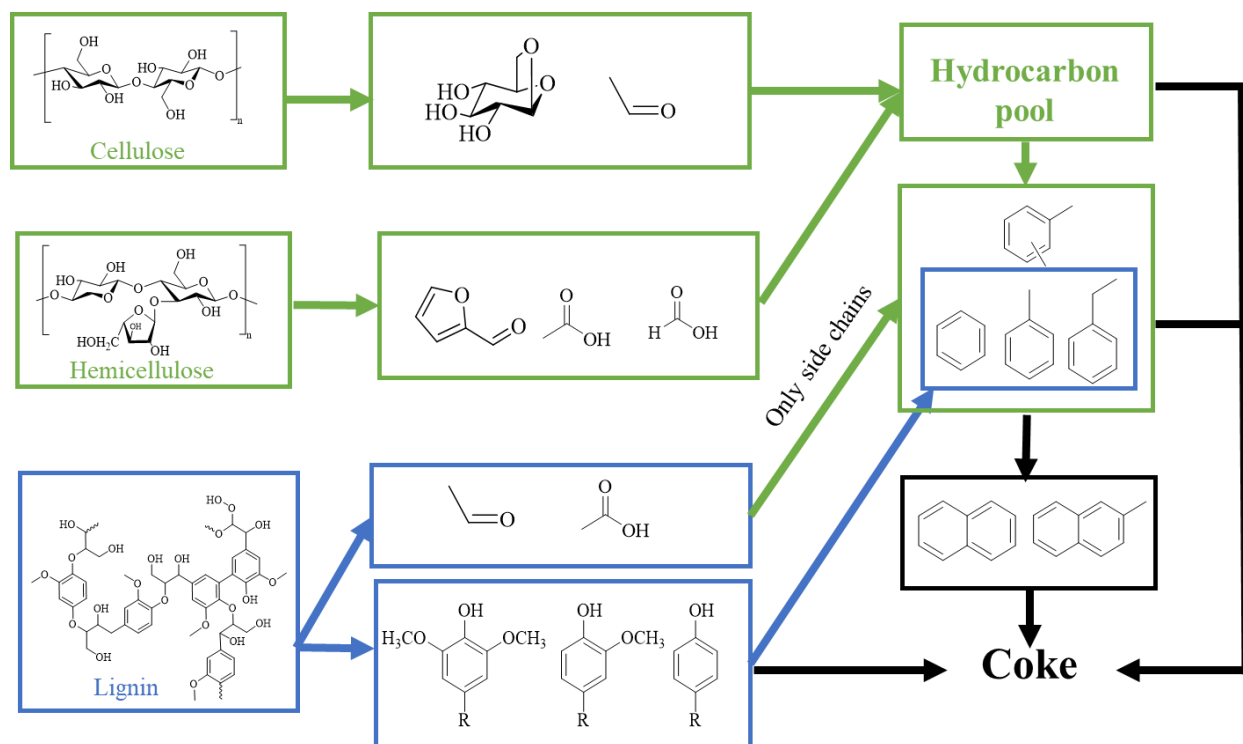


Figure 4.10 A proposed reaction pathway during catalytic fast pyrolysis.

4.5 Conclusion

Previous research demonstrated that labeled T87 cell lines, one with labelled holocellulose, the other with labelled lignin, could be used as a surrogate to investigate pyrolysis reaction pathways. In this work, catalytic fast pyrolysis reaction pathways were investigated by the same procedure. ^{13}C distribution results indicated that BTEX produced by carbohydrates was formed by light olefins. Carbohydrates underwent depolymerization and decomposition reactions, followed by deoxygenation to light hydrocarbons. Conversely, lignin's route to BTEX by CFP of T87 cells was different than carbohydrate's route as the aromatic rings were not opened. Due to HZSM-5's pore size, BTEX production decreased when the product's molecular size increased. In consideration of the production per mass, the conversion from lignin to benzene was slightly more than from carbohydrate while TEX conversions from carbohydrate were much higher than from lignin during catalytic pyrolysis of T87 cells.

CHAPTER 5. MONOCYCLIC AROMATICS PRODUCTION BY CATALYTIC FAST PYROLYSIS OF BIOMASS WITH METAL MODIFIED HZSM-5

5.1 Abstract

Six biomass types were characterized and examined for monoaromatic hydrocarbons (benzene, toluene, ethylbenzene, and xylenes, i.e. BTEX) production during catalytic fast pyrolysis with HZSM-5 with a silica to alumina ratio (SAR) of 23. Spent coffee grounds (SPG) yield the highest BTEX levels compared to poplar, wheat straw, switchgrass, corn stover, and sugarcane bagasse. Using SPG as a feedstock, HZSM-5 with different silica to alumina ratios (SAR) of 23, 50, and 80 was evaluated to determine BTEX product yields. Catalytic pyrolysis was performed using a microscale pyrolysis unit interfaced with a GC/MS to analyze pyrolysis products. Catalytic pyrolysis with a series of metal impregnated HZSM-5 catalysts was then performed to determine the highest aromatic yield. HZSM-5 with a SAR of 23 produced the highest yield of aromatic hydrocarbons. Chromium modified HZSM-5 (23) performed favorably when compared to gallium, iron (III), nickel, cobalt, titanium and copper. 1 wt.% loading of chromium on ZSM-5 was more selective to monoaromatic hydrocarbons and less selective to polycyclic aromatic hydrocarbons.

5.2 Introduction

Due to abundance and low cost, biomass has the potential for producing renewable energy. According to the Billion Ton Report published in 2016, harvested biomass in U.S. could achieve 1.3 billion dry ton with a price under \$60 per dry ton.[10] Determining how to effectively utilize this energy source is needed as part of the biofuel production design process. Hydrolysis and fermentation have been considered, but the carbon efficiency of fermentation is low and lignin,

constituting about 20-35 wt.% of lignocellulosic biomass and 40% of biomass energy, is not utilized.[39, 123]

Biomass fast pyrolysis is a promising process that converts biomass into non-condensable vapor, organic liquid fuel, and solid char in the absence of oxygen at intermediate temperature (400-600 °C) with a rapid heating rate (>500 °C/s).[30] Co-produced non-condensable gas, consisting of carbon monoxide, carbon dioxide, methane and hydrogen, can be combusted for energy. Solid char, also co-produced, can be used as an adsorbent, energy, or solid amendment to improve soil quality. The liquid product in fast pyrolysis, known as “bio-oil” is the dominant product that includes hundreds of organic compounds. However, these highly oxygenated compounds result in low energy content, high corrosiveness, and high acidity, that limits its application.

An upgrading process is needed to improve the bio-oil quality. Catalytic cracking plays an essential role in petroleum industry.[124] This application also works on upgrading bio-oil by removing the oxygen functionalities, and the integrated process is called catalytic fast pyrolysis. Zeolite catalyst has been commonly used in cracking since the 1960s due to their unique properties, such as low cost, larger surface area, distinctive pore structure, and good thermal stability.[125] Many researchers indicate that zeolites, especially ZSM-5, could yield a relatively high aromatic production and selectivity.[43-45] Among the aromatic products, monoaromatic compounds, such as benzene, toluene, ethylbenzene and xylenes (BTEX), are important industrial chemicals that are used in the print industry, leather industry, and rubber manufacture or as gasoline additives and solvents.[126] Moreover, metal modification on ZSM-5 was recommended by Iliopoulou et al. because the metal presence affects oxygen rejection by making more carbon oxides and less water, allowing for more hydrogen to be incorporated into hydrocarbons.[54]

Aromatic yields of catalytic pyrolysis of cell wall components have been studied.[39, 117, 118] However, results are contradictory, hindering feedstock selection. To alleviate this hindrance, this work studies the effect of feedstock by pyrolyzing six biomass types using analytical pyrolysis (py-GC/MS). The biomass with the highest monoaromatic yields is then selected as feedstock for further catalyst evaluation.

5.3 Methods and Materials

5.3.1 Characterization of biomass feedstocks

Six types of biomass were selected for catalytic fast pyrolysis: Poplar (DN-34, *Populus euramericana cv. Eugenei*), spent coffee grounds (The Coca-Cola Co. GA), wheat straw, corn stover, switchgrass, sugarcane bagasse. All biomass was ground and sieved with a particle size less than 0.5mm (35u.s. mesh) prior to the analysis.

5.3.1.1 Proximate analysis

The proximate properties of feedstocks were analyzed by a thermogravimetric analyzer (TGA/DSC-1, Mettler-Toledo, OH). Approximately 10-20 mg of sample was tested by TGA/DSC with a 20 ml/min flow of flue gas for either nitrogen or air. The moisture and volatile carbon contents were calculated by the mass difference through heating the biomass with a nitrogen flow from room temperature to 105 °C and 925 °C, respectively. The heating rate was set as 10 °C/min. After cooling the previous samples to 800 °C, the flue gas was switched to air and the residues were combusted to measure ash content and to compute fixed carbon by difference. Every step in the program was held at a set point temperature until the mass remained constant. The higher heating value (HHV) of SCG was determined using a Parr 1341 Jacket Calorimeter (Parr Instrument Company, Moline, IL).

5.3.1.2 Elemental analysis and H/C_{eff}

The samples were sent to Atalantic Microlabs for elemental analysis. Carbon, hydrogen, and nitrogen contents were quantified, and oxygen content was calculated by the difference. Chen's effective H/C ratio was calculated using Equation 3, where C, H, and O are in moles.[127]

$$H/C_{eff} = \frac{H - 2O}{C} \quad (3)$$

5.3.1.3 Compositional analysis and thioacidolysis

Cell wall polymer composition was determined by fiber analysis invented by NREL.[87] Biomass undergoes an acid hydrolysis with sulfuric acid to fractionate the biomass. Polymeric carbohydrates are hydrolyzed into their monomeric forms, which are measured by a high-performance liquid chromatography (HPLC, Angilent Technologies, Inc, CA) with a Bio-rad Aminex HPX-87P column (300 × 7.8mm). The insoluble lignin and ash were filtered, dried, and weighed. Thioacidolysis was also applied to each feedstock to obtain the composition of thioethylated lignin monomers through the cleavage of β -O-4 ether linkage.

5.3.2 Catalyst synthesis and characterization

HZSM-5 with different silicon-to-aluminum ratios (SAR) (23, 50, 80) were first tested to evaluate SAR effects in these pyrolysis experiments. Ammonia form ZSM-5 was purchased from Zeolyst Company (Conshohocken, PA). It was calcined in a furnace at 550 °C for 4 hours to obtain the acidic HZSM-5 form. According to previous research[45], HZSM-5(23) has the highest aromatic yield among five HZSM-5 catalysts with SAR ranging from 23-280. The calcined HZSM-5(23) was also used as the support of metal modified catalysts, which were synthesized by incipient wetness. Seven metal precursors were purchased from Sigma Aldrich, Inc (Gallium (III) nitrate hydrate, Chromium (III) acetylacetonate, Iron(III) chloride, Nickel(II) nitrate hexahydrate, Cobalt(II) acetate tetrahydrate, Titanium(IV) butoxide, and Cupric nitrate trihydrate) and were

dissolved in ethanol before mixing with HZSM-5 with three loadings (1 wt.%, 3 wt.%, 5 wt.%). After drying at 45 °C overnight, the catalysts were calcined at 550 °C for 4 hours to remove the volatile components within the solution, depositing the metals on the surface of HZSM-5.

Nitrogen adsorption/desorption isotherms were acquired from a Micromeritics ASAP2010 instrument. Approximately, 0.3 g catalyst was placed in a vacuum at 220 °C for 24 hours for pretreatment. The surface areas were computed using the standard Brunauer–Emmett-Teller (BET) equation. Total pore volumes were obtained from the single point of P/P_0 value at 0.97. The average pore diameters were calculated using Barret-Joyner-Halenda (BJH) analysis.

Temperature-programmed desorption of ammonia (NH_3 -TPD) was performed in a Micromeritics AutoChem 2910 with a thermal conductivity detector (TCD). In a typical run, 0.1g catalyst was treated in a flow of NH_3 (15% NH_3 in He, 50ml/min) at 60 °C for 1 hour after pretreatment at 550 °C in a flow of He (50ml/min). The physically absorbed NH_3 was removed by flushing the catalyst with He (50 mL/min) at 100 °C for 120 min before starting the TPD analysis. The amount of chemical adsorbed NH_3 was recorded by TCD by heating the sample from 100 °C to 550 °C at a ramp of 10 °C/min under He (50 mL/min).

5.3.3 Pyrolysis-GC/MS

Experiments were conducted using a microscale pyrolysis unit, CDS Pyroprobe 5250 (CDS Analytical Inc., Oxford, PA) interfaced to a Shimadzu QP-5050A gas chromatograph/mass spectrometer (Shimadzu Corp., MD). Approximately 0.5 mg of biomass sample was loaded between quartz wool in a quartz tube for fast pyrolysis. For catalytic pyrolysis experiments, catalysts were well-mixed with biomass at a weight ratio of 5:1. After that, approximately 3mg of mixture was packed between quartz wool. For each sample, three replicated experiments were examined.

Pyrolysis proceeded by setting the pyroprobe at 650 °C with a resident time of 20s at a heating rate of 999 °C/s. The GC used a Restek rtx-1701 column (Restek, Bellefonte, PA), 60 m × 0.25 mm with a 0.25 μm film thickness. The column gas flow was 1 ml/s with a split ratio of 1:100. The GC oven program started at 40 °C for 1 min, heated to 270 °C at 8.0 °C/min, and held at 270 °C for 10 min. The injector and detector temperature were set at 270 °C. The mass spectra were recorded in electron ionization mode for m/z 33–400.

Identification of compounds was performed by comparing the mass spectra of the peaks with standard spectra of other compounds using the NIST library to obtain the most similar matches. Pure compounds of aromatic hydrocarbon (Sigma–Aldrich Co., MO) were used to confirm the peak identities based on matching of retention times and mass spectra. Quantification was performed using external standards.

5.3.4 Pyrolysis-GC/FID

Pyrolysis proceeded the same as Part 5.3.4. The pyrolysis vapor was carried out by carrier gas. And a 50ml gas bag was filled by pyrolysis vapor and carrier gas. Then the mixed gas was injected into an Angilent-7890A GC-FID (Angilent Technologies, Inc, CA). The alkanes and alkenes in the pyrolysis vapor were separated in the column, then detected by the FID. Standard gases were used to all the alkanes and alkenes qualification and quantification.

5.4 Results and Discussion

5.4.1 Pyrograms of catalytic pyrolysis of spent coffee grounds with HZSM-5

Figure 5.1 represented the pyrogram of catalytic pyrolysis of spent coffee grounds with HZSM-5 (23). The products all belong to aromatic hydrocarbons. A similar pyrogram can be achieved by pyrolyzing other types of biomasses with HZSM-5. Table 5.1 listed the major compounds with retention time and the similarity based on the NIST library. The peak with a

retention time of 9.91 minute may be a mixture of *p*-xylene and *m*-xylene by checking the retention time of pure standard. In catalytic pyrolysis, deoxygenation reactions and cracking reactions produced more light gases hydrocarbons. In addition, more cracking and deoxygenation reactions took place, resulting in a high yield of alkenes.

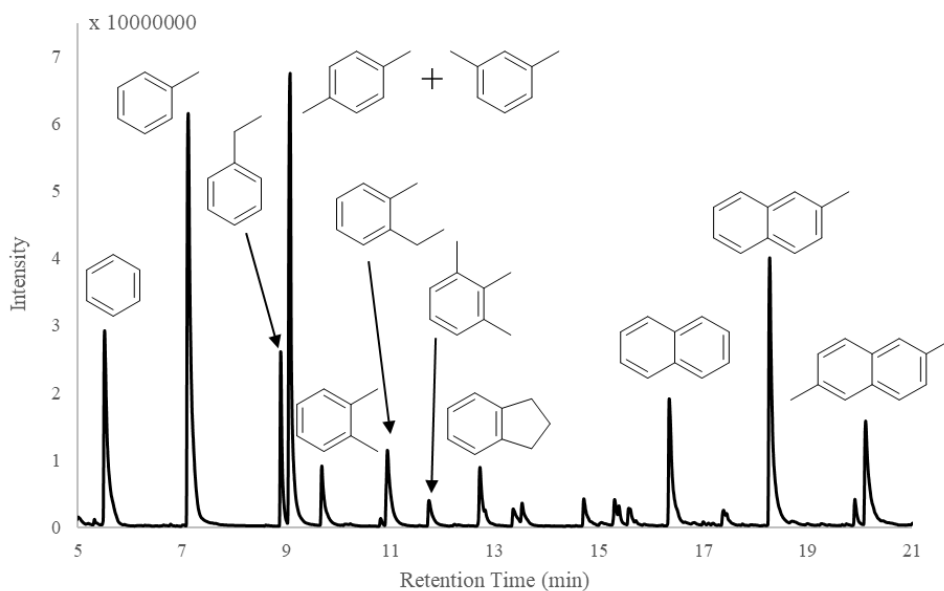


Figure 5.1 Pyrogram of spent coffee grounds with HZSM-5.

Table 5.1 Catalytic pyrolysis products from spent coffee grounds pyrogram identified by NIST library.

No.	Retention time (min)	CompoundName	Similarity
1	5.43	Benzene	96
2	6.34	Toluene	91
3	8.07	Ethylbenzene	98
4	9.91	p-Xylene	90
5	10.08	o-Xylene	98
6	10.69	Benzene, 1-ethyl-2-methyl-	97
7	11.97	Benzene, 1,2,3-trimethyl-	96
8	12.71	Indane	94
9	13.77	Indene	95
10	14.34	1H-Indene, 2,3-dihydro-2-methyl	96
11	14.56	1H-Indene, 2,3-dihydro-5-methyl-	96
12	15.74	Naphthalene	96
13	16.32	Naphthalene, 1-methyl-	91
14	17.47	Naphthalene, 2-ethyl-	97
15	19.41	Naphthalene, 2,6-dimethyl-	97

5.4.2 Biomass characterization and BTEX yield performance with HZSM-5 in CFP

5.4.2.1 Proximate analysis

As listed in Table 5.2, a proximate analysis has been completed for various feedstock. Even though poplar has the lowest ash content and highest volatile matter content, its higher heating value (HHV) examined by the calorimeter is lower than SCG. SCG has the lowest moisture content and a much larger HHV than any other feedstocks. It may be revealed that water content is the primary factor affecting HHV besides volatile carbon, fixed carbon, and ash. Wheat straw, corn stover and switchgrass have similar properties. Surprisingly, sugarcane bagasse has both lower moisture and ash content than wheat straw, corn stover, and switchgrass, but the lowest HHV.

Mariyam et al. indicated that the fixed carbon had positive effect on the pyrolysis yield, but adverse effects on biochar yield.[128]

Table 5.2 Feedstock proximate analysis. Moisture, volatile carbon, fixed carbon, and ash are in weight percentage based on dry biomass (a: Three replicates, b: single test).

	Poplar	Spent coffee grounds	Wheat straw	Corn stover	Switchgrass	Sugarcane bagasse
Moisture (%) ^a	6.42±0.63	3.13±0.09	6.05±0.39	6.31±0.26	6.31±0.72	5.55±0.18
Volatile carbon (%) ^b	80.89	78.45	74.23	72.25	73.22	72.11
Fixed carbon (%) ^b	12.05	17.18	14.98	16.29	13.49	18.06
Ash (%) ^a	0.64±0.10	1.22±0.30	5.07±0.35	5.15±0.39	6.67±0.18	4.28±0.60
HHV(MJ/Kg) ^a	19.46±0.70	23.14±0.77	16.60±1.35	16.76±1.12	16.15±0.76	14.61±1.97

5.4.2.2 Elemental analysis

Elemental analysis (Table 5.3) has been done by Atalantic Microlabs for carbon, hydrogen, and nitrogen in weight fraction. Oxygen content was calculated differently. SCG has the highest carbon and nitrogen content that leads to a lowest oxygen content. H/C_{eff} was found Based on Equation (1) and SCG with a H/C_{eff} value over 0.5 that indicates a higher yield may be obtained than the other biomass. The effective H/C ratio for petroleum-based fuels is between 1 to 2, while it is below 0.5 for pyrolysis oil and zero for glucose and cellulose. Most lignocellulosic biomass types have H/C_{eff} ratio from 0 to 0.3.[129]

Table 5.3 Elemental analysis from Atalantic Microlabs. Oxygen is calculated by difference. H/C_{eff} is computed by the hydrogen lost from biomass as oxygen is removed as water. The elemental analysis results in wt.%, while H/C_{eff} is based on molar.

	Poplar	Spent coffee grounds	Wheat straw	Corn stover	Switchgrass	Sugarcane bagasse
C	46.44± 0.13	51.99± 0.11	41.06± 0.03	43.46± 0.13	44.03± 0.15	44.41± 0.11
H	6.14± 0.12	7.07± 0.02	5.63± 0.08	5.91± 0.08	5.83± 0.08	5.75± 0.06
N	0.15± 0.02	2.26± 0.05	0.55± 0.03	0.60± 0.06	0.42± 0.04	0.22± 0.08
O	47.29± 0.28	38.69± 0.18	52.76± 0.14	50.04± 0.01	49.73± 0.27	49.63± 0.25
H/C_{eff}	0.06	0.51	-0.28	-0.1	-0.11	-0.12

5.3.2.3 Compositional analysis and thioacidolysis

Table 5.4 reports the cell wall fraction measured by NREL fiber analysis. The glucan content of SCG is low as they were processed by hot water. As glucan was removed from SCG, the xylan and lignin contents are relatively higher than biomass components. In total, the fiber content of SCG 88 wt.%.

Lignin is a combination of complex organic polymer consisting of three common monomer components: *p*-coumaryl alcohol (H type), coniferyl alcohol (G type) and sinapyl alcohol (S type). Table 5.5 reports the monolignol contents as molar ratios for each feedstock after using thioacidolysis. Liu et al. found that softwood was dominantly of G-lignin, hardwood lignin was mainly G and S type, while grass lignin included all three monomers.[130]

Table 5.4 Compositional analysis using NREL fiber analysis methods. All numbers are weight fractions.

	Poplar	Spent coffee grounds	Wheat straw	Corn stover	Switchgrass	Sugarcane bagasse
Glucan (%)	45.21±3.60	10.41±0.75	38.48±1.57	37.87±3.84	40.31±1.17	43.45±0.50
Xylan (%)	20.26±1.37	39.77±1.41	24.82±0.74	22.90±3.20	24.84±0.88	23.44±0.27
Lignin (%)	23.34±0.42	37.84±2.48	22.05±0.27	22.26±4.63	24.12±0.89	24.25±0.98
Total (%)	88.81±5.39	88.01±1.88	85.35±2.58	83.03±2.41	89.27±2.94	90.65±1.75

Table 5.5 Lignin monomer composition measured by thioacidolysis. The results are molar ratio.

Lignin Type	Poplar	Spent coffee	Wheat straw	Corn stover	Switchgrass	Sugarcane bagasse
H	0.51±0.04	0.30±0.01	5.03±0.28	4.19±0.13	2.50±0.26	2.26±0.26
G	36.83±1.59	49.75±0.30	41.70±1.91	44.29±2.21	62.37±1.01	40.45±2.71
S	62.66±1.62	49.95±0.29	53.28±2.19	51.52±2.27	35.13±0.78	57.29±2.60

5.3.2.4 BTEX yield performance of each feedstock

BTEX production levels from various biomass sources through catalytic pyrolysis with HZSM-5 (23) are shown in Table 5.2. SCG yielded the most BTEX as H/C_{eff} predicted. Moreover,

the same trend as in proximate analysis in Table 5.2, wheat straw, corn stover, and switchgrass performed a similar conversion to BTEX during CFP. SCG and poplar have larger HHV that leads to a high BTEX production. Only for sugarcane bagasse was the prediction based on proximate analysis in Table 5.2 was incorrect. SCG, the feedstock with the highest HHV and H/C_{eff} , resulted in the highest BTEX conversion. Thus, HHV and H/C_{eff} predict BTEX conversion for a given feedstock. Given the high yields, SCG was selected as feedstock for catalyst evaluation.

Table 5.6 BTEX yield produced by six types of biomasses during catalytic pyrolysis with HZSM-5(23).

Feedstocks	Biomass:Catalyst Ratio	BTEX Yield (wt.%)	Relative BTEX Yield
Poplar	1:5	7.79 ± 0.23	1
Spent coffee	1:5	11.27 ± 0.65	1.45
Wheat straw	1:5	6.65 ± 0.60	0.85
Corn stover	1:5	6.73 ± 0.57	0.86
Switchgrass	1:5	6.91 ± 0.49	0.89
Sugarcane bagasse	1:5	7.15 ± 0.11	0.92

5.4.3 Catalyst properties and yield performance of HZSM-5 with different SARs (23, 50, 80)

5.4.3.1 Catalyst properties of HZSM-5 with different SARs (23, 50, 80)

Table 5.7 compares the nitrogen adsorption/desorption properties of HZSM-5 with different SARs. The typical microporous HZSM-5 catalysts had an average pore size from 0.498-0.510 nm and the BET surface area and pore volume decreased with the increased SAR. More acidic sites are available if the surface area increases, resulting in a higher conversion and low production of coke. This result matched the previous research that HZSM-5 (23) provided the highest aromatic yield as acidity is the strong compared to ZSM-5 with a high SAR.[45]

Figure 5.2 shows the NH_3 desorption amounts of HZSM-5 catalysts with different SAR in NH_3 -TPD. The NH_3 desorption curves were correlated with the strength and amount of acid sites. The curves of the three HZSM-5 types have a peak located around 200°C corresponding to weak

acid sites. Another peak corresponding to strong acid sites occurs at about 370°C. Both peaks shifted to higher temperature with lower SAR, indicating the acid site strength increases with the decreasing of SAR. Additionally, with decreasing SAR, the peak areas increase significantly, demonstrating an increased number of acid sites.

Table 5.7 Structural properties of the HZSM-5 with different SARs (23, 50, 80) by nitrogen adsorption/desorption.

	BET Surface area(m ² /g)	Pore size(nm)	Pore volume(cm ³ /g)
HZSM-5(23)	357.74	0.501	0.184
HZSM-5(50)	315.08	0.498	0.157
HZSM-5(80)	259.71	0.51	0.132

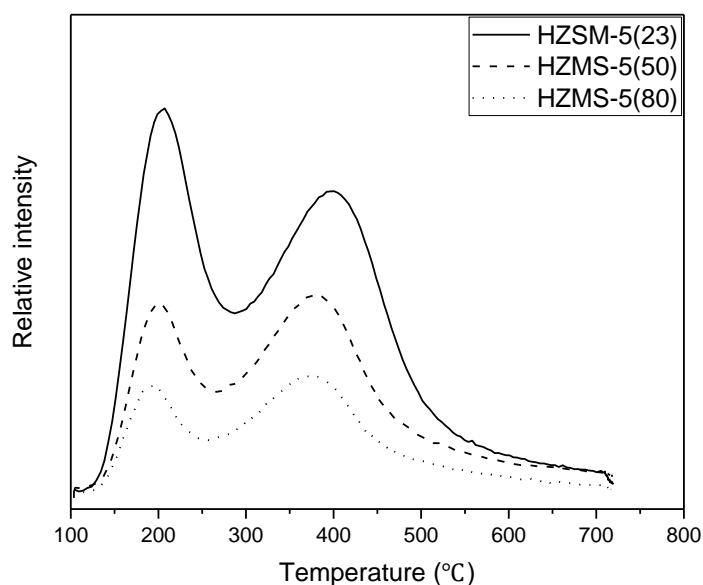


Figure 5.2 NH₃ desorption amount of HZSM-5(23, 50, 80) in NH₃-TPD.

5.4.3.2 Yield performance of HZSM-5 with different SARs during CFP

HZSM-5 is a crystalline aluminosilicate zeolite with a high silica and low aluminum content. The reduction in alumina probably enhances its Brønsted acid sites.[131] The gas product distribution and yield of catalytic pyrolysis of SCG with HZSM-5 of different SAR was shown in

Figure 5.3. HZSM-5 (23) with the most acid sites generated more alkanes and alkenes, with the highest yields of 1.83 wt.% and 4.09 wt.%, respectively. As SAR increases, the amount and strength of acid sites decreases. Accordingly, the alkane and alkene yield of HZSM-5(50) and HZSM-5(80) decreases with increasing SAR.

HZSM-5 (23) produced the greatest amount of monocyclic aromatic hydrocarbons (Figure 5.4), including C6 (benzene), C7 (toluene), C8 (ethylbenzene, xylene, and other isomers) and C9 (trimethylbenzene and other isomers). HZSM-5 (23), with the highest concentration of acidic sites, also produced the most PAH, including C10+PAH (naphthalene, methylnaphthalene, anthracene, and other isomers), a likely result of secondary polymerization reactions of monocyclic aromatic hydrocarbons. In total, SAR 23 produced 9.29 wt.% MAH and 4.11 wt.% PAH, respectively.

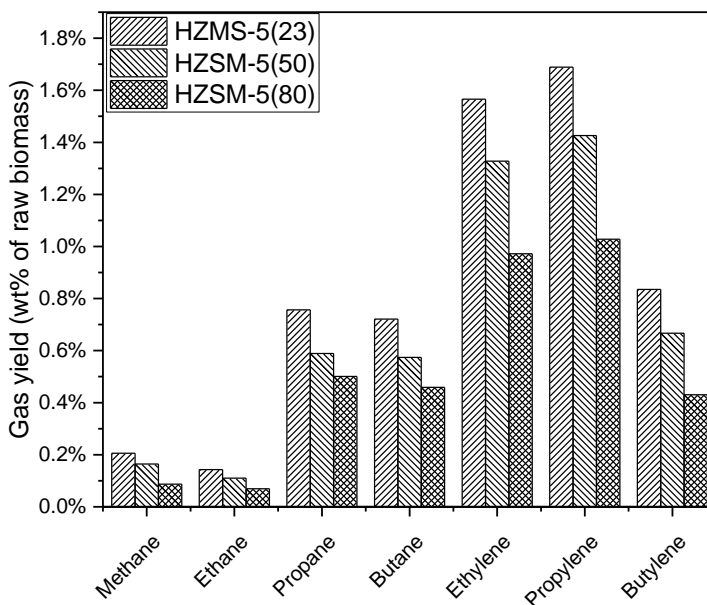


Figure 5.3 Alkanes and alkenes yields of catalytic pyrolysis with HZSM-5(23, 50, 80).

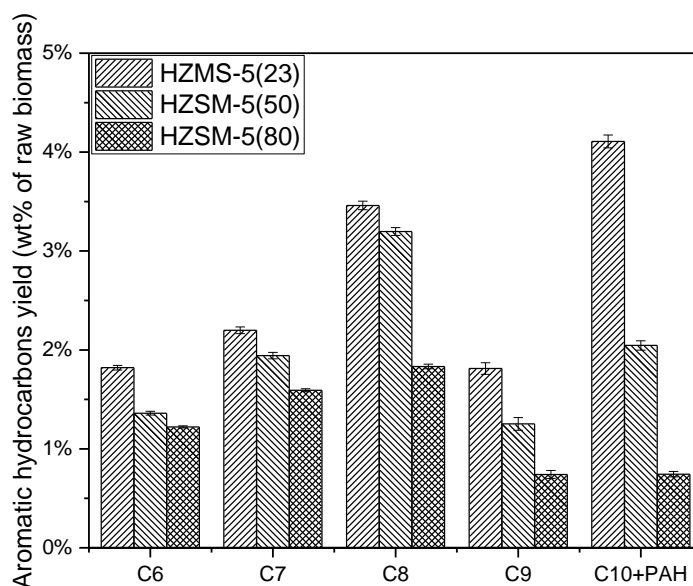


Figure 5.4 Aromatic hydrocarbon yields of catalytic pyrolysis with HZSM-5(23, 50, 80).

The aromatic hydrocarbon selectivity is defined as the mass of aromatic hydrocarbon divided by the total mass of aromatic hydrocarbons in condensable products. The C6 and C7 selectivity increased with SAR suggesting that a lower concentration of acidic sites tends to produce greater amount of benzene and methylbenzene molecules. Comparatively, SAR 50 had the highest selectivity in C8, while SAR 80 was particularly selective for C10+PAH. With the increase of SAR, HZSM-5 tended to produce more aromatic hydrocarbons with less molecular weight.

Table 5.8 Yield performance of HZSM-5 with different SARs (23, 50, 80) during catalytic pyrolysis of SCG.

Catalyst	Alkane	Alkene	Total gas yield	MAH yield	MAH selectivity	PAH yield	PAH selectivity	Total aromatic yield
HZMS-5(23)	1.83%	4.09%	5.92%	9.29%	69.34%	4.11%	30.66%	13.40%
HZSM-5(50)	1.44%	3.42%	4.86%	7.75%	79.12%	2.05%	20.88%	9.80%
HZSM-5(80)	1.12%	2.43%	3.55%	5.39%	87.86%	0.74%	12.14%	6.13%

5.4.4 Evaluation of metal modified HZSM-5 catalyst

Various metals were examined for the catalytic performance modified with HZSM-5 under three different loadings. Based on the results in Table 5.9, every type of metal achieved the highest BTEX production at 1 wt.% loading. Wherein, Ga/ZSM-5, Cr/ZSM-5 and Co/ZSM-5 yields exceed 10.6 wt.%. Zheng et al. tested several metals doped on ZSM-5 and listed an order of deoxygenation ability for each catalyst as follows (from low to high): H/ZSM5, Cu/ZSM-5, Mg/ZSM-5, Co/ZSM-5, Ni/ZSM-5, Zn/ZSM-5, and Ga/ZSM-5.[57] Increasing the loadings on ZSM5, less BTEX was produced during CFP, especially for cobalt. Haukka et al. mentioned that the weakness of incipient wetness was pH changes during drying and the adsorptive character of the surface changes.[132] Due to the uncertainty of metal loadings on the surface, catalyst performance is assessed, including conversion with three metal loading amounts, for each metal. Based on the results in Table 5.9, chromium was selected for evaluation with multiple metal loadings.

Table 5.9 BTEX yield of metal modified ZSM-5 during catalytic pyrolysis of spent coffee grounds.

Catalyst	Loading amount		
	1 wt.%	3 wt.%	5 wt.%
Ga/ZSM-5	10.63%	9.69%	9.23%
Cr/ZSM-5	10.61%	10.35%	10.13%
Fe ³⁺ /ZSM-5	10.24%	9.64%	9.99%
Ni/ZSM-5	10.50%	8.99%	6.88%
Co/ZSM-5	10.64%	8.56%	4.49%
Ti/ZSM-5	10.40%	10.08%	10.44%
Cu/ZSM-5	9.81%	9.13%	8.29%
HZSM-5	10.07%		

5.4.5 Evaluation of multiple loading amounts of Chromium on HZSM-5

Nitrogen adsorption/desorption described in Section 5.3.2 was applied for Cr/ZSM-5 with different loading amounts (1 wt.%, 3 wt.%, 5 wt.%) and the results are shown in Table 5.10. The surface area of three metal modified Cr/HZSM-5 decreased with increasing of chromium loading, which might be attributed to both the occupation of metal particles and some micropore structure collapse after calcination in incipient wetness. However, the average pore size increased from 0.501nm to 0.589 nm after chromium impregnation, which indicates that there were more micropores with smaller pore sizes occupied or collapsed than micropores with relatively larger pore sizes. The large pore sizes of Cr/HZSM-5 series catalysts are expected to reduce both the diffusion resistance of pyrolysis products and catalytic products.

Table 5.10 Structure properties of chromium modified HZSM-5 with different loading (1 wt.%, 3wt.%, 5 wt.%) by nitrogen adsorption/desorption.

Catalyst	BET Surface area(m ² /g)	Pore size(nm)	Pore volume(cm ³ /g)
1%Cr/HZSM-5(23)	332.44	0.536	0.178
3%Cr/HZSM-5(23)	328.89	0.566	0.186
5%Cr/HZSM-5(23)	309.34	0.589	0.182

In the previous section, BTEX production of Cr/ZSM-5 with different metal loadings was measured. More detailed yield performance was tested for Cr modified ZSM-5. As shown in Figure 5.5 HZSM-5(23) had the highest yield of ethane, propane, and butane. Comparatively, 1% Cr/ZSM-5 produced more alkenes, such as ethylene, propylene, and butylene. However, with the increase of chromium loading amount, the yields of all alkanes and alkenes decreased, perhaps because both the strong and weak acid sites decomposed. In total, HZSM-5(23) had the highest yield of 1.83% alkanes, and 1% Cr/ZSM-5 produced 4.82% of alkenes. Both the MAH and PAH yield of catalytic pyrolysis of SCG with HZSM-5(23) and 1%, 3% and 5% Cr/ZSM-5 are reported in Figure 5.6. All four catalysts result in nearly the same in C6 yield. Cr/HZSM-5 series catalysts

produced more C7, C8, and C9 MAH and less C10+PAH than HZSM-5(23). With increased chromium loading, the MAH yield decreased slightly and more C10+PAH were formed.

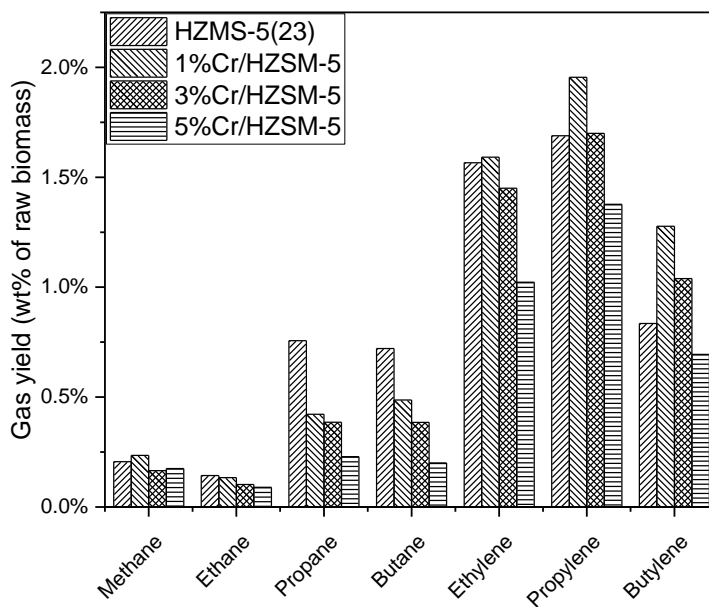


Figure 5.5 Alkanes and alkenes yields of catalytic pyrolysis with HZSM-5(23) and Cr/ZSM-5 (1 wt.%, 3 wt.%, 5 wt.%).

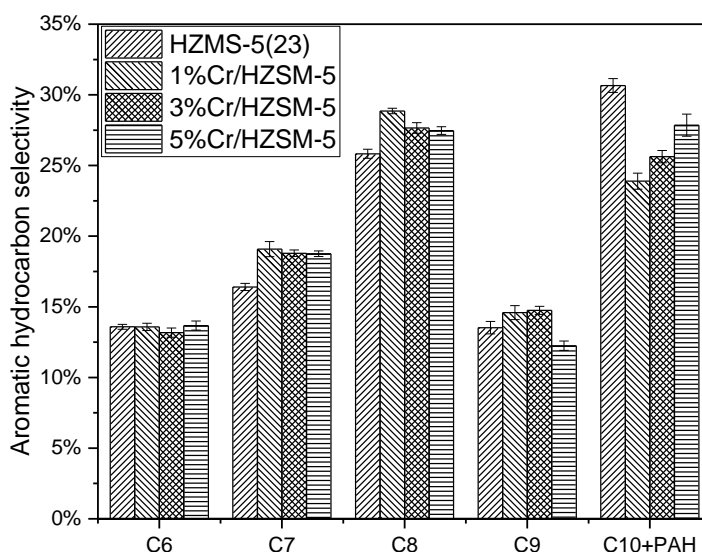


Figure 5.6 Aromatic hydrocarbon yields of catalytic pyrolysis with HZSM-5(23) and Cr/ZSM-5 (1 wt.%, 3 wt.%, 5 wt.%).

Table 5.11 Yield performance of with HZSM-5(23) and Cr/ZSM-5 (1 wt.%, 3 wt.%, 5 wt.%) during catalytic pyrolysis of SCG.

Catalyst	Alkane	Alkene	Total gas yield	MAH yield	MAH selectivity	PAH yield	PAH selectivity	Total aromatic yield
HZMS-5(23)	1.83%	4.09%	5.92%	9.29%	69.34%	4.11%	30.66%	13.40%
1%Cr/HZSM-5	1.28%	4.82%	6.10%	10.38%	76.11%	3.26%	23.89%	13.64%
3%Cr/HZSM-5	1.04%	4.19%	5.23%	10.36%	74.37%	3.57%	25.63%	13.93%
5%Cr/HZSM-5	0.69%	3.09%	3.79%	9.80%	72.15%	3.78%	27.85%	13.58%

5.5 Conclusion

Monoaromatic hydrocarbons, mainly benzene, toluene, ethylbenzene, and xylenes, are highly valuable chemicals. Aiming to improve BTEX production during catalytic pyrolysis, an investigation of feedstock selection, silicon-to-alumina ratio of HZSM-5(23, 50, 80), metal selection for modification, metal loadings on ZSM-5 (1 wt.%, 3 wt.%, 5 wt.%), and overall yield performance during catalytic fast pyrolysis was performed. Regarding biomass selection, spent

coffee grounds achieved the highest BTEX yields as it has the largest HHV and H/C_{eff} value. Compared to the results of poplar, wheat straw, corn stover, switchgrass and sugarcane bagasse, HHV and H/C_{eff} value are predictive of BTEX production. For SAR selection, the conclusion was consistent with other researcher[45], namely that a lower SAR resulting in high acidity and more acidic sites improved monoaromatic production. For different metal loadings, every metal type reached the highest BTEX yield at 1 wt.% loading. However, the yield reduced with increased metal loadings. Overall chromium modified ZSM-5 had the best performance. Compared to 3 wt.% and 5 wt.% loadings on ZSM-5, 1 wt.% Cr/ZSM-5 produced the most alkane, alkene, MAH, and the least PAH.

CHAPTER 6. CONCLUSIONS AND RECOMMENDATIONS

6.1 Conclusions

Biomass fast pyrolysis is a promising thermochemical conversion to produce renewable energy in liquid form. A methodology was developed to investigate pyrolysis reaction pathways by using isotopically labeled plant cell culture. Feeding ^{13}C labeled biosynthetic precursors can preferentially label the cell wall fraction, such as glucose to carbohydrate, phenylalanine to lignin. Adding excess phenylalanine into the media can block the biology metabolism pathway from glucose to phenylalanine. Meanwhile, the abundance of phenylalanine in the media prompted T87 cell to form lignin, where about four times more lignin was observed compared to without adding phenylalanine. No S-type lignin was detected through thioacidolysis.

When T87 cells were applied as a surrogate via analytical pyrolysis- GC/MS system (py-GC/MS), the pyrogram of T87 cells demonstrated a higher similarity to pyrolysis of *Arabidopsis* plant than the single compound or simple mixture, such as glucose, cellulose, and lignin. However, excess amount of phenylalanine cannot be rinsed away during harvesting of T87 cells. The residual phenylalanine stored in the cytosol, requiring a double rinsing procedure which needed to grind the cell, then rinsed, filtered, and dried. The pyrolysis behavior of double rinsed T87 cells was even closer to *Arabidopsis* plant, than single rinsed cells. Pyrolysis of either T87 cells or *Arabidopsis* plant is quite different from pyrolyzing lignocellulosic biomass. Toluene was observed during biomass fast pyrolysis without adding catalyst. The production of dehydrated sugars and phenolic compounds was much less than pyrolyzing lignocellulosic biomass, like poplar. By analyzing ^{13}C distribution in main products, we found that most aldehydes, for example, 2-methylpropanal, 3-methylbutanal, were formed by carbohydrate, while the monoaromatic

hydrocarbons, toluene, ethylbenzene, and styrene, were mainly derived from lignin. Phenol was produced by both carbohydrate and lignin.

The bio-oil directly produced by pyrolysis has limited application due to high acidity, high moisture, and low energy content. An upgrading process is needed to improve fuel quality and make desired products. Zeolite catalyst, especially ZSM-5, is typically used to form aromatic hydrocarbons. Monoaromatic hydrocarbons, like benzene, toluene, ethylbenzene, and xylenes, (BTEX) are widely utilized in printing, leather, and rubber industries. To probe catalytic reaction pathways, the same procedure was applied to obtain preferably labeled T87 cells. HZSM-5 with a silicon to alumina ratio of 23 was mixed with the cells and then subjected into py-GC/MS system. The tracking of ^{13}C isotope in products during catalytic pyrolysis illustrated that the reaction pathway from carbohydrate to BTEX was different than from lignin. Holocellulose was initially depolymerized and decomposed, and then formed a “hydrocarbon pool” via decarbonylation and decarboxylation. BTEX was eventually produced by a ring reforming, while the aromatic ring in lignin would not break. BTEX was generated by side chain cleavage of lignin in this respect. No *p*-xylene was derived from lignin because no S-lignin was observed in T87 cells. In consideration of pore size of the catalyst, *m*-xylene and *o*-xylene were barely produced by lignin.

Feedstock selection and catalyst behavior are critical during catalytic fast pyrolysis. Compared to poplar, wheat straw, corn stover, and sugarcane bagasse, spent coffee grounds yield a much higher BTEX production. The silicon to alumina ratio of HZSM-5 affects the acidity and number of available acidic sites on ZSM-5. HZSM-5 with a lower SAR led to a stronger acidity and larger amount of acidic sites, benefiting to yield higher monoaromatic production. Chromium modified ZSM-5 provided a more competitive performance in BTEX production than other metals including Gallium, Nickel, Iron (II), Copper, Titanium, and Cobalt. Among of three loadings of

Chromium on ZSM-5 (1 wt.%, 3wt.%, 5 wt.%), 1 wt.% Cr/ZSM-5 yield a highest alkane, alkene, monoaromatic hydrocarbon production and a lowest polyaromatic hydrocarbon production.

6.2 Future Work

The following points may prompt the performance in reaction pathway mappings by using isotopically labeled plant cell culture:

- Cultivate the plant cells for long time periods aiming to increase cell wall content.
- Investigate how toluene is formed during fast pyrolysis without adding catalyst.
- Statistically investigate how the characteristic properties of biomass are related to BTEX production.
- Improve the catalyst quality (pore size, acidity and acidic site, functional metals) used for catalytic pyrolysis.

BIBLIOGRAPHY

1. Weilhhammer, V., J. Schmid, I. Mittermeier, F. Schreiber, L.M. Jiang, V. Pastuhovic, C. Herr, and S. Heinze, *Extreme weather events in Europe and their health consequences - A systematic review*. International Journal of Hygiene and Environmental Health, 2021. **233**.
2. Navas-Martín, M.Á., M.-A. Ovalle-Perandones, J.A. López-Bueno, J. Díaz, C. Linares, and G. Sánchez-Martínez, *Population adaptation to heat as seen through the temperature-mortality relationship, in the context of the impact of global warming on health: A scoping review*. Science of The Total Environment, 2023: p. 168441.
3. Hansen, J., M. Sato, R. Ruedy, K. Lo, D.W. Lea, and M. Medina-Elizade, *Global temperature change*. Proceedings of the National Academy of Sciences of the United States of America, 2006. **103**(39): p. 14288-14293.
4. IPCC, *Climate Change 2023: Synthesis Report*. 2023: Geneva, Switzerland. p. 35-115.
5. Rahmstorf, S., G. Foster, and N. Cahill, *Global temperature evolution: recent trends and some pitfalls*. Environmental Research Letters, 2017. **12**(5).
6. Intergovernmental Panel Climate Change, W.G.I.I.I., *Climate Change 2014: Mitigation of Climate Change*. Climate Change 2014: Mitigation of Climate Change, 2014: p. 1-1435.
7. IEA, *CO2 Emissions in 2022*. 2023: IEA, Paris.
8. Downing, M., L.M. Eaton, R.L. Graham, M.H. Langholtz, R.D. Perlack, J. Turhollow, Anthony F., B. Stokes, and C.C. Brandt, *U.S. Billion-Ton Update: Biomass Supply for a Bioenergy and Bioproducts Industry*. 2011, ; Oak Ridge National Lab. (ORNL), Oak Ridge, TN (United States). p. Medium: ED.
9. McKendry, P., *Energy production from biomass (part 1): overview of biomass*. Bioresource Technology, 2002. **83**(1): p. 37-46.
10. Brandt, C.C., M.R. Davis, B. Davison, L.M. Eaton, R.A. Efroymson, M.R. Hilliard, K. Kline, M.H. Langholtz, A. Myers, S. Sokhansanj, T.J. Theiss, J. Turhollow, Anthony F., E. Webb, I. Bonner, G. Gresham, J.R. Hess, P. Lamers, E. Searcy, K.L. Abt, M.A. Buford, D.P. Dykstra, P.D. Miles, P. Nepal, J.H. Perdue, K.E. Skog, D.W. Archer, H.S. Baumes, P.D. Cassidy, K. Novak, R. Mitchell, N. Andre, B.C. English, C. Hellwinkel, L.H. Lambert, J. McCord, T.G. Rials, R.C. Abt, B.J. Stokes, A. Wiselogel, D. Adams, B. Boykin, J. Caul, A. Gallagher, J. Largent, M. Lucas, B. Mar, A. Moulton, K. Satalino, G. Shields, V. Owens, L.R. Johnson, C. Daly, M. Halbleib, J. Rogers, R. Davis, A. Milbrandt, N. Brown, K.C. Lewis, A. Coleman, C. Drennan, M. Wigmosta, T. Volk, S. Schoenung, and W. Salverson, *2016 Billion-Ton Report: Advancing Domestic Resources for a Thriving Bioeconomy, Volume 1: Economic Availability of Feedstocks*. 2016, ; Oak Ridge National Lab. (ORNL), Oak Ridge, TN (United States). p. Medium: ED; Size: 448 p.
11. McKendry, P., *Energy production from biomass (part 2): conversion technologies*. Bioresource Technology, 2002. **83**(1): p. 47-54.

12. Bridgwater, A.V., D. Meier, and D. Radlein, *An overview of fast pyrolysis of biomass*. *Organic Geochemistry*, 1999. **30**(12): p. 1479-1493.
13. Winsley, P., *Biochar and bioenergy production for climate change mitigation*. *New Zealand Science Review*, 2007. **64**(1): p. 5-10.
14. Wright, M.M., D.E. Daugaard, J.A. Satrio, and R.C. Brown, *Techno-economic analysis of biomass fast pyrolysis to transportation fuels*. *Fuel*, 2010. **89**: p. S11-S19.
15. Zhang, Q., J. Chang, T.J. Wang, and Y. Xu, *Upgrading bio-oil over different solid catalysts*. *Energy & Fuels*, 2006. **20**(6): p. 2717-2720.
16. Wan, S.L., T. Pham, S. Zhang, L. Lobban, D. Resasco, and R. Mallinson, *Direct catalytic upgrading of biomass pyrolysis vapors by a dual function Ru/TiO₂ catalyst*. *Aiche Journal*, 2013. **59**(7): p. 2275-2285.
17. Diebold, J.P. and S. Czernik, *Additives to lower and stabilize the viscosity of pyrolysis oils during storage*. *Energy & Fuels*, 1997. **11**(5): p. 1081-1091.
18. Darmstadt, H., M. Garcia-Perez, A. Adnot, A. Chaala, D. Kretschmer, and C. Roy, *Corrosion of metals by bio-oil obtained by vacuum pyrolysis of softwood bark residues. An X-ray photoelectron spectroscopy and auger electron spectroscopy study*. *Energy & Fuels*, 2004. **18**(5): p. 1291-1301.
19. Chiamonti, D., A. Bonini, E. Fratini, G. Tondi, K. Gartner, A.V. Bridgwater, H.P. Grimm, I. Soldaini, A. Webster, and P. Baglioni, *Development of emulsions from biomass pyrolysis liquid and diesel and their use in engines - Part 2: tests in diesel engines*. *Biomass & Bioenergy*, 2003. **25**(1): p. 101-111.
20. Scholze, B. and D. Meier, *Characterization of the water-insoluble fraction from pyrolysis oil (pyrolytic lignin). Part I. PY-GC/MS, FTIR, and functional groups*. *Journal of Analytical and Applied Pyrolysis*, 2001. **60**(1): p. 41-54.
21. Evans, R.J., D.N. Wang, F.A. Agblevor, H.L. Chum, and S.D. Baldwin, *Mass spectrometric studies of the thermal decomposition of carbohydrates using C-13-labeled cellulose and glucose*. *Carbohydrate Research*, 1996. **281**(2): p. 219-235.
22. Carlson, T.R., J. Jae, and G.W. Huber, *Mechanistic Insights from Isotopic Studies of Glucose Conversion to Aromatics Over ZSM-5*. *Chemcatchem*, 2009. **1**(1): p. 107-110.
23. Lin, Y.C., J. Cho, G.A. Tompsett, P.R. Westmoreland, and G.W. Huber, *Kinetics and Mechanism of Cellulose Pyrolysis*. *Journal of Physical Chemistry C*, 2009. **113**(46): p. 20097-20107.
24. Patwardhan, P.R., R.C. Brown, and B.H. Shanks, *Product Distribution from the Fast Pyrolysis of Hemicellulose*. *Chemsuschem*, 2011. **4**(5): p. 636-643.

25. Zhou, X.W., M.W. Nolte, B.H. Shanks, and L.J. Broadbelt, *Experimental and Mechanistic Modeling of Fast Pyrolysis of Neat Glucose-Based Carbohydrates. 2. Validation and Evaluation of the Mechanistic Model*. Industrial & Engineering Chemistry Research, 2014. **53**(34): p. 13290-13301.
26. Ingram, L.O., H.C. Aldrich, A.C.C. Borges, T.B. Causey, A. Martinez, F. Morales, A. Saleh, S.A. Underwood, L.P. Yomano, S.W. York, J. Zaldivar, and S.D. Zhou, *Enteric bacterial catalysts for fuel ethanol production*. Biotechnology Progress, 1999. **15**(5): p. 855-866.
27. Brown, R.C. and T.R. Brown, *Thermochemical Processing of Lignocellulosic Biomass*. Biorenewable Resources: Engineering New Products from Agriculture, 2nd Edition, 2014: p. 195-236.
28. Bridgwater, A.V., *Review of fast pyrolysis of biomass and product upgrading*. Biomass & Bioenergy, 2012. **38**: p. 68-94.
29. Isahak, W.N.R.W., M.W.M. Hisham, M.A. Yarmo, and T.Y.Y. Hin, *A review on bio-oil production from biomass by using pyrolysis method*. Renewable & Sustainable Energy Reviews, 2012. **16**(8): p. 5910-5923.
30. Czernik, S. and A.V. Bridgwater, *Overview of applications of biomass fast pyrolysis oil*. Energy & Fuels, 2004. **18**(2): p. 590-598.
31. Lu, Q., W.Z. Li, and X.F. Zhu, *Overview of fuel properties of biomass fast pyrolysis oils*. Energy Conversion and Management, 2009. **50**(5): p. 1376-1383.
32. Zhang, Q., J. Chang, T.J. Wang, and Y. Xu, *Review of biomass pyrolysis oil properties and upgrading research*. Energy Conversion and Management, 2007. **48**(1): p. 87-92.
33. Dhyani, V. and T. Bhaskar, *Pyrolysis of Biomass*. Biofuels: Alternative Feedstocks and Conversion Processes for the Production of Liquid and Gaseous Biofuels, 2nd Edition, 2019: p. 217-244.
34. Wang, S.R., B. Ru, H.Z. Lin, and Z.Y. Luo, *Degradation mechanism of monosaccharides and xylan under pyrolytic conditions with theoretic modeling on the energy profiles*. Bioresource Technology, 2013. **143**: p. 378-383.
35. Dhyani, V., M.K. Awasthi, Q. Wang, J. Kumar, X.N. Ren, J.C. Zhao, H.Y. Chen, M.J. Wang, T. Bhaskar, and Z.Q. Zhang, *Effect of composting on the thermal decomposition behavior and kinetic parameters of pig manure-derived solid waste*. Bioresource Technology, 2018. **252**: p. 59-65.
36. Kawamoto, H., *Lignin pyrolysis reactions*. Journal of Wood Science, 2017. **63**(2): p. 117-132.

37. Han, Y.L., M. Gholizadeh, C.C. Tran, S. Kaliaguine, C.Z. Li, M. Olarte, and M. Garcia-Perez, *Hydrotreatment of pyrolysis bio-oil: A review*. Fuel Processing Technology, 2019. **195**.
38. Elliott, D.C., T.R. Hart, G.G. Neuenschwander, L.J. Rotness, M.V. Olarte, A.H. Zacher, and Y. Solantausta, *Catalytic Hydroprocessing of Fast Pyrolysis Bio-oil from Pine Sawdust*. Energy & Fuels, 2012. **26**(6): p. 3891-3896.
39. Wang, K.G., K.H. Kim, and R.C. Brown, *Catalytic pyrolysis of individual components of lignocellulosic biomass*. Green Chemistry, 2014. **16**(2): p. 727-735.
40. Carlson, T.R., G.A. Tompsett, W.C. Conner, and G.W. Huber, *Aromatic Production from Catalytic Fast Pyrolysis of Biomass-Derived Feedstocks*. Topics in Catalysis, 2009. **52**(3): p. 241-252.
41. Jae, J., G.A. Tompsett, A.J. Foster, K.D. Hammond, S.M. Auerbach, R.F. Lobo, and G.W. Huber, *Investigation into the shape selectivity of zeolite catalysts for biomass conversion*. Journal of Catalysis, 2011. **279**(2): p. 257-268.
42. Zhou, C.H., X. Xia, C.X. Lin, D.S. Tong, and J. Beltramini, *Catalytic conversion of lignocellulosic biomass to fine chemicals and fuels*. Chemical Society Reviews, 2011. **40**(11): p. 5588-5617.
43. Lappas, A.A., K.G. Kalogiannis, E.F. Iliopoulou, K.S. Triantafyllidis, and S.D. Stefanidis, *Catalytic pyrolysis of biomass for transportation fuels*. Wiley Interdisciplinary Reviews-Energy and Environment, 2012. **1**(3): p. 285-297.
44. Carlson, T.R., T.R. Vispute, and G.W. Huber, *Green gasoline by catalytic fast pyrolysis of solid biomass derived compounds*. Chemsuschem, 2008. **1**(5): p. 397-400.
45. Kelkar, S., C.M. Saffron, K. Andreassi, Z.L. Li, A. Murkute, D.J. Miller, T.J. Pinnavaia, and R.M. Kriegel, *A survey of catalysts for aromatics from fast pyrolysis of biomass*. Applied Catalysis B-Environmental, 2015. **174**: p. 85-95.
46. Williams, C.L., C.C. Chang, P. Do, N. Nikbin, S. Caratzoulas, D.G. Vlachos, R.F. Lobo, W. Fan, and P.J. Dauenhauer, *Cycloaddition of Biomass-Derived Furans for Catalytic Production of Renewable -Xylene*. Acs Catalysis, 2012. **2**(6): p. 935-939.
47. Cheng, Y.T., Z.P. Wang, C.J. Gilbert, W. Fan, and G.W. Huber, *Production of p-Xylene from Biomass by Catalytic Fast Pyrolysis Using ZSM-5 Catalysts with Reduced Pore Openings*. Angewandte Chemie-International Edition, 2012. **51**(44): p. 11097-11100.
48. Ashraf, M.T., R. Chebbi, and N.A. Darwish, *Process of p-Xylene Production by Highly Selective Methylation of Toluene*. Industrial & Engineering Chemistry Research, 2013. **52**(38): p. 13730-13737.

49. Choudhary, V.R., A.K. Kinage, and T.V. Choudhary, *Direct aromatization of natural gas over H-gallosilicate (MFI), H-galloaluminosilicate (MFI) and Ga/H-ZSM-5 zeolites*. Applied Catalysis a-General, 1997. **162**(1-2): p. 239-248.
50. Aboul-Gheit, A.K., M.S. El-Masry, and A.E. Awadallah, *Oxygen free conversion of natural gas to useful hydrocarbons and hydrogen over monometallic Mo and bimetallic Mo-Fe, Mo-Co or Mo-Ni/HZSM-5 catalysts prepared by mechanical mixing*. Fuel Processing Technology, 2012. **102**: p. 24-29.
51. Mullen, C.A. and A.A. Boateng, *Production of Aromatic Hydrocarbons via Catalytic Pyrolysis of Biomass over Fe-Modified HZSM-5 Zeolites*. Acs Sustainable Chemistry & Engineering, 2015. **3**(7): p. 1623-1631.
52. Du, Z.Y., X.C. Ma, Y. Li, P. Chen, Y.H. Liu, X.Y. Lin, H.W. Lei, and R. Ruan, *Production of aromatic hydrocarbons by catalytic pyrolysis of microalgae with zeolites: Catalyst screening in a pyroprobe*. Bioresource Technology, 2013. **139**: p. 397-401.
53. Cheng, Y.T., J. Jae, J. Shi, W. Fan, and G.W. Huber, *Production of Renewable Aromatic Compounds by Catalytic Fast Pyrolysis of Lignocellulosic Biomass with Bifunctional Ga/ZSM-5 Catalysts*. Angewandte Chemie-International Edition, 2012. **51**(6): p. 1387-1390.
54. Iliopoulou, E.F., S.D. Stefanidis, K.G. Kalogiannis, A. Delimitis, A.A. Lappas, and K.S. Triantafyllidis, *Catalytic upgrading of biomass pyrolysis vapors using transition metal-modified ZSM-5 zeolite*. Applied Catalysis B-Environmental, 2012. **127**: p. 281-290.
55. French, R. and S. Czernik, *Catalytic pyrolysis of biomass for biofuels production*. Fuel Processing Technology, 2010. **91**(1): p. 25-32.
56. Varzaneh, A.Z., A.H.S. Kootenaei, J. Towfighi, and A. Mohamadalizadeh, *Optimization and deactivation study of Fe-Ce/HZSM-5 catalyst in steam catalytic cracking of mixed ethanol/naphtha feed*. Journal of Analytical and Applied Pyrolysis, 2013. **102**: p. 144-153.
57. Zheng, Y.W., F. Wang, X.Q. Yang, Y.B. Huang, C. Liu, Z.F. Zheng, and J.Y. Gu, *Study on aromatics production via the catalytic pyrolysis vapor upgrading of biomass using metal-loaded modified H-ZSM-5*. Journal of Analytical and Applied Pyrolysis, 2017. **126**: p. 169-179.
58. Veses, A., B. Puértolas, J.M. López, M.S. Callén, B. Solsona, and T. García, *Promoting Deoxygenation of Bio-Oil by Metal-Loaded Hierarchical ZSM-5 Zeolites*. Acs Sustainable Chemistry & Engineering, 2016. **4**(3): p. 1653-1660.
59. Antal, M.J., *Biomass Pyrolysis: A Review of the Literature Part 1—Carbohydrate Pyrolysis*, in *Advances in Solar Energy: An Annual Review of Research and Development, Volume 1 · 1982*, K.W. Böer and J.A. Duffie, Editors. 1983, Springer New York: Boston, MA. p. 61-111.

60. Antal, M.J., *Biomass Pyrolysis: A Review of the Literature Part 2—Lignocellulose Pyrolysis*, in *Advances in Solar Energy: An Annual Review of Research and Development Volume 2*, K.W. Böer and J.A. Duffie, Editors. 1985, Springer US: Boston, MA. p. 175-255.
61. Glassner, S. and A.R. Pierce, *Gas Chromatographic Analysis of Products from Controlled Application of Heat to Paper and Levoglucosan*. Analytical Chemistry, 1965. **37**(4): p. 525-&.
62. Shafizadeh, F., *Pyrolysis of cellulose*. Carbohydrate research, 1973. **29**(1): p. 113-122.
63. Shafizadeh, F., C.W. Philpot, and N. Ostojic, *Thermal Analysis of 1,6-Anhydro-Beta-D-Glucopyranose*. Carbohydrate Research, 1971. **16**(2): p. 279-+.
64. Milne, T.A. and M.N. Soltys, *Direct Mass-Spectrometric Studies of the Pyrolysis of Carbonaceous Fuels .1. A Flame-Pyrolysis Molecular-Beam Sampling Technique*. Journal of Analytical and Applied Pyrolysis, 1983. **5**(2): p. 93-110.
65. Evans, R.J., T.A. Milne, M.N. Soltys, and H.R. Schulten, *Mass-Spectrometric Behavior of Levoglucosan under Different Ionization Conditions and Implications for Studies of Cellulose Pyrolysis*. Journal of Analytical and Applied Pyrolysis, 1984. **6**(3): p. 273-283.
66. Evans, R.J., T.A. Milne, and M.N. Soltys, *Direct Mass-Spectrometric Studies of the Pyrolysis of Carbonaceous Fuels .3. Primary Pyrolysis of Lignin*. Journal of Analytical and Applied Pyrolysis, 1986. **9**(3): p. 207-236.
67. Van der hage, E.R.E., M.M. Mulder, and J.J. Boon, *Structural Characterization of Lignin Polymers by Temperature-Resolved in-Source Pyrolysis Mass-Spectrometry and Curie-Point Pyrolysis-Gas Chromatography Mass-Spectrometry*. Journal of Analytical and Applied Pyrolysis, 1993. **25**: p. 149-183.
68. Ponder, G.R. and G.N. Richards, *Mechanisms of Pyrolysis of Polysaccharides .7. Pyrolysis of Some C-13-Labeled Glucans - a Mechanistic Study*. Carbohydrate Research, 1993. **244**(1): p. 27-47.
69. Paine, J.B., Y.B. Pithawalla, J.D. Naworal, and C.E. Thomas, *Carbohydrate pyrolysis mechanisms from isotopic labeling. Part 1: The pyrolysis of glycerin: Discovery of competing fragmentation mechanisms affording acetaldehyde and formaldehyde and the implications for carbohydrate pyrolysis*. Journal of Analytical and Applied Pyrolysis, 2007. **80**(2): p. 297-311.
70. Paine, J.B., Y.B. Pithawalla, and J.D. Naworal, *Carbohydrate pyrolysis mechanisms from isotopic labeling. Part 2. The pyrolysis of D-glucose: General disconnective analysis and the formation of C-1 and C-2 carbonyl compounds by electrocyclic fragmentation mechanisms*. Journal of Analytical and Applied Pyrolysis, 2008. **82**(1): p. 10-41.
71. Paine, J.B., Y.B. Pithawalla, and J.D. Naworal, *Carbohydrate pyrolysis mechanisms from isotopic labeling. Part 3. The Pyrolysis of D-glucose: Formation of C-3 and C-4 carbonyl*

- compounds and a cyclopentenedione isomer by electrocyclic fragmentation mechanisms.* Journal of Analytical and Applied Pyrolysis, 2008. **82**(1): p. 42-69.
72. Paine, J.B., Y.B. Pithawalla, and J.D. Naworal, *Carbohydrate pyrolysis mechanisms from isotopic labeling Part 4. The pyrolysis Of D-glucose: The formation of furans.* Journal of Analytical and Applied Pyrolysis, 2008. **83**(1): p. 37-63.
73. Paine, J.B., Y.B. Pithawalla, and J.D. Naworal, *Carbohydrate pyrolysis mechanisms from isotopic labeling. Part 5. The pyrolysis of D-glucose: The origin of the light gases from the D-glucose molecule.* Journal of Analytical and Applied Pyrolysis, 2019. **138**: p. 70-93.
74. Zhou, X.W., M.W. Nolte, H.B. Mayes, B.H. Shanks, and L.J. Broadbelt, *Experimental and Mechanistic Modeling of Fast Pyrolysis of Neat Glucose-Based Carbohydrates. 1. Experiments and Development of a Detailed Mechanistic Model.* Industrial & Engineering Chemistry Research, 2014. **53**(34): p. 13274-13289.
75. Zhou, X.W., W.J. Li, R. Mabon, and L.J. Broadbelt, *A mechanistic model of fast pyrolysis of hemicellulose.* Energy & Environmental Science, 2018. **11**(5): p. 1240-1260.
76. Mayes, H.B. and L.J. Broadbelt, *Unraveling the Reactions that Unravel Cellulose.* Journal of Physical Chemistry A, 2012. **116**(26): p. 7098-7106.
77. McCann, M., *Architecture of the primary cell wall.* The cytoskeletal basis of plant growth and form, 1992: p. 109-129.
78. Carpita, N.C. and D.M. Gibeaut, *Structural models of primary cell walls in flowering plants: consistency of molecular structure with the physical properties of the walls during growth.* The Plant Journal, 1993. **3**(1): p. 1-30.
79. Schwender, J., J. Ohlrogge, and Y. Shachar-Hill, *Understanding flux in plant metabolic networks.* Current Opinion in Plant Biology, 2004. **7**(3): p. 309-317.
80. Spielbauer, G., L. Margl, L.C. Hannah, W. Romisch, C. Ettenhuber, A. Bacher, A. Gierl, W. Eisenreich, and U. Genschel, *Robustness of central carbohydrate metabolism in developing maize kernels.* Phytochemistry, 2006. **67**(14): p. 1460-1475.
81. Arabidopsis Genome, I., *Analysis of the genome sequence of the flowering plant Arabidopsis thaliana.* Nature, 2000. **408**(6814): p. 796-815.
82. Cosgrove, D.J., *Growth of the plant cell wall.* Nature Reviews Molecular Cell Biology, 2005. **6**(11): p. 850-861.
83. Anderson, M., *Climate Change 2014: Synthesis Report.* Library Journal, 2016. **141**(9): p. 28-28.
84. Mazo, J., *Climate Change Impacts in the United States: The Third National Climate Assessment.* Survival, 2014. **56**(4): p. 175-183.

85. Agency, I.E., *CO2 Emissions from Fuel Combustion 2019*. 2019.
86. UNFCCC, *Adoption of the Paris Agreement—FCCC/CP/2015/L.9/rev.1*. 2015.
87. Sluiter, A., B. Hames, R. Ruiz, C. Scarlata, J. Sluiter, D. Templeton, and D. Crocker, *Determination of Structural Carbohydrates and Lignin in Biomass—NREL/TP-510-42618*. Laboratory Analytical Procedure (LAP), 2008.
88. Herr, J.M., Jr., *New uses for calcium chloride solution as a mounting medium*. *Biotech Histochem*, 1992. **67**(1): p. 9-13.
89. Davidson, R.S., H. Choudhury, S. Origgi, A. Castellan, V. Trichet, and G. Capretti, *The Reaction of Phloroglucinol in the Presence of Acid with Lignin-Containing Materials*. *Journal of Photochemistry and Photobiology a-Chemistry*, 1995. **91**(1): p. 87-93.
90. Zhao, Q.A., H.Z. Wang, Y.B. Yin, Y. Xu, F. Chen, and R.A. Dixon, *Syringyl lignin biosynthesis is directly regulated by a secondary cell wall master switch*. *Proceedings of the National Academy of Sciences of the United States of America*, 2010. **107**(32): p. 14496-14501.
91. Derikvand, M.M., J.B. Sierra, K. Ruel, B. Pollet, C.T. Do, J. Thevenin, D. Buffard, L. Jouanin, and C. Lapierre, *Redirection of the phenylpropanoid pathway to feruloyl malate in Arabidopsis mutants deficient for cinnamoyl-CoA reductase 1*. *Planta*, 2008. **227**(5): p. 943-956.
92. Yamamura, M., S. Wada, N. Sakakibara, T. Nakatsubo, S. Suzuki, T. Hattori, M. Takeda, N. Sakurai, H. Suzuki, D. Shibata, and T. Umezawa, *Occurrence of guaiacyl/p-hydroxyphenyl lignin in Arabidopsis thaliana T87 cells*. *Plant Biotechnology*, 2011. **28**(1): p. 1-8.
93. de Kraker, J.W., K. Luck, S. Textor, J.G. Tokuhisa, and J. Gershenzon, *Two Arabidopsis genes (IPMS1 and IPMS2) encode isopropylmalate synthase, the branchpoint step in the biosynthesis of leucine*. *Plant Physiology*, 2007. **143**(2): p. 970-986.
94. Jabeen, S., Z. Zeng, M. Altarawneh, X. Gao, A. Saeed, and B.Z. Dlugogorski, *Thermal decomposition of model compound of algal biomass*. *International Journal of Chemical Kinetics*, 2019. **51**(9): p. 696-710.
95. Strecker, A., *On a peculiar oxidation by alloxan*. *Justus Liebigs Ann Chem.*, 1862. **123**: p. 363-367.
96. Smit, B.A., W.J.M. Engels, and G. Smit, *Branched chain aldehydes: production and breakdown pathways and relevance for flavour in foods*. *Applied Microbiology and Biotechnology*, 2009. **81**(6): p. 987-999.
97. Wang, M., J.M. Lu, X.C. Zhang, L.H. Li, H.J. Li, N.C. Luo, and F. Wang, *Two-Step, Catalytic C-C Bond Oxidative Cleavage Process Converts Lignin Models and Extracts to Aromatic Acids*. *Acs Catalysis*, 2016. **6**(9): p. 6086-6090.

98. Wang, M., J.M. Lu, L.H. Li, H.J. Li, H.F. Liu, and F. Wang, *Oxidative C(OH)-C bond cleavage of secondary alcohols to acids over a copper catalyst with molecular oxygen as the oxidant*. Journal of Catalysis, 2017. **348**: p. 160-167.
99. Wang, M., L.H. Li, J.M. Lu, H.J. Li, X.C. Zhang, H.F. Liu, N.C. Luo, and F. Wang, *Acid promoted C-C bond oxidative cleavage of β -O-4 and β -1 lignin models to esters over a copper catalyst*. Green Chemistry, 2017. **19**(3): p. 702-706.
100. Liu, H.F., M. Wang, H.J. Li, N.C. Luo, S.T. Xu, and F. Wang, *New protocol of copper-catalyzed oxidative C(CO)single bondC bond cleavage of aryl and aliphatic ketones to organic acids using O₂ as the terminal oxidant*. Journal of Catalysis, 2017. **346**: p. 170-179.
101. Chu, S., A.V. Subrahmanyam, and G.W. Huber, *The pyrolysis chemistry of a β -O-4 type oligomeric lignin model compound*. Green Chemistry, 2013. **15**(1): p. 125-136.
102. Huang, J., C. Liu, D. Wu, H. Tong, and L. Ren, *Density functional theory studies on pyrolysis mechanism of β -O-4 type lignin dimer model compound*. Journal of analytical and applied pyrolysis, 2014. **109**: p. 98-108.
103. Jiang, W.K., S.B. Wu, L.A. Lucia, and J.Y. Chu, *A comparison of the pyrolysis behavior of selected β -O-4 type lignin model compounds*. Journal of Analytical and Applied Pyrolysis, 2017. **125**: p. 185-192.
104. Shen, Q.R., Z.W. Fu, R. Li, and Y.L. Wu, *A study on the pyrolysis mechanism of a β -O-4 lignin dimer model compound using DFT combined with Py-GC/MS*. Journal of Thermal Analysis and Calorimetry, 2021. **146**(4): p. 1751-1761.
105. Zhang, Y.Y., H.W. Lei, Z.X. Yang, D.L. Duan, E. Villota, and R. Ruan, *From Glucose-Based Carbohydrates to Phenol-rich Bio-oil Integrated with Syngas Production via Catalytic Pyrolysis over Activated Carbon Catalyst* Green Chemistry, 2018. **20**(14): p. 3346-3358.
106. Yan, J., Q.L. Meng, X.J. Shen, B.F. Chen, Y. Sun, J.F. Xiang, H.Z. Liu, and B.X. Han, *Selective valorization of lignin to phenol by direct transformation of Csp²-Csp³ and C-O bonds*. Science Advances, 2020. **6**(45).
107. Huber, G.W., S. Iborra, and A. Corma, *Synthesis of transportation fuels from biomass: Chemistry, catalysts, and engineering*. Chemical Reviews, 2006. **106**(9): p. 4044-4098.
108. Brown, R.C. and T.R. Brown, *Biorenewable Resources: Engineering New Products from Agriculture, 2nd Edition*. Biorenewable Resources: Engineering New Products from Agriculture, 2nd Edition, 2014: p. 1-375.
109. Moens, L., S.K. Black, M.D. Myers, and S. Czernik, *Study of the Neutralization and Stabilization of a Mixed Hardwood Bio-Oil*. Energy & Fuels, 2009. **23**(5-6): p. 2695-2699.

110. Yang, Z.X., A. Kumar, and R.L. Huhnke, *Review of recent developments to improve storage and transportation stability of bio-oil*. *Renewable & Sustainable Energy Reviews*, 2015. **50**: p. 859-870.
111. Wang, K.G., P.A. Johnston, and R.C. Brown, *Comparison of in-situ and ex-situ catalytic pyrolysis in a micro-reactor system*. *Bioresource Technology*, 2014. **173**: p. 124-131.
112. Stefanidis, S.D., K.G. Kalogiannis, E.F. Iliopoulou, A.A. Lappas, and P.A. Pilavachi, *In-situ upgrading of biomass pyrolysis vapors: Catalyst screening on a fixed bed reactor*. *Bioresource Technology*, 2011. **102**(17): p. 8261-8267.
113. Guo, X.Y., Y. Zheng, B.H. Zhang, and J.Y. Chen, *Analysis of coke precursor on catalyst and study on regeneration of catalyst in upgrading of bio-oil*. *Biomass & Bioenergy*, 2009. **33**(10): p. 1469-1473.
114. Carlson, T.R., J. Jae, Y.C. Lin, G.A. Tompsett, and G.W. Huber, *Catalytic fast pyrolysis of glucose with HZSM-5: The combined homogeneous and heterogeneous reactions*. *Journal of Catalysis*, 2010. **270**(1): p. 110-124.
115. Yamaguchi, D. and M. Hara, *Starch saccharification by carbon-based solid acid catalyst*. *Solid State Sciences*, 2010. **12**(6): p. 1018-1023.
116. Boerjan, W., J. Ralph, and M. Baucher, *Lignin biosynthesis*. *Annual Review of Plant Biology*, 2003. **54**: p. 519-546.
117. Srinivasan, V., S. Adhikari, S.A. Chattanathan, M.B. Tu, and S. Park, *Catalytic Pyrolysis of Raw and Thermally Treated Cellulose Using Different Acidic Zeolites*. *Bioenergy Research*, 2014. **7**(3): p. 867-875.
118. Mullen, C.A. and A.A. Boateng, *Catalytic pyrolysis-GC/MS of lignin from several sources*. *Fuel Processing Technology*, 2010. **91**(11): p. 1446-1458.
119. Wu, Y., S.L. Wu, H.Y. Zhang, and R. Xiao, *Cellulose-lignin interactions during catalytic pyrolysis with different zeolite catalysts*. *Fuel Processing Technology*, 2018. **179**: p. 436-442.
120. Liu, Q.A., Z.P. Zhong, S.R. Wang, and Z.Y. Luo, *Interactions of biomass components during pyrolysis: A TG-FTIR study*. *Journal of Analytical and Applied Pyrolysis*, 2011. **90**(2): p. 213-218.
121. Choudhary, V.R., V.S. Nayak, and T.V. Choudhary, *Single-component sorption/diffusion of cyclic compounds from their bulk liquid phase in H-ZSM-5 zeolite*. *Industrial & Engineering Chemistry Research*, 1997. **36**(5): p. 1812-1818.
122. Yang, Y., Z.Y. Luo, S.M. Li, K.Y. Lu, and W.B. Wang, *Catalytic Pyrolysis of Hemicellulose to Produce Aromatic Hydrocarbons*. *Bioresources*, 2019. **14**(3): p. 5816-5831.

123. Luo, L., E. van der Voet, G. Huppel, and H.A.U. de Haes, *Allocation issues in LCA methodology: a case study of corn stover-based fuel ethanol*. International Journal of Life Cycle Assessment, 2009. **14**(6): p. 529-539.
124. Marcilly, C., *Present status and future trends in catalysis for refining and petrochemicals*. Journal of Catalysis, 2003. **216**(1-2): p. 47-62.
125. Perot, G. and M. Guisnet, *Advantages and Disadvantages of Zeolites as Catalysts in Organic-Chemistry*. Journal of Molecular Catalysis, 1990. **61**(2): p. 173-196.
126. Su, F.S., C.Y. Lu, K.R. Johnston, and S.K. Hu, *Kinetics, Thermodynamics, and Regeneration of BTEX Adsorption in Aqueous Solutions via NaOCl-Oxidized Carbon Nanotubes*. Environanotechnology, 2010: p. 71-97.
127. Taarning, E., C.M. Osmundsen, X.B. Yang, B. Voss, S.I. Andersen, and C.H. Christensen, *Zeolite-catalyzed biomass conversion to fuels and chemicals*. Energy & Environmental Science, 2011. **4**(3): p. 793-804.
128. Mariyam, S., M. Alherbawi, S. Pradhan, T. Al-Ansari, and G. McKay, *Biochar yield prediction using response surface methodology: effect of fixed carbon and pyrolysis operating conditions*. Biomass Conversion and Biorefinery, 2023.
129. Zhang, H.Y., Y.T. Cheng, T.P. Vispute, R. Xiao, and G.W. Huber, *Catalytic conversion of biomass-derived feedstocks into olefins and aromatics with ZSM-5: the hydrogen to carbon effective ratio*. Energy & Environmental Science, 2011. **4**(6): p. 2297-2307.
130. Liu, Q.Q., L. Luo, and L.Q. Zheng, *Lignins: Biosynthesis and Biological Functions in Plants*. International Journal of Molecular Sciences, 2018. **19**(2).
131. Niwa, M., S. Sota, and N. Katada, *Strong Bronsted acid site in HZSM-5 created by mild steaming*. Catalysis Today, 2012. **185**(1): p. 17-24.
132. Haukka, S., E.L. Lakomaa, and T. Suntola, *Adsorption controlled preparation of heterogeneous catalysts*. Adsorption and Its Applications in Industry and Environmental Protection, Vol I: Applications in Industry, 1999. **120**: p. 715-750.